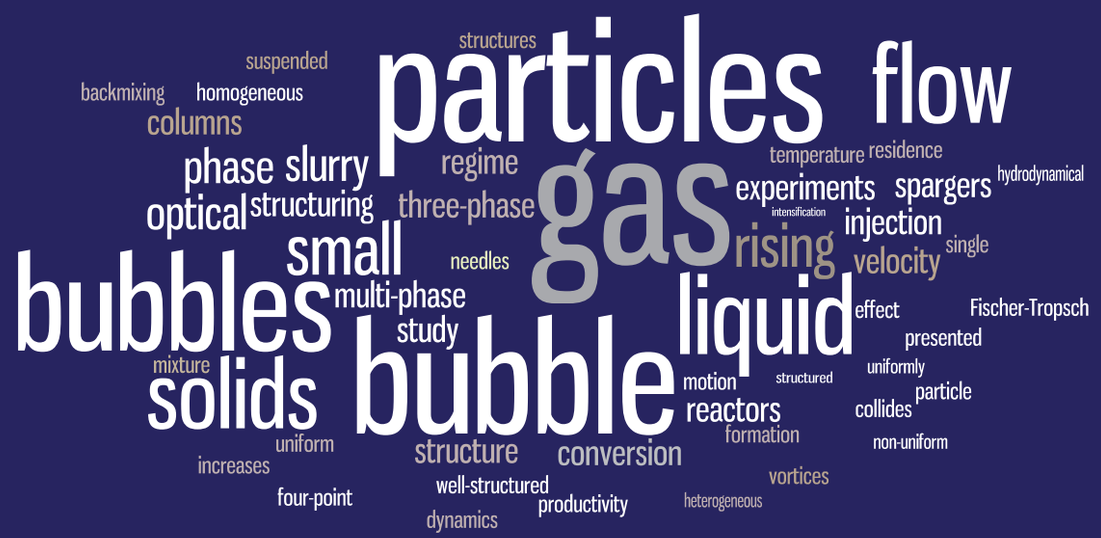

Hydrodynamics of Structured Slurry Bubble Columns

Nasim Hooshyar

Hydrodynamics of Structured Slurry Bubble Columns

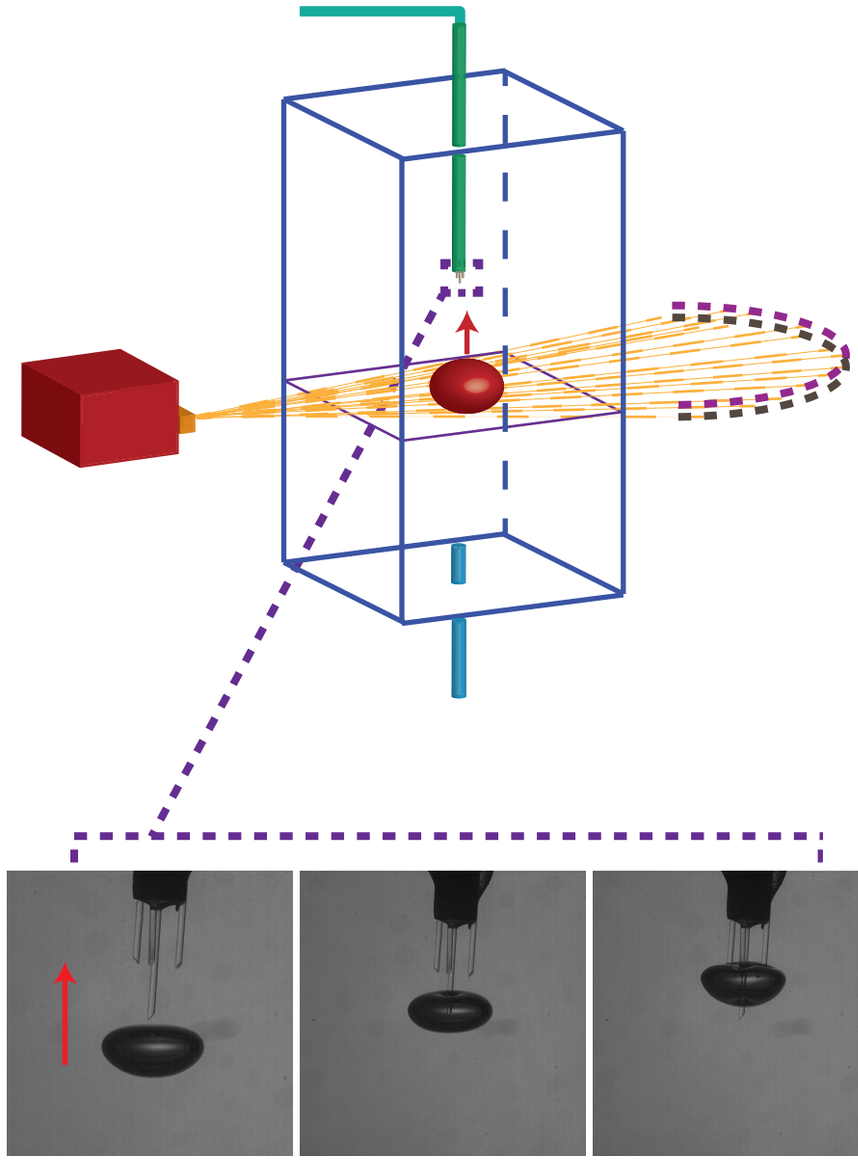

Nasim Hooshyar

Hydrodynamics of Structured Slurry Bubble Columns

PROEFSCHRIFT

ter verkrijging van de graad van doctor
aan de Technische Universiteit Delft,
op gezag van de Rector Magnificus Prof. ir. K.C.A.M. Luyben,
voorzitter van het College voor Promoties,
in het openbaar te verdedigen op 14 januari 2013 om 15:00 uur

door

Nasim HOOSHYAR

Master of Science in Chemical Engineering
University of Tehran, Iran

geboren te Shiraz, Iran

Dit proefschrift is goedgekeurd door de promotor:
Prof. dr. R. F. Mudde

Copromotor:
Dr. ir. J. R. van Ommen

Samenstelling promotiecommissie:

Rector Magnificus	voorzitter
Prof. dr. R. F. Mudde	Technische Universiteit Delft, promotor
Dr. ir. J. R. van Ommen	Technische Universiteit Delft, copromotor
Prof. dr. ir. A. I. Stankiewicz	Technische Universiteit Delft
Prof. dr. S. Sundaresan	Princeton University, Princeton
Prof. dr. ir. J. A. M. Kuipers	Technische Universiteit Eindhoven
Dr. ir. B. van Wachem	Imperial College, London
Prof. dr. ir. H. E. A. van den Akker	Technische Universiteit Delft, reservelid

Dr. ir. P. J. Hamersma heeft als begeleider in belangrijke mate aan de totstandkoming van het proefschrift bijgedragen.

This work was financially supported by the Delft University of Technology.

Printed by: SIECA REPRO

ISBN 978-94-6186-108-5

In the memory of my father
Hossein Hooshyar,
Who led me into science and literature but left us
before his dream came true.
To my mother
To Farzad

"Narrow minds devoid of imagination. Intolerance, theories cut off from reality, empty terminology, usurped ideals, inflexible systems. Those are the things that really frighten me. What I absolutely fear and loathe."

-Haruki Murakami, Kafka on the Shore

Summary

Slurry Bubble Columns (SBCs) are widely used in industry e.g. for production of algae, water treatment and Fischer-Tropsch synthesis to perform reactions involving gas, liquid and solids. SBCs are an example of multi-phase flow systems in which three phases, i.e. gas, liquid and solids are present. The gas is dispersed from the bottom region of the column via a gas sparger to a pool of liquid and solids mixture. The solids are normally fine catalyst particles which are suspended in the liquid in contrast to systems with immobilized solid phase such as fixed bed reactors. The easy construction and working near isothermal conditions have made these three-phase catalytic reactors attractive for industry and specially for many exothermic three-phase reacting systems. However, solids separation, scale-up and backmixing are typical disadvantages in these multi-phase flow systems. Structuring the flow is an attractive way to tackle the disadvantages of the multi-phase reactors.

The work presented in this thesis aims at process intensification in SBCs by means of structuring the flow and on the effect of particles on the dynamics of the gas bubbles rising in the slurry systems. Several approaches are possible to structure the flow in SBCs, e.g. staging the reactor or inducing vibration to the SBC. Less attention has been paid to a well-structured gas injection system. This research focuses on manipulating the gas phase to structure the flow in SBCs. It is shown in this study, both theoretically and experimentally, that structuring can increase the gas residence time and the conversion in a SBC.

Experiments show that although backmixing, up to a certain level, is required to prevent the particles from settling down, it causes the bubbles to coalesce or cluster together. These larger bubbles or clusters rise faster than small or isolated bubbles. The follow-up of the low residence time of the gas bubbles are the low conversion and productivity of the reactor. However, the uniform distribution of the gas bubbles, regular both in time and space, can lead to the formation of small bubbles, less vortices and the extension of more regular structures of the homogeneous regime to higher gas velocities than attainable for regular spargers.

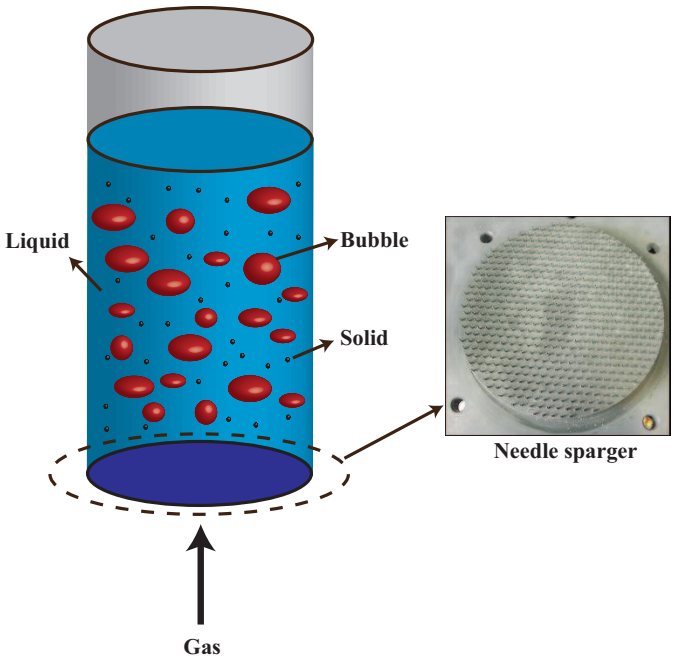

FIGURE 1: Schematic diagram of a Slurry Bubble Column and the applied needle sparger for process intensification.

We study the influence of structuring and reducing the degree of liquid mixing in an industrial SBC by simulation. The Fischer-Tropsch synthesis is chosen as one of the most important examples of the application of the SBCs. The results indicate that with a 75% reduction in the liquid axial dispersion coefficient, the syngas conversion and the productivity of the C_{5+}, hydrocarbons with five or more atoms, increases by 20%.
To structure the flow, reduce the vortices and increase the number of small bubbles in a SBC, a well-structured gas injection system consisting of several needles is used. The experiments are performed both in a 2D and a 3D column which are equipped with the needles as their spargers (see Fig. 1). These spargers can provide both uniform and non-uniform gas injections. We consider the situations in which the air bubbles formed are of the same size and injected uniformly to the entire bottom of the column with the same velocity. Water is used as the liquid phase and very fine glass beads as the solids particles. The pressure of the inlet gas is 2.0 bar and the temperature is the ambient temperature in all the experiments in the slurry bubble columns. Fig. 2 shows the sequence of the formation of an air bubble at the exit of a needle.

The gas fraction in the cross section of the columns is measured using single point optical probes and the bubble dynamics using a four-point optical probe facing downward. The results show that using a structured gas injection system, we can extend the homogeneous flow regime and have more small bubble in the heterogeneous flow regime. In addition, visual observations indicate that the strength and number of vortical structures

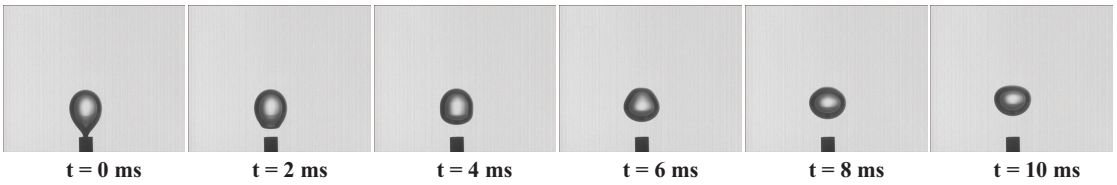

FIGURE 2: Bubble formation at the exit of the needles.

has been reduced.

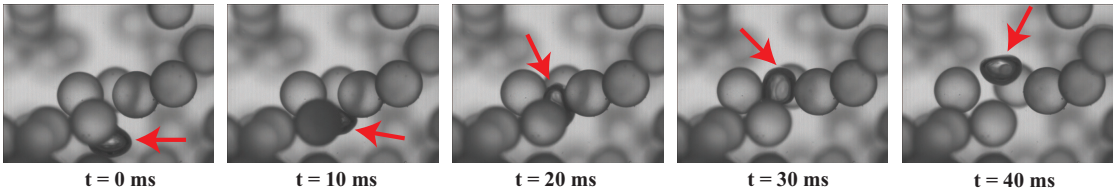

FIGURE 3: The rising motion of a 3 mm gas bubble in a glycerol-water mixture containing neutrally buoyant 4.0 mm polystyrene particles. The bubble encounters the particles, gets squeezed in between the particles, pushes them aside and rises. The arrows point to the bubble.

Addition of the particles changes the hydrodynamical characteristics of the slurry systems. The experiments show that an increase in the solids volume fraction increases the bubble velocity by 100% but the bubble size stays rather constant. To get a better insight in the effect of solids particles on the motion of rising bubbles, we apply X-ray densitometry and a high speed camera in combination with the four-point optical probe and zoom in on the motion of a single rising bubble in a liquid-solids suspension. To keep the particles suspended and slip free relative to the liquid, the liquid (a water and glycerol mixture) is neutrally buoyant to the particle's density. We use different sizes of polystyrene particles. The results show that the rising bubble does not collide with the particles when these are small. The novelty of our study is in the case of large particles where the rising bubble collides with particles (see Fig. 3); upon each collision, the bubble deforms and slows down, separates from the particle, re-accelerates and collides with the next particle. A simple model for the average bubble rise velocity that captures the essence of this repeating cycle of events is also presented. The later study helps us to understand the hydrodynamics of slurry bubble columns and classify a system with small particles as a pseudo two phase bubble column and a system with large particles as a three-phase system in which frequent interaction between the bubbles and particles are felt.

Samenvatting

Slurrie-bellenkolommen (SBK) worden in de industrie veel toegepast om reacties uit te voeren waarbij een gasfase, een vloeistoffase en een vaste gedispergeerde fase betrokken zijn. Voorbeelden zijn de productie van algen, afvalwaterzuivering en de Fischer-Tropsch-synthese. De gasfase wordt door middel van een verdeler via de bodem van de kolom in de vloeistof met vaste, gedispergeerde deeltjes gebracht. De vaste deeltjes zijn meestal katalysatordeeltjes die in de vloeistof zijn gesuspendeerd, in tegenstelling tot systemen waarbij de vaste fase niet mobiel is, zoals in een gepakt bed. De eenvoudige constructie en het opereren bij nagenoeg isotherme procesomstandigheden maken driefasen-reactoren aantrekkelijk voor de chemische industrie, in het bijzonder voor processen waarbij exotherme reacties optreden. Echter, het scheiden van de disperse vaste fase, het opschalen en de terugmenging zijn nadelen van deze meerfasen systemen. Het structureren van de stroming is een aantrekkelijke manier om de nadelen van de meerfasen-reactoren aan te pakken.

Het werk dat in dit proefschrift wordt beschreven is gericht op procesintensivering van SBK door middel van het structureren van de stroming, en op het effect van deeltjes op de dynamica van gasbellen in deze driefasen systemen. Verschillende benaderingen zijn mogelijk om de stroming te structureren in een SBK, bijvoorbeeld door op verschillende hoogtes poreuze platen aan te brengen (het zogenaamde “staging”) of door middel van vibratie van de SBK. Minder aandacht is besteed aan goed gedefinieerde gas injectiesystemen. Dit onderzoek richt zich op het manipuleren van de gasfase om meer structuur aan te brengen in het stromingsgedrag in de SBK. Deze studie laat, zowel theoretisch als experimenteel, zien dat het aanbrengen van een structuur de gasverblijftijd en de omzettingsgraad in SBK kan verhogen. Experimenten laten zien dat hoewel terugmenging tot een zeker niveau is gewenst om de deeltjes in suspensie te houden, het clustering en coalescentie van bellen veroorzaakt. De grotere bellen stijgen sneller dan kleine gesoleerde bellen. Het gevolg van de kortere verblijftijd van de gasbellen zijn de lagere omzetting en productiviteit van de reactor. Een uniforme distributie van gasbellen, regelmatig in tijd en plaats, kan leiden tot de formatie van kleine bellen, minder

wervels en verlenging van het homogene stromingsregime tot hogere superficile gasnelheden dan bij traditionele gasinjectiesystemen.
Wij hebben het effect van structurering en het verminderen van de graad van menging bestudeerd in een industrile SBK door middel van simulaties. De Fischer-Tropsch-synthese is gekozen als een van de meest belangrijke voorbeelden van de toepassing van de SBK. De resultaten van de simulaties laten zien dat door een reductie van 75% van de axiale dispersiecoefficient, de synthesegas omzetting en de vorming van de C_{5+} koolstofmoleculen toenemen met 20%.
Om de stroming te structureren, het reduceren van wervels en het toenemen van kleine bellen in een SBK, is een goed gestructureerd gasinjectiesysteem bestaande uit verschillende naalden gebruikt. De experimenten zijn uitgevoerd in zowel een 2D als een 3D kolom beide voorzien van een naaldinjectiesysteem als gasinlaat (zie Figuur 1; Zie de figuren in de Engelse samenvatting).
Deze gasinjectiesystemen kunnen zowel een uniforme als een niet-uniforme gasbel distributie creren. Wij beschouwen de situaties waarbij luchtbellen met dezelfde grootte en snelheid uniform worden genjecteerd over de kolomdoorsnede. Water is gebruikt als vloeistoffase en zeer kleine glasbolletjes als de vaste deeltjesfase. De druk van de gasinlaat is 2 bar en de temperatuur is gelijk aan de omgevingstemperatuur in alle experimenten verricht met de SBK. Figuur 2 laat de formatie van een luchtbel aan het uiteinde van een naald zien.
De volumefractie gas in de dwarsdoorsnede van de kolommen is gemeten met een 1-punts optische sonde en de dynamica van bellen met een 4-punts optische sonde die naar beneden is gericht. Door gebruik te maken van deze optische sondes zijn we in staat om metingen te verrichten gedurende een langere tijd. De resultaten laten zien dat, als we een gestructureerd gas injectiesysteem gebruiken, we het homogene stromingsregime kunnen verlengen en dat we meer kleinere bellen hebben in het heterogene stromingsregime. In aanvulling hierop, tonen visuele waarnemingen aan dat de intensiteit van en het aantal wervels in de vloeistoffase zijn afgenomen.
Toevoeging van deeltjes verandert de hydrodynamische karakteristieken van een slurriebellensysteem. De experimenten laten zien, dat bij een toename van de volumefractie van de vaste deeltjes, de belsnelheid toeneemt met 100% maar de belgrootte nagenoeg constant blijft. Om een beter inzicht te krijgen in het effect van deeltjes op het stromingsgedrag van bellen hebben we gebruik gemaakt van een dichtheidsbepaling met rntgenstraling, en een hoge snelheid camera gecombineerd met de 4-punts optische sonde om in te zoomen op de bewe ging van 1 stijgende bel in een vloeistof-vaste stof suspensie. Om de deeltjes in suspensie te houden, en slipvrij ten opzichte van de vloeistoffase te laten zweven, hebben de vloeistof (een water-glycerol mengsel) en de deeltjes dezelfde dichtheid. We hebben gebruik gemaakt van van polystyreen deeltjes van verschillende diameters. De resultaten laten zien dat de stijgende bellen niet botsen met deeltjes als ze

heel klein zijn. De nieuwheid van onze studie is dat in het geval van grote deeltjes, waar de stijgende bel botst met deeltjes (zie Figuur 3), tijdens elke botsing de bel deformeert en snelheid vermindert, bel en deeltje van elkaar scheiden. Vervolgens versnelt de bel weer en botst met het volgende deeltje.

Een eenvoudig model voor de gemiddelde belstijgsnelheid dat de essentie van dit herhalende gedrag beschrijft, wordt gepresenteerd. Deze laatgenoemde studie helpt ons om het hydrodynamisch gedrag van SBK te begrijpen en een systeem met kleine deeltjes te classificeren als een pseudo-twee-fasen-bellenkolom en een systeem met grote deeltjes als een drie-fasen-systeem waarin regelmatig interactie tussen bellen en deeltjes plaatsvinden.

Contents

Symbols

a	Gas-liquid specific area for bubbles	m^2/m^3
d_b	Bubble diameter	m
d_s	Solid diameter	m
D_T	Column diameter	m
E_L	Liquid axial dispersion coefficient	m^2/s
I	Intensity of the beam	cd
I_0	Original intensity of the beam	cd
K_L	Volumetric mass transfer coefficient	$1/s$
r	Radial position	m
R	Column Radius	m
St	Stokes number ($St = \tau_p/\tau_b$)	$-$
t_f	Time of the flight of a bubble	s
U_{sg}	Superficial gas velocity	m/s
v_b	Bubble velocity	m/s
x	Distance from the beam source	m
μ	Attenuation coefficient	$-$
μ_L	Viscosity of the liquid	$Pa.s$
ρ_L	Density of the liquid	kg/m^3
ρ_p	Density of the particles	kg/m^3
τ_b	Characteristic time of a bubble	s
τ_p	Stokes relaxation time of a bubble	s

Chapter 1

Introduction

Slurry bubble columns (SBCs) are an example of multi-phase flow systems in which three phases, i.e. gas, liquid and solids are present (see Fig. 1.1). The gas is dispersed in the bottom region [1, 2] of the column from a gas sparger into a pool of liquid and solids mixture [3]. The solids are normally fine catalyst particles which are suspended in the liquid, in contrast to systems with immobilized solid phase such as fixed bed reactors. SBCs are used in numerous fields such as biotechnology [4, 5], water treatment [6] and oil and gas [7–11]. Depending on the application, they are operated in a continuous or semi-batch manner regarding the slurry phase. These three-phase reactors have complicated hydrodynamics. Therefore, the hydrodynamical characteristics of them have been studied for a long time [12–18]. The design, scale-up [19–22] and process intensification [23] of a SBC requires enough information about the hydrodynamical aspects of it. Flow regimes basically characterize the hydrodynamics of the SBC. The shift from one flow regime to another one mainly depends on the superficial gas velocity, U_{sg}, which affects the flow pattern and the dynamics of the gas bubbles. The geometry of the column and the operational conditions e.g. the pressure and the solids loading can also affect the flow regimes and the motion of the bubbles in the system. The flow pattern of the column as well as the dynamics of the bubble represents the absence or presence of the vortical structures in the SBC which is tightly connected to the residence time of the reactant gas bubbles in the reactor.

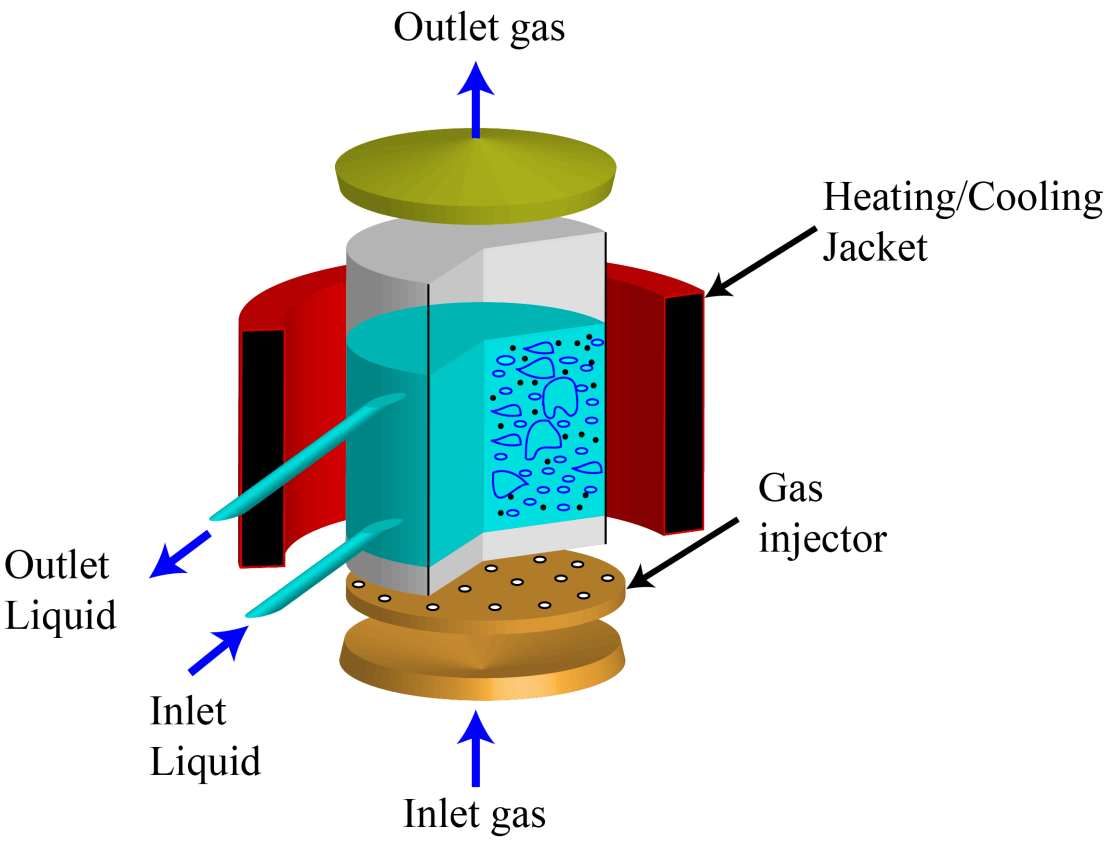

FIGURE 1.1: Schematic representation of a three-phase slurry bubble column.

1.1 Hydrodynamics

1.1.1 Flow Regime

Two main flow regimes are observed in a SBC: homogeneous (bubbly flow) and heterogeneous which depend on the physical properties of the liquid, the solids and the superficial gas velocity. The homogeneous regime exists at low superficial gas velocities and changes to heterogeneous regimes with an increase in the superficial gas velocity. In the homogeneous regime the gas velocity is usually less than 0.05 m/s. Under this condition, the gas bubbles do not affect the overall liquid motion and almost no liquid mixing is observed. As the gas velocity and the gas fraction are increased, the uniform flow looses its stability and the flow regime changes from homogeneous to heterogeneous. Then the instability quickly develops and there is a strong interaction among gas bubbles and both coalescence and break up of bubbles are observed. This is the "churn-turbulent" regime as a part of heterogeneous flow [24–26], where the larger gas bubbles move in a plug flow manner, creating liquid recirculation and thus back mixing (see Fig. 1.2). The smaller gas bubbles, on the other hand are partially entrained within the liquid recirculation [27] .

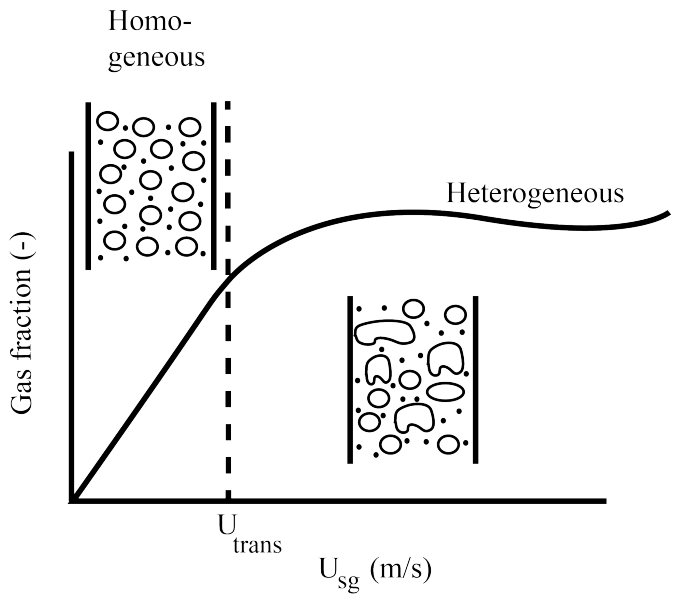

FIGURE 1.2: Flow regime diagram in a SBC.

1.1.2 Liquid flow pattern

Generally, the gas phase in SBCs is not distributed uniformly over the cross section of the column: there is typically a larger gas fraction in the central part of the column than close to the wall. Consequently, an internal circulation is induced with liquid flowing upwards in the center and downwards close to the wall [28].

Yang et al. [29] studied the flow pattern in bubble columns and reported that in the inner region around the column axis a so-called bubble-street is formed, with liquid flowing upward with maximum velocity near the column axis, whereas in the region near the reactor wall the liquid flows downwards. Between these two regions there is the shear zone, where the flow direction changes and the averaged velocity of the liquid becomes zero. The radial position of this inversion of flow depends on the properties of the gas-liquid system and the operating conditions, and it can be used to characterize liquid velocity profiles. Yang et al. [29] found that the mean value for the inversion point in liquid flow in a bubble column is $r/R = 0.70 - 0.73$ for low viscosity fluids. In liquids of high viscosity, the inversion point is nearer to the central axis of the column; the shape of the liquid velocity profile in these liquids is different too. Mudde et al. [26] have shown that by applying a very even gas supply obtained by a special needle sparger, the inversion point could be shifted to $r/R > 0.9$, which represents a very strong homogeneity .

1.1.3 Bubble dynamics

In the design of SBCs, the bubble size, shape and velocity distribution are important parameters. The other hydrodynamic parameters such as liquid velocity as well as the operational conditions may affect the bubble dynamics. To study the bubble dynamics, different techniques have been used such as high speed camera, optical probes and pressure sensors. Previous studies show that the bubble velocity and size depend on the gas injection system design, physical properties of liquid and solids, superficial gas velocity and solids volume fraction in the gas-liquid-solid system.
It has been shown that at low superficial gas velocities the bubbles are small and uniform [30]. With an increase in the superficial gas velocities and consequently the gas fraction in the system the flow regime changes to heterogeneous flow regime and the bubble velocity increases. A further increase causes the uniform flow to loose its stability [26]. When the superficial gas velocity is high enough the interaction between the bubbles increases and coalescence and break up of the bubbles widens the size distribution of the bubbles. The investigation of the effect of solids concentration on the bubble dynamics shows that an increase in the solids volume fraction and liquid viscosity increases the average bubble size.

1.2 Why structuring?

SBC have a number of important advantages: the simplicity of the construction; the absence of moving parts; low construction and operation costs; working near isothermal conditions; limited pressure drop; adaptability to different processes. However, they also have some serious drawbacks: a considerable amount of backmixing; the pressure drop is higher than in trickle beds; their scale-up is complicated; the separation of solids from the slurry is a challenge. Structuring the SBCs is a way to tackle the disadvantages of these multi-phase system. Several approaches have been used for process intensification by means of structuring these systems.
An important aim of looking for structuring of the flow in SBCs is to decrease the liquid axial dispersion. This will decrease the deviation from plug flow, and will increase the conversion and selectivity. Following, we give a brief literature overview of the various approaches that have been investigated to achieve this goal.
Ellenberger and Krishna [23, 31] studied vibrated bubble columns with a 12-capillary gas inlet device and showed that the application of low-frequency vibrations, in the 40-120 Hz range, to the liquid phase of an air-water bubble column causes the formation of smaller bubbles. They have shown that the application of vibration to the liquid phase

helps to overcome the surface tension forces and therefore break-up of bubbles will happen. Vibrations delay the transition to the heterogeneous flow regime and lead to a more uniform bubble size distribution and radial spreading of the bubbles. Another effect of the vibration is increasing the gas fraction. Ellenberger and Krishna [23, 31] show that the higher the vibration frequency, the higher the gas fraction, and that the higher the vibration amplitude, the higher the gas fraction. They also reported the enhancement in k_La by a factor of two or more. Their results suggest that the k_La improvement is a consequence of both increase in interfacial area and a higher value of k_L. The physical reason for higher k_L is that the gas bubbles and liquid oscillate at different velocities as a result of the added mass force [32], which leads to an increase in surface renewal.
Knopf and co-workers [33] also subjected the liquid phase of a batch bubble column to low frequencies (10-30 Hz) and measured the gas fraction, mass transfer and bubble size distribution at both low and jetting gas rates. Their results showed that at low gas flow rates (up to 0.083 cm/s), liquid and gas phases inside the injector undergo expulsion and that suck-back of liquid into the injector causes bubble breakage inside the injector. For higher superficial gas velocities, the large momentum of the gas which flowed through the injector could overcome the expulsion and suck-back and larger-sized bubbles formed near the injector. As bubbles moved through the column, the turbulence or shear forces induced started to break the bubbles up and smaller sized bubbles were formed. When the rate of bubble breakage and coalescence became equal, the bubble size distribution reached a constant shape. Similarly to Ellenberger and Krishna [23], Knopf and co-workers [33] reported that application of vibrations delays the transition from homogeneous to heterogeneous flow. Although the results at lab-scale are promising, applying vibration to large-scale reactors will probably yield serious mechanical problems.
There are other strategies that have been reported in literature to structure the flow and thereby decrease the back mixing. The impact of structured packings on mass transfer in bubble columns was investigated by Lakota et al. [34]. They measured the volumetric mass transfer coefficient in a system of tap water and oxygen and their results indicate that using a polyethylene structured packing (Sulzer SMV 16) reduced the axial dispersion coefficient in the liquid, E_L, by about 50% at low gas velocity but only 20% at high gas velocity. They showed that E_L is affected by both liquid and gas superficial velocity in a packed system, whereas in an unpacked system only the superficial gas velocity affects E_L [35, 36].
Urseanu et al. [37] measured the gas fraction and axial dispersion coefficient in structured bubble columns which consist of two parts of a structured packed section containing KATAPAK-S elements in the lower part and an unstructured bubble column section in the upper part. They showed that the presence of structures decreases the backmixing of the liquid phase, and that the superficial gas velocity does not have a significant effect on the axial dispersion in the structured part.

Maretto and Krishna [11] modeled and optimized a multi-stage bubble column slurry reactor for FischerTropsch synthesis. They divided the column into four stages by introducing sieve plates as baffles, approaching plug flow conditions instead of well-mixed. As a consequence, higher syngas conversion and higher productivity were achieved.
Dreher and Krishna [38] applied one or two partition plates in their bubble columns with the aim of reduction of liquid backmixing in bubble columns. They made a comparison with previous work [39–41]. Experimental studies on backmixing in the liquid phase have shown an increasing axial dispersion coefficient with increasing column diameter, D_T, in two-phase bubble columns without partitions.
In conclusion we can say that none of the previous studies have studied the structuring of the flow by manipulating the gas phase in a *slurry* bubble column. Moreover, the presence of solids in the column affect the hydrodynamics of the system a lot and makes it more complicated. Consequences of adding solids particles to a bubble column are: changes in the flow regime, appearance of vortical structures and variations in the bubble dynamics. Since there is a lack of fundamental understanding of the effect of particles on the hydrodynamical parameters of the SBC, in addition to the research on structuring of the slurry systems, the influence of adding solids particles to the bubble column needs to be studied.

1.3 Research objective

The research on structuring the SBCs has three main levels: (1) the process intensification by structuring the SBCs to get better conversion and selectivity under similar operational conditions(2) finding the desired modes of operation that cannot be achieved with the current steady-state operation (see Fig. 1.3) and the idea is to introduce dynamic structuring in SBCs. (3) which kind of structuring should be used in a SBC?
Previous studies show that several approaches are possible to impose structure on the hydrodynamics of the bubble columns or the SBCs. The question posed here is: *How can we structure the flow by manipulating the gas phase injection?* The effect of the sparger design on the hydrodynamics of a bubble column has been studied in various papers (see e.g. Kulkarni et al. [42], Herbrard et al. [43] and Thorat [44]). Harteveld et al. [26, 45] studied a needle sparger, leading to bubble distribution with a very homogeneous nature, regular both in time and space. Using this sparger, they were able to extend the more regular structure of the homogeneous regime in bubble columns to higher superficial gas velocities than are attainable for regular spargers. In this work, we demonstrate that this is also feasible for *slurry* bubble columns. Our hypothesis is that if we inject the gas to the entire bottom of the column in a very even way, the transition

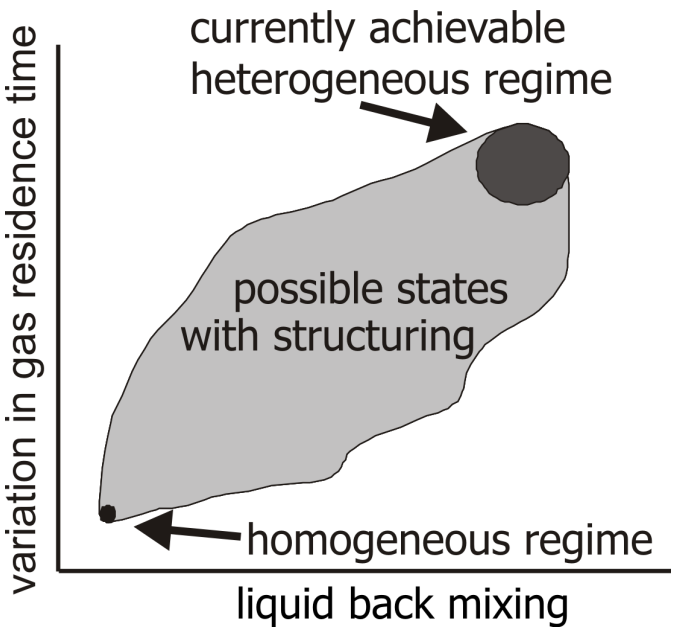

FIGURE 1.3: Graphical representation of extended operation modes.

from homogeneous to heterogeneous flow regime take place at a higher gas velocity and a higher gas fraction.

The second question we would like to answer is: *What is the underlying mechanism of bubble-particle interaction when a single bubble rises in a neutrally buoyant system?* The motivation for this question is under which conditions the mixture of solids and liquid can be considered as a pseudo liquid or when real collisions of the bubble with the particles are felt. This is important from a fundamental point of view and for practical applications in a SBC. We consider the ratio between the Stokes relaxation time of the particles and the characteristic time of the rising bubble: $St = \tau_p/\tau_b$ where $\tau_p = \rho_p d_s^2/18\mu_L$ and $\tau_b = d_b/v_b$ as an important parameter and show that this ratio is the relevant dimensionless number to understand the bubble dynamics. The hypothesis is that at low Stokes number ($St \ll 1$) once the particles are neutrally buoyant, the bubbles behave as in a pure liquid, i.e. the bubbles react to the hydrodynamical drag as if the particles are absent, but the liquid viscosity has increased. At high St number the bubbles collide with the particles, i.e. a direct momentum and energy exchange between the bubble and the particles takes place. The different response to the microscopic structure of the liquid-solids mixture gives an important clue to the behavior of bubbles, liquid and solids.

1.4 Outline of the thesis

This thesis consists of an introduction and overview and four, related papers published in or submitted to international journals. Chapter 2 describes the experimental systems used in our research and briefly describes the involved measurement techniques to obtain the relevant hydrodynamical properties in our study. Chapter 3 presents the conclusions of the work and the outlook.

A brief summary of the published papers is given bellow:

Paper I presents the results of a model study on Fischer-Tropsch synthesis in two different structured reactors. The influence of the structured flow on the performance, conversion and production of C_{5+} is discussed as well as the one-dimensional model in a SBC and a fixed bed reactor.

Paper II discusses different hydrodynamic parameters in SBCs and reviews different approaches for structuring theses reactors. The effect of the reduction in liquid axial dispersion coefficient on the conversion of a SBC is discussed. The main focus of this paper is on dispersing the gas phase via a needle sparger to the slurry system in a very even way.

Paper III deals with the hydrodynamical parameters in a structured SBC. The measurement of the gas fraction and bubble dynamics with the four-point optical probe is extensively described. Fitting our experimental data to the Richardson and Zaki and Garnier models shows that we cannot use the model coefficients they report in their papers. However, fitting our data results in realistic values for the terminal bubble velocity in a swarm.

Paper IV reports a fundamental study on the dynamics of a single rising bubble in a liquid-solids mixture while the liquid is neutrally buoyant to the density of the particles. This paper illustrates how we can classify slurry systems based on the physical properties of the particles and bubble dynamics.

Chapter 2

Experimental

2.1 Experimental systems

To answer the two main research questions of this thesis we needed two different types of experimental set-ups. To study the process intensification by means of structuring the gas phase we needed a macro-scale equipment. To study the influence of solids particles on the dynamics of a single rising bubble in a neutrally buoyant system we used a micro-scale set-up.

2.1.1 Macro-scale

The experiments related to the process intensification were carried out in 2D (width $\times$ depth $\times$ height =240 $\times$ 40 $\times$ 1000 mm) and 3D (ID =150 mm and H=2000 mm) set-ups equipped with a special gas injection systems consisted of a needle sparger. Using such a gas injection system the gas bubbles were homogeneously distributed over the entire bottom of the column in a very even way. The relative high pressure drop over the needles resulted in an effective decoupling of the gas supply system and the bubbles were formed at the outlet of the needle. This resulted in the generation of mono-sized bubbles and a very uniform bubble size distribution in the entire bottom region of the column. The other advantage of such an injection system was to have control on each of the individual needles (see Fig. 2.1). The needles with an ID of 0.8 mm and height of 200 mm were placed in a rectangular pattern with a pitch of 6 mm and the upper tip was located 5 mm above the plate. The gas injection system of the 2D column consisted of 95 needle and the cylindrical 3D column with 559 needles [45].

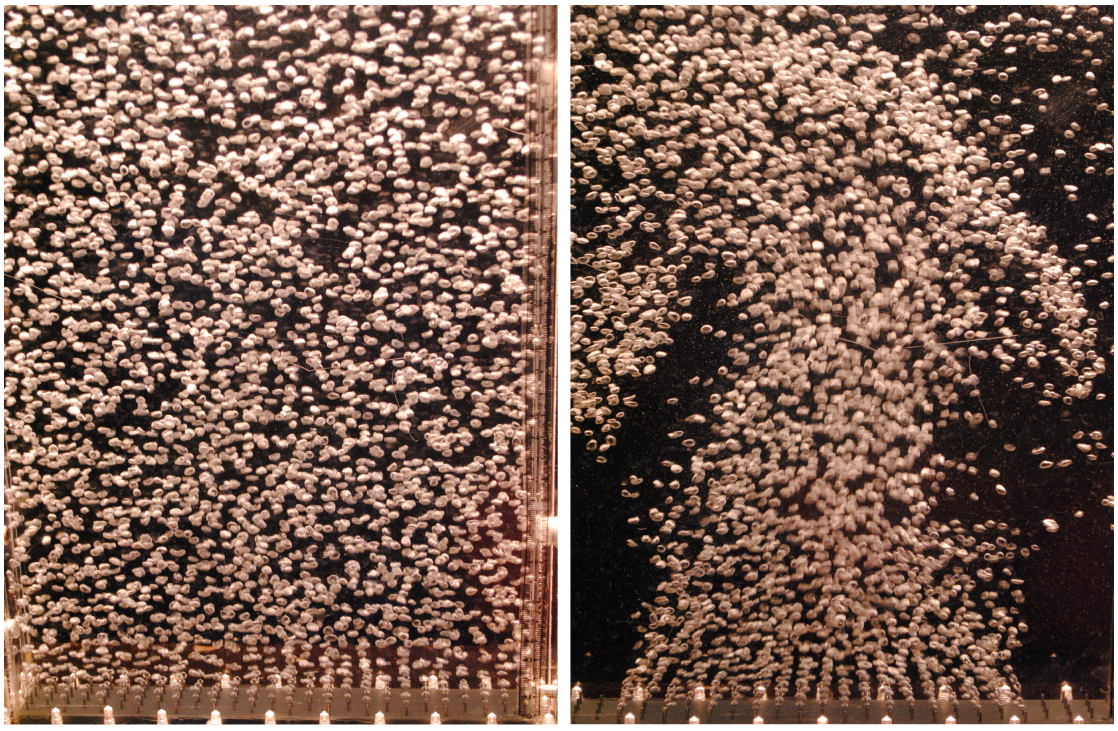

(a) (b)

FIGURE 2.1: Applying a needle sparger in a 2D column with a possibility of full control on the gas flow: (a) Keeping all the needles open causes in uniform gas distribution over the entire bottom of the column (B) Partially used needles leads to non-uniform gas distribution.

In our study we have used water as the liquid phase, air as the gas phase and glass beads with a density of 2500 kg/m^3 as solid phase. The range of superficial gas velocities that has been applied is given in Table 2.1. This table also shows the size and the volume fractions of the glass beads that have been used.

TABLE 2.1: Dimensions and operating conditions of macro-scale experiments.

Parameters	2D column	3D column
Range of superficial gas velocity, U_{sg} (m/s)	0-0.1	0-0.106
Solids mean size, d_s (μm)	108 $\pm$ 13	78 $\pm$ 12
Range of solids volume fraction, C_s (%)	0-10	0-20

2.1.2 Micro-scale

The set-up used to zoom in on a single rising bubble was a rectangular column with width $\times$ depth $\times$ height = 50 $\times$ 50 $\times$ 200 mm. One needle with an ID of 0.8 mm and length of 200 mm was placed in the bottom centre of the set-up. A heating jacket

connected to a thermostatic bath was used to control the temperature. A mass flow controller adjusted the inlet gas to the column to inject the bubbles at U_{sg} of 15 mm/s one after each other into the liquid and solids mixture.

TABLE 2.2: Dimensions and operating conditions of micro-scale experiments.

Parameters	value
Superficial gas velocity, U_{sg} (mm/s)	15
Solids mean size, d_s (μm)	78, 587, 2.0×10^3 and 4.0×10^3
Range of solids volume fraction, C_s (%)	0-20

The liquid phase was a mixture of water and glycerol and the fraction of glycerol was tuned such that the density of the liquid was matched to the density of the polystyrene particles. The reason of making the liquid phase neutrally buoyant to the particles was to keep the particles suspended and slip free relative to the liquid phase. Four different sizes of Polystyrene particles were used in this research: d_s=78 μm, 587 μm and 2 mm and 4 mm (see table 2.2). The liquid mixture density was 1054 kg/m^3, slightly varying with the different particles used.

2.2 Measurement techniques

Different experimental techniques have been used to study different hydrodynamic parameters of a slurry bubble column. The opaque character of a gas-liquid-solids system makes the measurements and especially the visualization troublesome. On the other hand, the presence of solids particles might damage the intrusive fragile techniques such as optical probes. In this research we used a high speed camera, a four-point optical probe and X-ray densitometry. These techniques are discussed in more detail in the next section.

2.2.1 High speed camera

An Olympus high speed camera (CMOS 800 $\times$ 600 sensor) was used for visualization and measurement of the size and rise velocity of single bubbles. The high-speed camera measurements (made at 1000 fps) were used to validate the four-point optical probe and X-ray densitometry. The displacement of the centre of gravity in two consecutive frames was first calculated in pixels and (using a ruler) subsequently converted to mm, from which the bubble velocity was computed. Given the opaque nature of our suspensions

at appreciable solids loading levels, the high speed camera could be used to make measurements at no or ultra-low ($\sim 0.03\%$) particle loading levels only.

2.2.2 Optical probe

Both single and four-point optical probes were used in this research to measure the local gas fraction, bubble velocity and chord length. The single probe had sufficient accuracy to measure the local gas fraction in a slurry bubble column while the four-point probe was used to measure the bubble dynamics. Several studies have been performed on the bubble dynamics in a two-phase bubble column with optical probes [46, 47] while Wu et al. [48] have used it also in a slurry system. The optical probe works on the principle of light reflection between the gas, liquid and the probe material. The probe can either be made of plastic or glass. The glass probes are very fragile. Therefore, in our study we chose to use the plastic probes.

A more detailed discussion on this topic is given in paper II and III.

2.2.3 X-ray densitometry

The opaque character of the gas-liquid-solids systems made observations with the camera impossible. Moreover, experiments with a four-point optical probe on a single bubble surrounded by solids particles were confronted with a lot of challenges such as the deviation of bubbles from a vertical motion. Since the solids were to some extent transparent to X-rays or γ- radiation, these non-intrusive techniques could be used for the measurements in the gas-liquid-solid experiments [49]. The X-ray facility was in our research used to measure the velocity of a single bubble in a solid-liquid mixture. The time of flight of the bubbles from one detector plane to the other one was measured while the distance between the two horizontal parallel planes was known. The effect of the solids size and the volume fraction on the bubble velocity have been studied with this method.

In Appendix A, a more detailed description of this technique can be found.

Chapter 3

Conclusions and outlook

3.1 Conclusions

The research presented in this thesis focused on both process intensification in slurry bubble columns by structuring the flow, specifically by manipulating the gas phase injection and on the influence of the particles on the hydrodynamical parameters of the slurry systems. Typical challenges in a slurry reactor are reducing backmixing and optimizing solids separation. Structuring the flow has been considered as a way to tackle the disadvantages of the multi-phase reactors and to introduce extra degrees of freedom to optimize the design objectives independently. The advantage of a structured reactor is that it may be designed in full detail up to the local surroundings of the catalyst, allowing ultimate precision. Such a rational design can strongly enhance the productivity of three-phase reactors.

In this research we targeted on controlling the backmixing in slurry bubble columns. Backmixing occurs at high superficial gas velocities and therefore the heterogeneous flow regime. Many industrial columns are operated at high gas velocities to obtain a sufficiently high throughput. At high gas velocities lots of eddies and vortices appear in the reactor. The degree of mixing cannot be controlled; this is one of the disadvantages of working in the heterogeneous flow regime. The high level of liquid backmixing, increases the number of interactions between the bubbles, but also changes the velocity of the bubbles and lifts them. The high interaction between the bubbles causes coalescence and breakup of the bubbles and a wide range of bubble sizes. The larger the bubbles the faster they rise in the column. The low residence time of the bubbles may to some extent govern the high mass transfer of the large bubbles and reduces the conversion and productivity of the slurry bubble columns. We showed in paper (I) by simulations that reducing the level of liquid backmixing, improved the performance of the slurry bubble

column. We used the Fischer-Tropsch Synthesis as a working example for this purpose. Our experimental work revealed that a considerable number of small bubbles in a slurry system can be achieved using a dynamic structuring.

The modelling results showed how reducing the liquid axial dispersion in a slurry bubble column and improving the heat transfer and lowering the diffusion length in a fixed bed improves the productivity of a reactor. Moreover, we illustrated, what gains can be expected when these bottlenecks are relieved by structuring. The results demonstrated that the potential for increasing the productivity per reactor volume for both reactor types is tens of percentages.

To impose a structure on the hydrodynamics in a bubble column or slurry bubble column, several approaches are possible. The focus was on structuring by manipulating the gas phase. In this case, two approaches were possible: temporal manipulation and spatial manipulation of the gas supply to come to structured hydrodynamics. The first approach - varying the gas supply in times - could in principle be done using a feedback control. Earlier work showed that it was possible to change the chaotic motion of a single train of gas bubbles rising in a liquid into a self-stabilized periodic motion by controlling the gas supply to the injector, keeping the average gas supply constant. In practice, however, it was far from straightforward to measure the relevant properties in a bubble column or slurry bubble column and use this information for feedback control. The alternative approach was to apply "open loop control": oscillating the gas supply without a feedback mechanism. To the author's best knowledge, this had not been tried before, but other researchers have oscillated or vibrated the liquid or the whole system. In our experimental work we injected the bubbles with a very homogeneous nature, regular both in time and space via a well structured gas injection system. The idea was to impose a desired flow pattern on the system in order to obtain lower axial dispersion by structuring. Using a needle sparger for gas injection gave us the possibility to control the local flow rate and generate uniform flow without any large-scale structures over the entire column for higher superficial gas velocities. We have been able to extend the more regular structure of the homogeneous regime in slurry bubble columns to ten % higher velocities than attainable for regular spargers.

The gas fraction and the bubble size and velocity are hydrodynamical parameters of a slurry bubble column that can be measured in time experimentally in order to have direct information about the gas residence time and consequently the gas conversion. These parameters are dependent on gas velocity, solids loading, liquid viscosity and injection systems as well as operational pressure and temperature. It had been shown that at low gas velocities in a regular slurry bubble column, the gas bubbles do not affect the liquid motion and almost no liquid mixing is observed. The bubbles were small and uniform. Increasing the gas fraction increases the bubble size. A further increase results in bubble size enhancement beyond a critical size in which the uniform flow looses its

stability. At high superficial gas velocities, coalescence and breakup cause a wide range of bubble sizes. The average bubble size in the transition from homogeneous to heterogeneous increases rapidly with increasing superficial gas velocity due to coalescence. Upon further increasing the gas velocity the increase of bubble size becomes slower. An increase in the solids loading and liquid viscosity widens the bubble velocity and size distribution and the probability density functions shift to higher the bubble velocities. Our experimental study in a structured slurry bubble column in paper (II) and (III) showed that the transition from homogeneous to heterogeneous flow regime can be shifted to higher gas velocities with a needle sparger. Moreover, using an optical probe we showed that the average size of gas bubbles at high gas velocities and solids loading can be kept rather small and the change in the average bubble size is not comparable with the change in the average bubble velocity. From these observation we can conclude that the bubble velocity is changing not because coalescence is widening the bubble size but instead because the flow changes from homogeneous with almost zero liquid velocity to heterogeneous flow with vortical structures and overall liquid circulation.

To study the physics underlying the effect of particles loading on the hydrodynamical characteristics of a slurry bubble column, first, we treated the slurry as a pseudo two-phase flow and consider a simple force balance on a gas bubble rising in a liquid-solid suspension. Assuming an ellipsoidal shape and constant drag coefficient for the bubbles the relation between the bubble slip velocity and chord length would be: v_s proportional to $\sqrt{L_b}$. Our experimental data indicated that the effect of solids is more complicated: the drag coefficient is not a constant for the various cases. To study the influence of particles on the dynamics of gas bubbles in more detail and look into the underlying mechanism of bubble-particle interaction, we designed our experiments in paper (IV). We studied bubble rise in suspensions made of liquid and particles. We used spherical particles and made them neutrally buoyant to prevent direct momentum exchange of particles colliding with a bubble due to their gravitational settling. We used the high speed camera, four-point optical probe and X-ray densitometry in our study. We categorized the system in terms of the ratio between the Stokes relaxation time of the particles ($\tau_p = \rho_p d_s^2/18\mu$, with the particle density ρ_p, the solid diameter d_s, and the liquid viscosity μ) and the characteristic time of the rising bubble ($\tau_b = d_b/v_b$, with the bubble diameter d_b and the bubble velocity v_b), St=τ_p/τ_b . We experimentally showed that the St number is the most important parameter for understanding the bubble dynamics with a regime transition from the direct to indirect particle interaction around St=1. The theoretical and experimental results showed that the rising bubble does not collide with fine particles (St $\ll$ 1); increasing particle loading increases the viscosity of the suspension and decreases the bubble rise velocity. In contrast, when the particles are large (St $\gg$ 1), the rising bubble collides with particles; upon each collision, the bubble deforms and slows down, separates from the particle, re-accelerates and collides

with the next particle. The average bubble rise velocity is dictated by this repeating cycle of events.
Comparing the bubble velocity profiles in the slurry bubble column and the single bubble system showed that an increase in the solids loading enhances the bubble velocity at the macro-scale system (stronger circulation patterns) while decreases the bubble velocity at the micro-scale. The conclusion is that the effect of liquid velocity is dominant and the liquid with the upward direction of motion in the center of the column carries the bubbles along and enhances their rise velocities.

3.2 Perspectives

This thesis focused on structuring the slurry bubble columns and the hydrodynamics of slurry systems using optical probes, a high-speed camera and the X-ray densitometry as measurement techniques. However, there are still many potential topics for future work which will be briefly discussed in the following sections.

3.2.1 Gas injection and measurement techniques

The research on uniform distribution of the gas bubbles in the entire bottom section of a slurry bubble column showed the importance of structuring the flow in a multi-phase system. The high pressure drop over the needles results in an effective decoupling of the gas supply system and the bubbles formed at the outlet of the needles. This results in the uniform formation of bubbles, regular both in time and space. However, reactor maintenance in the presence of solid particles was troublesome e.g. cleaning the clogged needles specially after operating at low gas velocities. The industrial application of such a needle sparger may not be feasible. Nevertheless, the idea of a uniform gas injection system can be beneficial to make a well-structured gas sparger which can be used for process intensification in industry.
Previous work on process intensification in slurry bubble columns or bubble columns has focused on one specific structuring method e.g. staging the column or inducing vibration to the system. It may be possible to combine two or more techniques to achieve a better performance of the reactor. For instance, structured gas injection in combination with staging can be used to improve the productivity of a slurry bubble column.
The effect of the needle sparger on bubble dynamics and gas fraction in slurry systems has been monitored but the influence of the structuring on the level of liquid mixing has not been measured directly. It will be worthwhile to determine experimentally how

much the backmixing is reduced in a structured slurry bubble column in comparison to a regular one. It may be possible by measuring the liquid velocity in combination with the gas fraction and bubble dynamics measurements.

3.2.2 Fundamental research

The influence of polystyrene particles of different size and volume fraction on the dynamics of a single bubble rising in a water-glycerol mixture has been studied. The motion of a single bubble rising in a suspension of particles is a fundamental problem underlying the slurry bubble columns. The system we have investigated, is categorized in terms of the ratio between the Stokes relaxation time of the particles and the characteristic times of the rising bubble: St=τ_p/τ_b where $\tau_p = \rho_p d_s^2/18\mu$ and $\tau_b = d_b/v_b$. We conclude that at low St, the bubble will not collide with the particles and will experience the suspension as a pseudo-pure liquid. We compare the experimental results with theory. We think that the drag coefficient in a pseudo-pure-liquid system (proposed by previous studies) is underestimated and needs more work.
In this fundamental research we have isolated the hydrodynamic interaction between the bubble, particles and liquid. The hydrodynamic interaction in a macro-scale system is accompanied by gravitational settling of the particles. It will be interesting to study the effect of particles on a single rising bubble in a non-neutrally buoyant system e.g. the influence of settling particles on a rising bubble.

Appendix A

X-ray densitometry

A.1 Introduction

When dealing with suspensions having high particle loading, observation with a camera is not possible because of the opacity. Furthermore, the trajectory of the bubble departs significantly from a vertical path, especially for the large particles (2.0 and 4.0 mm) which makes optical probe placement for accurate measurements difficult. Since the particles are to some extent transparent to X-ray, non-intrusive techniques based on X-ray densitometry or γ-scans can be used for the measurements in the gas-liquid-solid experiments [49]. Previous research on the measurement of the gas fraction in a gas-liquid stirred reactor using γ-CT [50, 51] and bubble dynamics in a fluidized bed with X-ray [49, 52, 53] demonstrated the usefulness of these techniques. Kong et al. [51] reported that using a γ-CT they have been able to study the distribution of the gas fraction near the impeller region of a stirred tank at different impeller speed. Ong et al. [54] used γ-ray computed tomography (CT) technique to study the influence of gas injection design on the gas fraction profile in a bubble column.

We choose the X-ray densitometry to get local information in time and position about the velocity of a single bubble in a solid-liquid mixture. Doing the measurements with the X-ray densitometry is much faster in comparison to the rotating CT. The normal time for the rotating CT to rotate around the set-up to reconstruct the time-averaged parameters is one hour while in X-ray technique we used the needed time for the experiments is reduced to a couple of minutes. We study the effect of the solids size and concentration on the bubble velocity with this method.

This appendix provides a description of the X-ray densitometry that has been used in the bubble velocity investigation in this thesis.

A.2 Experimental

A.2.1 Set-up

A rectangular column with width × depth × height = 50 × 50 × 200 mm is used to investigate the velocity of a bubble rising in a mixture of water-glycerol and Polystyrene particles. The density of the water-glycerol mixture is neutrally buoyant to the density of the Polystyrene particles (ρ=1054 kg/m^3, slightly varying with the particle's diameter). Therefore, the particles are slip free relative to the liquid phase. The air bubbles are injected via a needle (ID= 0.8 mm) in the mixture one by one to prevent them from having any interaction with each other. Fig. A.1 represents a schematic of the set-up we used to study the velocity of a single rising bubble. The position of the capillary generating the air bubbles is 250 mm from the X-ray source.

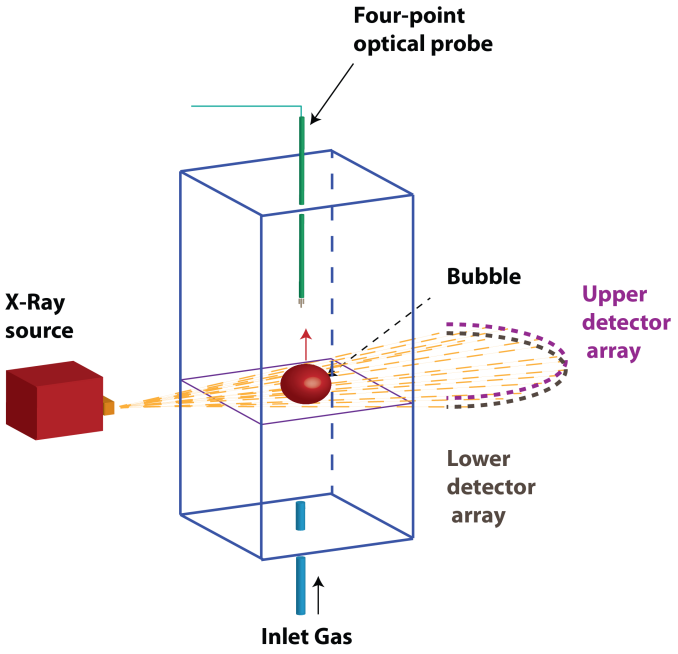

FIGURE A.1: Set-up of the measurement in the plane of the X-ray densitometer.

A.2.2 Facility

The X-ray source used in this study is manufactured by Yxlon Intentional GmbH. The maximum X-ray energy and tube current are 150 kV and 22.5 mA, respectively. The X-ray source generates a fan beam that is detected by two sets of 32 sensors placed opposite to the source. These two sets of detectors form two measuring planes 4 cm apart at the detector's position. The detectors are manufactured by Hamamatsu (type:

S 1337- 1010BR). Fig. A.2 schematically shows the arrangement of the detectors. The estimation of each measuring plane thickness at the measurement location is 1.5 mm.

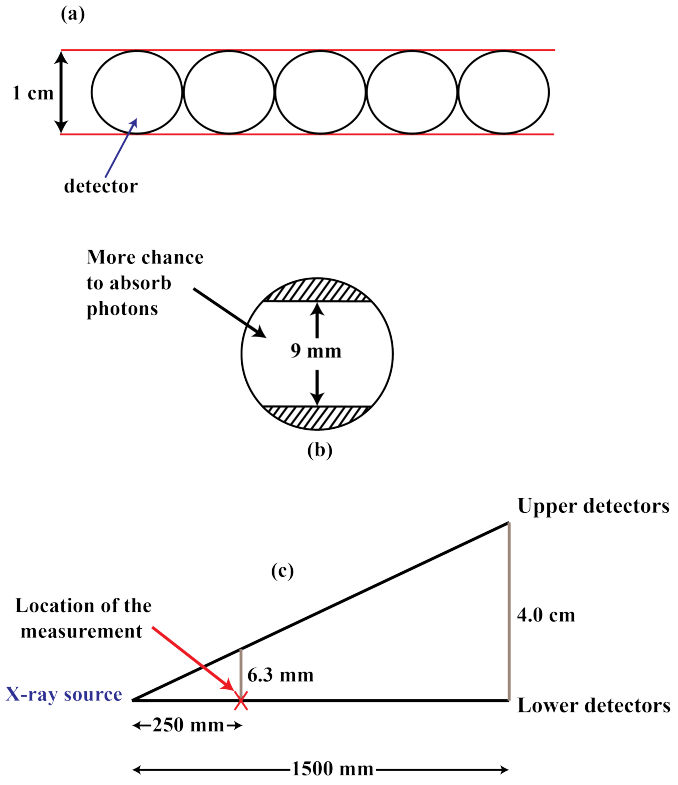

FIGURE A.2: Schematic arrangement of the detectors in one plane: (a) series of detectors in one array, the distance between two sheets is 1 cm, (b) highlights the sensitive area of one sensor and (c) the distance between the source, measurement location and detectors. Note: the cross shows the location of the measurements in our study.

A.3 Measuring principle

The Lambert-Beer law describes the attenuation of the incoming mono-chromatic radiation through a homogeneous substance by:

$$I = I_0 e^{-\mu x} \tag{A.1}$$

where I_0 is the original intensity of the beam, I is the intensity of the beam at distance x into the substance and μ is the attenuation coefficient. μ is a function of the photon energy. The transmitted radiation intensity for a beam traversing a bubble will be higher than when the beam only traverses the mixture. This mechanism is used for the measurements of the terminal velocities as it results in a peak in the detection of the

beam intensity. Fig. A.3 shows the peaks in the signals due to a passing bubble both in the lower and upper detector plane.

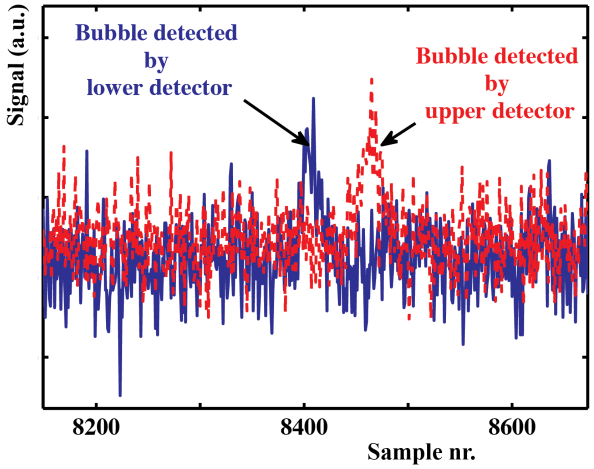

FIGURE A.3: Raw signals: a detected bubble by upper and lower detector is high lighted.

A.4 Measurements

The velocities of bubbles surrounded by 78 μm, 2.0 mm and 4.0 mm Polystyrene particles are measured using X-ray densitometry. The bubble is injected from the bottom of the column. It rises from the lower plane to the higher one. We start the experiments from a solids free liquid and continue with 5, 10, 15 and 20 volume %. The velocity estimation is based on the raw data of the attenuation of the X-ray beam after passing through the rectangular column. In each experiment, the typical duration of recording was 30 sec and each experiment is repeated four times. The raw data corresponding to the X-ray are collected from 32 detectors per plane. The next important step is to analyze the raw data.

A.5 Signal analysis

The passage of a bubble through the X-ray beams causes peaks in the intensities of the signals. We need to extract the data related to a bubble from the time-series and estimate the time of the flight of a bubble from the lower detector plane to the higher one. The rise velocity of the bubbles, v_b, can be estimated by $v_b = \Delta z/\Delta t_f$ in which Δz is the distance between the lower and upper planes and Δt_f is the time of flight of

a bubble. Fig. A.4 summarizes the procedure of the bubble velocity estimation.

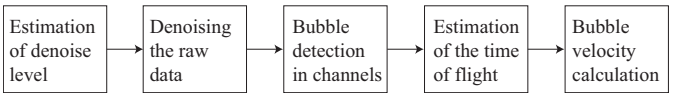

FIGURE A.4: Procedure of signal analysis for bubble velocity measurement.

As can be seen in the Fig. A.3, the signals are rather noisy which make the signal processing difficult. This is a consequence of the stochastic nature of X-ray beams. The first step in the data analysis is to de-noise the raw data. Different methods for filtering the noise in signals are possible such as Fourier transform and Wavelet. We choose the Wavelet method and apply the Matlab *wdencmp* function for this purpose.

A.5.1 Fourier transform

When a signal is defined on an infinite interval, the Fourier transform decomposes the signal in its-frequency components $\{f\}$ which can be any real or complex number [55]. If g is a continuously differentiable function with $\int_{-\infty}^{\infty} |g(t)|\, dt < \infty$, then

$$g(x) = \frac{1}{\sqrt{2\pi}} \int_{-\infty}^{\infty} \widehat{g}(f) e^{ifx} df \tag{A.2}$$

where the $\widehat{g}(f)$ (the Fourier transform of g) is given by:

$$\widehat{g}(f) = \frac{1}{\sqrt{2\pi}} \int_{-\infty}^{\infty} g(t) e^{-ift} dt \tag{A.3}$$

The idea will be illustrated in the following example. We compute the Fourier transform of the $g(t) = cos(3t)$ when $-\pi \leq t \leq \pi$ (see Fig. A.5). The results is $\widehat{g}(t) = \sqrt{2} f sin(f\pi)/(\sqrt{\pi}(9 - f^2))$. The graph of $\widehat{g}$ is given in Fig. A.5. The Fourier transform peaks at f=3 and -3. This should be expected since $g(t) = cos(3t)$ vibrates with frequency 3 on the interval $-\pi \leq t \leq \pi$.

The Fourier transform can be used to design a filter. An input signal to be processed and modified can be introduced to the filter. An application of a filter would be in

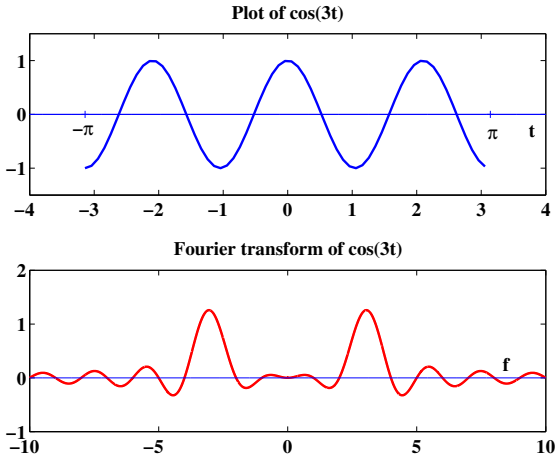

FIGURE A.5: Plot of $cos(3t)$ and the Fourier transform of $cos(3t)$ with $-\pi \leq t \leq \pi$.

de-nosing a signal.

The Fourier transform can only provide frequency information but it gives no direct information *when* an oscillation occurred (see Fig. A.6). The Fourier transform only works when the frequency is constant and not when it evolves over time [56]. The short-time Fourier transform is better. The full time interval is divided into a number of small, equal time intervals which are individually analysed using the Fourier transform. The results contain time and frequency information but the equal time intervals are not adjustable and the times when very short duration, high-frequency bursts occur are hard to detect. Wavelets can keep track of time and frequency information. They can be used to zoom in on short bursts or zoom out to detect long and slow oscillations.

A.5.2 Wavelet method

Wavelets are used for signal processing and to extract data from unknown signals. Wavelet analysis is appropriate for signals that contain features localized in both time and frequency. We use the standard definition of the Wavelet transform:

$$WT(t,a) = \frac{1}{\sqrt{2\pi}} \int s(u)\psi^*(\frac{u-t}{a})du \tag{A.4}$$

$$= \sqrt{a} \int e^{jwt}\widehat{s}(\omega)\widehat{\psi}^*(a\omega)d\omega \tag{A.5}$$

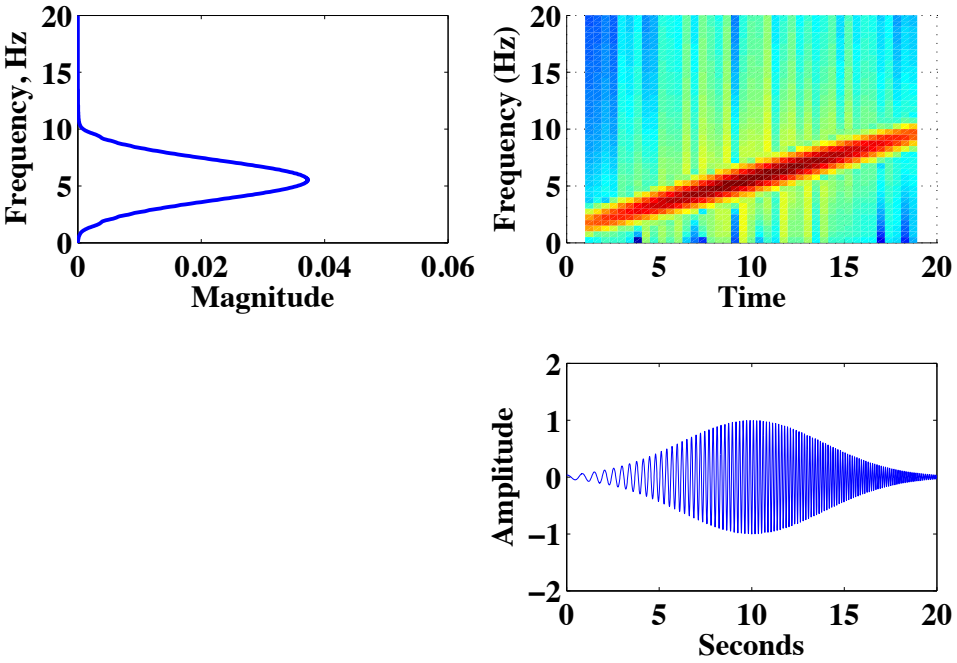

FIGURE A.6: Frequency bandwidth increases as the frequency changes.

where $s(t)$ is the signal and $\psi(t)$ is the Wavelet. The $\widehat{s}(\omega)$ and $\widehat{\psi}(\omega)$ are, respectively, the Fourier transforms:

$$\widehat{s}(\omega) = \sqrt{\frac{1}{2\pi}} \int s(t) e^{jwt} dt \tag{A.6}$$

$$\widehat{\psi}(\omega) = \sqrt{\frac{1}{2\pi}} \int \psi(t) e^{jwt} dt \tag{A.7}$$

The Wavelet theory can be used in a continuous or discrete wave. To denoise the signals we use the discrete Wavelet transforms [57].

One disadvantage of Fourier series is that it relies on sines and cosines which continue forever. This may be useful for filtering time-independent signals but not for signals with more localized features. Wavelets are designed to model these types of signals. As an example consider the graphs given in Fig. A.7: the top one is the original signal which needs to be filtered and the bottom one is the constructed signal with the Daubechies Wavelet. The wavelet analysis provides immediate access to information that can be obscured by the other time frequency methods.

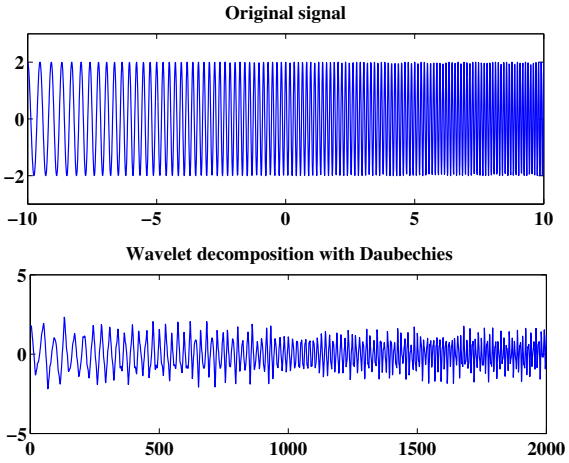

FIGURE A.7: Wavelet transform of a signal with a localized feature. The order of Daubechies is three (db3).

A.5.3 Bubble velocity estimation

The signal analysis starts with choosing a de-noising method to filter the noise from the raw data using Wavelets. The next step is to find an appropriate filtering level. As can be seen in Fig. A.8 the level of de-noising plays an important role in the accuracy of our calculations. Using a high level of filtering, the accuracy of finding the bubble peak location is low. Fig. A.8 illustrates that the high level of filtering will shift the peak from its real value shown in the original signal to a wrong one.

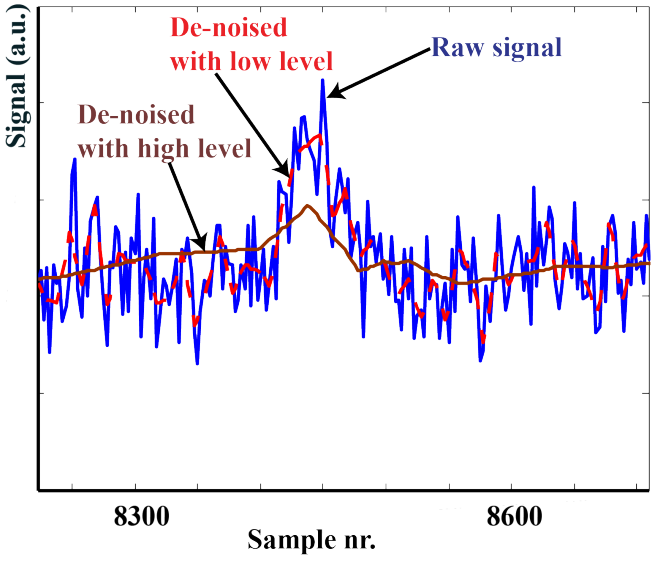

FIGURE A.8: Wavelet analysis is used to filter the noise from the signals. It is highlighted that the too high de-noise level might shift the peak from its actual position.

After choosing a proper method and level we filter the noise from the raw signals. The next step is to detect the bubble within the signals recorded by both upper and lower detectors. The peaks should be distinguished from the random fluctuations. A bubble with an equivalent diameter of 3 mm and average velocity of 0.25 m/s is expected to give a width of around 45 data points as the frequency of the measurement is 2500 Hz and the thickness of the measuring plane is 1.5 mm. Fig. A.9 represents the difference between the signals related to a bubble and a fluctuation appearing in the measurements.

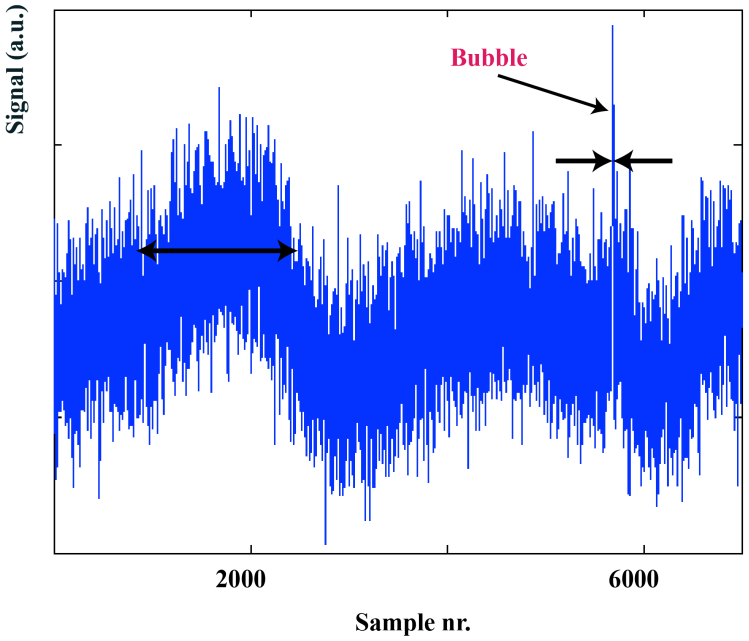

FIGURE A.9: Bubble detection: the arrow points to a narrow peak caused by a bubble and the wide peak highlights a fluctuation.

The distinguished peaks in the lower and appear detector planes are shown in Fig. A.3. The time difference between these two peaks is called the time of flight. The difference between the sample numbers, which can be seen in the figure A.3 is multiplied by 2500 Hz generating the time in second. To estimate the average bubble velocity the distance between the plane is divided by this time.

A.6 Uncertainty analysis

The uncertainty in the time-value of the peaks affects the uncertainty of the bubble velocity which is estimated via measuring the time of flight. To calculate this uncertainty, first we assume that an ideal ellipsoidal bubble is passing the upper and lower planes of detectors. The generated master curve is plotted is Fig. A.7. Assuming the noise

having a Gaussian shape, we generate random Gaussian noise with a frequency of 20 Hz around the master curve. Peak finding procedure (based on 10000 bubble) shows that we have an uncertainty of 15% in the determination of the time value of each individual peak. Measuring the velocity of a sufficient number of bubbles (N=100) there is no bias in the measurements. The average peak value will be estimated with an uncertainty of about $15\%/\sqrt{N}$ with N the number of bubbles measured. Thus for 100 bubbles, the uncertainty of the average is 1.5%. Fig. A.10 is an example of generated curves for the error analysis.

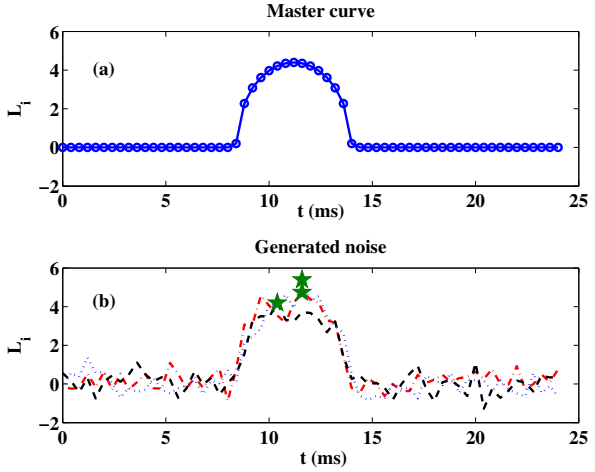

FIGURE A.10: Uncertainty in the peak value estimation: (a) Master curve and (b) three of generated noise. The stars are the peaks of three curves.

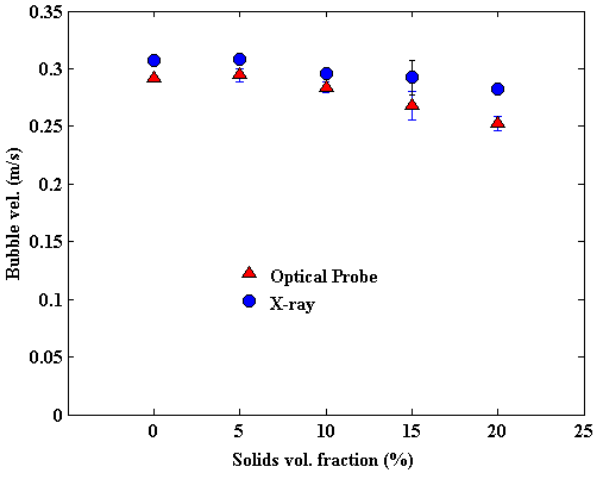

FIGURE A.11: Comparison of the bubble velocity measured by X-ray densitometry and four-point optical probe. Note that the size of the Polystyrene particles are 78 μm. Note: the error in the measurements with X-ray has been shown in one data point.

A.7 X-ray results versus Optical probes

To validate the experimental results obtained from X-ray densitometry, we compare the rising velocity of a bubble measured with the four-point optical probe in different solids volume fractions with the ones measured with the X-ray. Fig. A.11 shows the reduction in the bubble velocity with an increase in the solids volume fraction in both sets of data. Bubble rise velocities measured by X-ray densitometry and the four-point optical probe are comparable at low particle volume fractions (see A.11). The intrusive optical probe slows down the bubble, an effect that appears to be more pronounced at higher particle loading levels. Furthermore, at high solids loading, the signals of the X-ray and optical probe becomes progressively noisier as the particle loading level increases; this, in turn, leads to larger uncertainties in measurements and analysis.

Bibliography

[1] R. F. Mudde. Gravity-driven bubbly flows. *Annu. Rev. Fluid Mech.*, 37:393–423, 2005.

[2] A. Shaikh and M. H. Al-Dahhan. A review on flow regime transition in bubble columns. *Int. J. Chem. React. Eng.*, 5:art. no. R1, 2007.

[3] P. A. Ramachandran and R. V. Chaudhari. *Three-phase catalytic reactors*. Gordon and Breach Science Publishers, 1983.

[4] E. M. R. Porcel, J. L. Casas López, J. A. S. Pérez, and Y. Chisti. Lovastatin production by aspergillus terreus in a two-staged feeding operation. *J. Chem. Technol. Biotechnol.*, 83(9):1236–1243, 2008.

[5] L. Rodolfi, G. C. Zittelli, N. Bassi, G. Padovani, N. Biondi, G. Bonini, and M. R. Tredici. Microalgae for oil: Strain selection, induction of lipid synthesis and outdoor mass cultivation in a low-cost photobioreactor. *Biotechnol. Bioeng.*, 102(1):100–112, 2009.

[6] K. Pujara, S.P Kamble, and V.G Pangarkar. Photocatalytic degradation of phenol-4-sulfonic acid using an artificial UV/TiO_2 system in a slurry bubble column reactors. *Ind. Eng. Chem. Res.*, 46(12):4257–4264, 2007.

[7] N. Rados, M.H Al-Dahhan, and M.P Dudukovic. Modeling of the Fischer-Tropsch synthesis in slurry bubble column reactors. *Catal. Today*, 79-80:211–218, 2003.

[8] W. D. Deckwer, Y. Serpemen, M. Ralek, and B. Schmidt. Modeling the Fischer-Tropsch synthesis in the slurry phase. *Ind. Eng. Chem. Proc. D. D.*, 21(2):231–241, 1982.

[9] A. A. Troshko and F. Zdravistch. Cfd modeling of slurry bubble column reactors for Fisher-Tropsch synthesis. *Chem. Eng. Sci.*, 64(5):892–903, 2009.

[10] C. Maretto and R. Krishna. Modelling of a bubble column slurry reactor for Fischer-Tropsch synthesis. *Catal. Today*, 52(2-3):279 – 289, 1999.

[11] C. Maretto and R. Krishna. Design and optimisation of a multi-stage bubble column slurry reactor for Fischer-Tropsch synthesis. *Catal. Today*, 66(2-4):241–248, 2001.

[12] J. W. A. Krishna, R.and de Swart, D. E. Hennephof, J. Ellenberger, and H. C.J. Hoefsloot. Influence of increased gas density on hydrodynamics of bubble-column reactors. *AIChE J.*, 40(1):112–119, 1994.

[13] J. W. A. De Swart and R. Krishna. Influence of particles concentration on the hydrodynamics of bubble column slurry reactors. *Chem. Eng. Res. Des.*, 73(A3): 308–313, 1995.

[14] J. W. A. De Swart, R. E. Van Vliet, and R. Krishna. Size, structure and dynamics of 'large' bubbles in a two-dimensional slurry bubble column. *Chem. Eng. Sci.*, 51 (20):4619–4629, 1996.

[15] R. Krishna, J. W .A. De Swart, J. Ellenberger, G. B. Martina, and C. Maretto. Gas holdup in slurry bubble columns: Effect of column diameter and slurry concentrations. *AIChE J.*, 43(2):311–316, 1997.

[16] F. Magaud, M. Souhar, G. Wild, and N. Boisson. Experimental study of bubble column hydrodynamics. *Chem. Eng. Sci.*, 56(15):4597–4607, 2001.

[17] J.E. Julia, L. Hernandez, S. Chiva, and A. Vela. Hydrodynamic characterization of a needle sparger rectangular bubble column: Homogeneous flow, static bubble plume and oscillating bubble plume. *Chem. Eng. Sci.*, 62(22):6361–6377, 2007.

[18] G. Olivieri, M. Elena Russo, M. Simeone, A. Marzocchella, and P. Salatino. Effects of viscosity and relaxation time on the hydrodynamics of gas-liquid systems. *Chem. Eng. Sci.*, 66(14):3392–3399, 2011.

[19] R. Krishna and S. T. Sie. Design and scale-up of the fischer-tropsch bubble column slurry reactor. *Fuel Process. Technol.*, 64(1):73–105, 2000.

[20] R. Krishna. A scale-up strategy for a commercial scale bubble column slurry reactor for fischer-tropsch synthesis. *Oil Gas Sci. Technol.*, 55(4):359–393, 2000.

[21] R. Krishna, J. M. Van Baten, M. I. Urseanu, and J. Ellenberger. Design and scale up of a bubble column slurry reactor for fischer- tropsch synthesis. *Chem. Eng. Sci.*, 56(2):537–545, 2001.

[22] D. Liu, X. Hua, and D. Fang. Mathematical simulation and design of three-phase bubble column reactor for direct synthesis of dimethyl ether from syngas. *J. Nat. Gas Chem.*, 16(2):193–199, 2007.

[23] J. Ellenberger and R. Krishna. Intensification of slurry bubble columns by vibration excitement. *Can. J. Chem. Eng.*, 81(3-4):655–659, 2003.

[24] J.-W. Tzeng, R. C. Chen, and L.-S. Fan. Visualization of flow characteristics in a 2-d bubble column and three-phase fluidized bed. *AIChE J.*, 39(5):733–744, 1993.

[25] G. Q. Yang and L-S Fan. Axial liquid mixing in high-pressure bubble columns. *AIChE J.*, 49(8):1995–2008, 2003.

[26] R. F. Mudde, W. K. Harteveld, and H. E. A. van den Akker. Uniform flow in bubble columns. *Ind. Eng. Chem. Res.*, 48(1):148–158, 2009.

[27] N. Hooshyar, S. Fatemi, and M. Rahmani. Mathematical modeling of fischer-tropsch synthesis in an industrial slurry bubble column. *Int. J. Chem. React. Eng.*, 7:A23, 2009.

[28] J. S. Groen, R. G. C. Oldemam, R. F. Mudde, and H. E. A. van den Akker. Coherent structures and axial dispersion in bubble column reactors. *Chem. Eng. Sci.*, 51(10): 2511–2520, 1996.

[29] Z. Yang, U. Rustemeyer, R. Buchholz, and U. Onken. Profile of liquid flow in bubble column. *Chem. Eng. Commun.*, 49(1-3):51–67, 1986.

[30] T. Wang, J. Wang, and Y. Jin. Slurry reactors for gas-to-liquid processes: A review. *Ind. Eng. Chem. Res.*, 46(18):5824–5847, 2007.

[31] J. Ellenberger and R. Krishna. Improving mass transfer in gas-liquid dispersions by vibration excitement. *Chem. Eng. Sci.*, 57(22-23):4809 – 4815, 2002.

[32] J. De Vries, S. Luther, and D. Lohse. Induced bubble shape oscillations and their impact on the rise velocity. *Eur Phys J B*, 29(3):503–509, 2002.

[33] F. C. Knopf, J. Ma, R. G. Rice, and D. Nikitopoulos. Pulsing to improve bubble column performance: I. low gas rates. *AIChE J.*, 52(3):1103–1115, 2006.

[34] A. Lakota, M. Jazbec, and J. Levee. Impact of structured packing on bubble column mass transfer charasteristics: Part 1. backmixing in the liquid phase. *Acta Chim. Slov.*, 48(4):453–468, 2001.

[35] M. H. I. Baird and R. G. Rice. Axial dispersion in large unbaffled columns. *Chem. Eng. J.*, 9(2):171–174, 1975.

[36] Y. T. Shah, B. G. Kelkar, S. P. Godbole, and W. D. Deckwer. Design parameters estimations for bubble column reactors. *AIChE J.*, 28(3):353–379, 1982.

[37] M. I. Urseanu, J. Ellenberger, and R. Krishna. A structured catalytic bubble column reactor: Hydrodynamics and mixing studies. *Catal. Today*, 69(1-4):105–113, 2001.

[38] A. J. Dreher and R. Krishna. Liquid-phase backmixing in bubble columns, structured by introduction of partition plates. *Catal. Today*, 69(1-4):165 – 170, 2001.

[39] R. Krishna, J. M. van Baten, and M. I. Urseanu. Three-phase eulerian simulations of bubble column reactors operating in the churn-turbulent regime: A scale up strategy. *Chem. Eng. Sci.*, 55(16):3275–3286, 2000.

[40] R. Krishna, M. I. Urseanu, J. M. van Baten, and J. Ellenberger. Liquid phase dispersion in bubble columns operating in the churn-turbulent flow regime. *Chem. Eng. J.*, 78(1):43–51, 2000.

[41] R. Krishna, M. I. Urseanu, J. M. Van Baten, and J. Ellenberger. Influence of scale on the hydrodynamics of bubble columns operating in the churn-turbulent regime: Experiments vs. eulerian simulations. *Chem. Eng. Sci.*, 54(21):4903–4911, 1999.

[42] A. V. Kulkarni, S. V. Badgandi, and J. B. Joshi. Design of ring and spider type spargers for bubble column reactor: Experimental measurements and cfd simulation of flow and weeping. *Chem. Eng. Res. Des.*, 87(12):1612–1630, 2009.

[43] G. Hebrard, D. Bastoul, and M. Roustan. Influence of the gas sparger on the hydrodynamic behaviour of bubble columns. *Chem. Eng. Res. Des.*, 74(3):406–414, 1996.

[44] B. N. Thorat. Effect of sparger design and height to diameter ratio on fractional gas hold-up in bubble columns. *Chem. Eng. Res. Des.*, 76(A7):823–834, 1998.

[45] W. K. Harteveld. *Bubble columns: structures or stability?* PhD thesis, Delft university of technology, Delft, the netherlands, 2005.

[46] J. Xue, M. Al-Dahhan, M P Dudukovic, and R F Mudde. Bubble velocity, size, and interfacial area measurements in a bubble column by four-point optical probe. *AIChE J.*, 54(2):350–363, 2008.

[47] R. F. Mudde and T. Saito. Hydrodynamical similarities between bubble column and bubbly pipe flow. *J. Fluid Mech.*, 437:203–228, 2001.

[48] C. Wu, K. Suddard, and M. H. Al-Dahhan. Bubble dynamics investigation in a slurry bubble column. *AIChE J.*, 54(5):1203–1212, 2008.

[49] R. F. Mudde. Bubbles in a fluidized bed: A fast x-ray scanner. *AIChE J.*, 57(10): 2684–2690, 2011.

[50] Y.-J. Liu, W. Li, L.-C. Han, Y. Cao, H.-A. Luo, M. Al-Dahhan, and M. P. Dudukovic. γ ct measurement and cfd simulation of cross section gas holdup distribution in a gas-liquid stirred standard rushton tank. *Chem. Eng. Sci.*, 66(17): 3721–3731, 2011.

[51] L.-N. Kong, W. Li, L.-C. Han, Y.-J. Liu, H.-A. Luo, M. Al Dahhan, and M. P. Dudukovic. On the measurement of gas holdup distribution near the region of impeller in a gas-liquid stirred rushton tank by means of γ -ct. *Chem. Eng. J.*, 188: 191–198, 2012.

[52] R. F. Mudde. Double x-ray tomography of a bubbling fluidized bed. *Ind. Eng. Chem. Res.*, 49(11):5061–5065, 2010.

[53] R. F. Mudde. Time-resolved x-ray tomography of a fluidized bed. *Powder Technol.*, 199(1):55–59, 2010.

[54] B. C. Ong, P. Gupta, A. Youssef, M. Al-Dahhan, and M. P. Dudukovic. Computed tomographic investigation of the influence of gas sparger design on gas holdup distribution in a bubble column. *Ind. Eng. Chem. Res.*, 48(1):58–68, 2009.

[55] Albert Boggess and J. Narcowich Francis. *A first course in wavelets with Fourier analysis*. John Wiley and Sons, 2009.

[56] Shie Qian. *Introduction to time-frequency and wavelet transforms*. 2002.

[57] I. Mappe-Fogaing, L. Joly, G. Durry, N. Dumelie, T. Decarpenterie, J. Cousin, B. Parvitte, and V. Zeninari. Wavelet denoising for infrared laser spectroscopy and gas detection. *Appl. Spectrosc.*, 66(6):700–710, 2012.

Acknowledgements

Foremost, I would like to thank my promoter Prof. Rob Mudde and my supervisors Dr. Ruud van Ommen and Dr. Peter Hamersma for providing me with the opportunity to complete my PhD thesis at the Delft University of Technology. Rob, thank you for all your encouraging support and guidance during my career as a PhD student. I especially appreciate my many progress meetings that ended up teaching me new physics and your on-line language correction! You have taken a sincere interest in my work and have always been available to advise me, mostly about the last chapter of my thesis work. It took me a while to figure out that it is easier to come to your office between 7:30 to 8:00 am to discuss my work with you then, since finding time in your busy schedule can be a nightmare! Ruud, I am indebted to you for providing me the opportunity to be a member of your research group. I appreciate all your support during my PhD and your friendly and respectful manner. Assisting you in teaching two courses was a joyful learning experience. I would also like to specifically thank you for promptly replying to my e-mails, which made my project in many aspects go much faster. Peter, what I will always remember from you is to smile at all the challenges that will appear in any research and development project and also in my life. Thank you for your support and for the critical reading and corrections of my manuscripts and thesis, and also for your critical feedback before my first oral presentation at an international conference in Philadelphia. The single bubble study discussed in this dissertation would not have been possible without the discussion and collaboration with Prof. Sundaresan from Princeton University. I appreciate all his contributions of time and ideas. I also gratefully acknowledge Henk Nugteren, Johan Grievink, Chris Kleijn, Harry van den Akker and Peter Appel for their valuable feedback and guidance.

I also thank all the members of the Product and Process Engineering and Transport Phenomena in the Chemical Engineering Department of TU Delft, especially the chairman of the Product and Process Engineering section, Prof. Michiel Kreutzer. Michiel, you made our section very active and taught us to be ambitious and creative. Encouraging me to attend the APS-DFD conference was a big step towards finishing the last part of my work. Pouyan and Volkert, thank you for chairing all the nice Tuesday group

meetings and journal clubs, which sometimes made me bored but at the end I learnt a great deal on various technical and research issues. Mark, thank you for your support in the laboratory and also introducing the Ado den Haag to me and your reasoning of supporting Ado instead of Ajax!

I would like to thank our nice secretaries Caroline, Elly, Els, Angela, and Anita. Many thanks go to the cool former and current PPE members: David Vervloet, Renske, David Newsome, Barbara, Mahsa, Lilian, Michiel, Aris, Bhaskar, Duong, Stephanie, Amer, David Valdesueiro, Rajat, Andrea and Venky, my PhD journey would not be as pleasant without your company. I would like to thank the MSc and BSc students who I supervised during my PhD : Nicola, Sibren, Arentien, Adriana, Avinash, Nichola, Steven, Merel and Marc - supervising you was one of the most rewarding parts of my research career. I also would like to thank all the other students in Proeffabriek for all the amazing coffee breaks, BBQs, Sinterklaas, New Years, and other social events we had. I would like to express my appreciation to the technicians of Kramers laboratorium, Jaap van Ramt, Evert, and Lodi, for all their technical support and assistance during my experiments.

I now take this opportunity to thank all my primary and high school teachers. In particular, I acknowledge Mrs. Entezarian, my lovely 4th grade primary school teacher, who taught me to work hard to achieve what I want; Mr. Fani, my high school math teacher, who taught me that to always be well organized; Mr. Amirani, my physics teacher, for his enthusiastic teaching and wonderful and enjoyable classes. I am very thankful to my professors in Amrikarbir University of Technology and the University of Tehran.

I am thankful to my precious friends: Bahar, to be always with me in last eighteen years and her amazing understanding; Nasim, for all the golden moments we spent together since high school time and to listen to me whenever I needed support and friendship; and Avishan, for being an amazing friend. Many thanks go to Salimeh, Solmaz, Mona, Elham, Bahareh and Mohsen, Ali Vakili, Elaheh, and cutie pie Tara (who brought joy and happiness to our life in these past two years), Kathy, Hanieh, Rouhi and René, Stephanie, Veronica and Stefan, Goodarz, Semiramis and little Aria, Anna, Sepideh Babaie, Mahshid, Mahla, Sogol and Stephan, Seyran and Nader, Ammar, Farid, Milad, Naghmeh and Babak, Mahnoush and Mojtaba, Sepideh Tabatabaie and Hamed, Aiyleen and Pieter for all their support and friendship, which insured that I would never feel alone. I would like to thank my dear paranymphs Mojgan and Sepideh for all their help and valuable friendship inside and outside the working hours.

Lastly, I would like to thank my family and in-laws for all their love and encouragements. My dear Mom, thank you for your everlasting love and for being there when I was feeling down. You showed me how to follow my dreams and to be proud of being a woman even in a masculine society. You are my inspiration and thanks for everything. My baby brother, Navid, thanks for your love and for introducing Metallica and trance to me. Auntie Beli and uncle Ahmad, I appreciate all your support and guidance during

my study in the Netherlands. My lovely Farzad, words cannot express my overwhelming appreciation of your help, support, encouragement, love, and sympathy.
My loving Dad! You physically left us twelve days after I had started my PhD, but I know that no matter what challenges I face, you will be always with me and that has made me more confident. I think about you every moment and will be Daddy's heart (Djigar-e-baba, as you used to call me) forever.

Curriculum-vitae

Nasim Hooshyar was born on 16 of April 1981 in Shiraz, Iran. In 1999 she got her diploma in mathematics and physics from the Dr. Afshar high school. She studied petrochemical engineering in 2000 and got her BSc from Tehran polytechnic (Amikabir university of technology). She continued her MSc in university of Tehran and graduated on December 2007. In October 2008 she moved to Delft to do her PhD in the faculty of Applied Sciences in the department of chemical engineering. Her promoter was Prof. Robert Mudde and her supervisors were Dr. Ruud van Ommen and Dr. Peter Hamersma. Since November 2012 she has worked in R&D of Unilever in Vlaardingen as a research scientist.

Paper I

Intensifying the Fischer-Tropsch Synthesis by reactor structuring – A model study

Has been published in Chemical Engineering Journal.

Chemical Engineering Journal 207–208 (2012) 865–870

Contents lists available at SciVerse ScienceDirect

Chemical Engineering Journal

journal homepage: www.elsevier.com/locate/cej

Intensifying the Fischer–Tropsch Synthesis by reactor structuring – A model study

N. Hooshyar *, D. Vervloet, F. Kapteijn, P.J. Hamersma, R.F. Mudde, J.R. van Ommen

Department of Chemical Engineering, Delft University of Technology, Julianalaan 136, 2628 BL, The Netherlands

HIGHLIGHTS

- Modelling of Fischer–Tropsch Synthesis in a fixed bed and a slurry bubble column.
- Increasing the productivity in a structured slurry bubble column by 20%.
- Improving the conversion by 40% in a fixed bed by process intensification.
- Structuring can be used to reduce reactor volume rather than increasing conversion.

ARTICLE INFO

Article history:
Available online 13 August 2012

Keywords:
Slurry bubble column
Fixed bed
Fischer–Tropsch
Process intensification
Structured reactors

ABSTRACT

This paper investigates the intensification of Fischer–Tropsch Synthesis in two types of three-phase catalytic reactors: slurry bubble columns and multi-tubular fixed beds. A simple mathematical model is used to analyse the effect of structuring on the C_{5+} productivity of these two types of reactors. The results of the model show that decreasing the liquid axial dispersion coefficient with a factor 4 in a slurry bubble column considerably enhances the production of C_{5+}. On the other hand in a fixed bed reactor a similar improvement is obtained when the heat transfer coefficient is improved with a factor 2.5 and the diffusion length in catalyst particles is decreased with a factor 2. Both reactors show a potential improvement in productivity per reactor volume; 20% in the slurry bubble column and 40% in the fixed bed reactor.

1. Introduction

Intensifying the operation of slurry bubble columns and multi-tubular fixed beds can be achieved by structuring. The advantage of a structured reactor is that it may be designed in full detail up to the local surroundings of the catalyst, allowing ultimate precision [1]. Such a rational design can strongly enhance the productivity of three-phase reactors.

Typical challenges in a slurry reactor are reducing backmixing and optimizing solids separation, while in a multi-tubular fixed bed reactor these are improving temperature gradients and catalyst effectiveness. Several methods have been proposed to structure the systems with a fixed catalyst structure [1–8] and systems with a mobile catalyst [9–13]. In each of these approaches, structuring introduces extra degrees of freedom to optimize the design objectives independently [14].

In this paper we show how reducing the backmixing in a slurry bubble column (SBC) and improving the heat transfer and lowering the diffusion length in a fixed bed (FB) improves the productivity of a reactor. Moreover, we illustrate, using a simple model, what gains can be expected when these bottlenecks are relieved by structuring. We use the Fischer–Tropsch Synthesis (FTS) as a working example for this purpose. The results demonstrate that the potential for increasing the productivity per reactor volume for both reactor types is tens of %.

2. Structuring

Structuring as a way of process intensification has been proposed for different type of industrial reactors in which three phases of gas–liquid–solid are present [15,16]. Although the structuring is more common in the area of fixed catalyst reactors [4,5], it can be also applied in fluidized beds [17] and slurry bubble columns [9,18].

The backmixing of both gas phase and slurry phase in a SBC is detrimental to conversion and selectivity. By restricting the vortical structures, for examples by injecting the gas bubbles with a narrow size distribution and with approximately the same velocities [9,19], we constrict the residence time distribution, increase the average residence time and therefore, intensify the process. Fig. 1 shows a photo of a needle sparger that has been used in a SBC for process intensification. In another example of structuring a SBC, Maretto and Krishna [20] modelled and optimized a staged reactor for FTS. Their results show that using sieve plates, they can approach plug flow condition instead of well-mixed.

* Corresponding author.
E-mail address: n.hooshyar@tudelft.nl (N. Hooshyar).

1385-8947/$ - see front matter © 2012 Elsevier B.V. All rights reserved.
http://dx.doi.org/10.1016/j.cej.2012.07.105

Nomenclature

a_0	kintetic parameter (mol/s kg_{cat} bar^2)
a_{large}	gas–liquid specific area for large bubbles (m^2/m^3)
a_{small}	gas–liquid specific area for small bubbles (m^2/m^3)
a_w	cooling tube specific external surface area referred to the total reactor volume (m^2/m^3)
b_0	adsorption coefficient (1/bar)
$C_{i,g0}$	concentration of i in the gas phase at reactor inlet (mol/m^3)
$C_{i,g,small}$	concentration of i in small bubbles (mol/m^3)
$C_{i,g,large}$	concentration of i in large bubbles (mol/m^3)
$C_{i,L}$	concentration of i in liquid (mol/m^3)
C_s	solids volume fraction in gas free slurry (–)
D_T	column diameter (m)
d_p	catalyst average diameter (m)
$E_{g,large}$	axial dispersion coefficient of the large bubbles (m^2/s)
$E_{g,small}$	axial dispersion coefficient of the small bubbles (m^2/s)
E_L	axial dispersion coefficient of the liquid phase (m^2/s)
F	catalyst improvement factor (–)
H	reactor height (m)
$K_{L,i,small}$	volume mass transfer coefficient of i with small bubbles (1/s)
$K_{L,i,large}$	volume mass transfer coefficient of i with large bubbles (1/s)
m_i	Henry's coefficient (–)
P	reactor pressure (Pa)
R_i	reaction rate expression ($mol_i/kg_{cat}/s$)
S_{C5+}	C_{5+} selectivity by weight (kg kg^{-1})
STY	space time yield ($kg/kg_{cat}/h$)
STY'	hydrocarbon production per reactor volume excluding the cooling medium ($kg/m^3_{G+L+cat}/h$)
STY''	hydrocarbon production per reactor volume including the cooling medium ($kg/m^3_{reactor}/h$)
T	temperature (K)
T_c	cooling temperature (K)
U_{sg}	superficial gas velocity (m/s)
U_{ss}	superficial slurry velocity (m/s)
U_{ov}	overal heat transfer (W/m^2 K)
z	reactor coordinate (m)
α	probability factor of hydrocarbon chain growth (–)
α_{eff}	liquid/slurry to internal coil wall conversion heat transfer coefficient (W/m^2 K)
ε_{large}	gas hold-up in large bubbles (–)
ε_{small}	gas hold-up in small bubbles (–)
ε_{bed}	catalyst hold-up (–)
ε_L	liquid hold-up (–)
λ_{ax}	effective axial heat conductivity of the liquid–solid suspension (W/m K)
v_i	stoichiometric ratio of species i (–)
ρ_p	solid density (kg/m^3)

We study the effect of the liquid backmixing on the output of the SBC. We use a typical axial dispersion coefficient of the liquid phase, $E_{L,SB}$, for a non-structured system for the base case. It is obtained using the relation proposed by Deckwer et al. [21]:

$$E_{L,SB} = 0.768 U_{sg}^{0.32} D_{T,SB}^{1.34} \quad (1)$$

As can be seen in the Eq. (1) the liquid axial dispersion coefficient is dependent on the superficial gas velocity, U_{sg}, and reactor diameter, $D_{T,SB}$. In our base case with U_{sg} = 0.3 m/s and $D_{T,SB}$ = 7.5 m, we find that $E_{L,SB}$ = 7.77 m^2/s.

Cheng et al. [22] investigated the reduction of backmixing in a bubble column by interrupting the global liquid circulation and eliminating the downward flow of the liquid. They have reported that installation of four channels at different heights of the column (i.e., local restriction of the column diameter) causes a strong reduction in the liquid backmixing.

Cheng et al. [22] measured the residence time distribution (RTD) of the liquid to test the effect of channels on the liquid backmixing in a bubble column. They used the tanks-in-series model to interpret their results and introduced the tank number N and the dimensionless variance for the liquid flow σ_θ^2. Their results show that by structuring, the number of stirred tanks in series increases from 1.4 to 3.2 and the dimensionless variance decreases from 0.7 to 0.3. Because of the linear relation between the dimensionless variance and axial dispersion coefficient [23], the $E_{L,SB}$ would decrease about 60%.

Dreher and Krishna [12] studied the influence of partition plates on the liquid backmixing in bubble columns with different diameters and different gas velocities. They staged the columns with perforated brass plates and determined the RTD of the liquid phase. They reported that using partition in a bubble column and staging it, the magnitude of the liquid circulation and therefore the $E_{L,SB}$ can be decreased by 90%. The reason would be restricting the liquid circulation between the compartments.

In the case of multi-tubular FB reactors, diffusion length and heat transfer are the most important challenges. Long diffusion lengths (catalyst effectiveness <1) give an ineffective use of the reactor volume. Large temperature gradients lead to non-uniform behavior in terms of selectivity, activity and deactivation. These points can be alleviated by replacing a bed of random particles by structured catalyst packings [1]. An example of structured packing in a FB was studied by Vervloet et al. [5]. Their investigation on cross flow structured packing elements shows that these types of packings can greatly improve the radial heat transport characteristics compared to randomly packed beds. In practice this leads to much flatter temperature profiles. Furthermore, using a structured catalyst support allows decoupling of the diffusion length from pressure drop effects, similar to monolith packings, effectively negating costly pressure losses, while realizing a degree of freedom in catalyst design. Fig. 2 represents two types of such packings.

3. Model

To facilitate a fair comparison between the two reactor types we used the same simple 1-D model for both SBC and FB. For this purpose, i.e., a qualitative exploration and comparison of the production sensitivity of certain reactor specific characteristics, the use of a 1D model is sufficient [24]. Although more detailed modelling approaches are available – such as a 2D modelling approach for the FB [24], which is more precise in predicting, for example, reactor runaway behavior the added value for our objective would be negligible. For the SBC, we distinguish the slurry phase consisting of liquid and mono dispersed particles, the large bubble phase and the small bubble phase [20,25]. We assume the absence of mass transfer limitations inside the small SBC catalyst particles (d_p = 50 μm) and a catalyst effectiveness of 1 [21]. For the FB, we assume that the gas and liquid are in equilibrium, while the most important mass transfer limitations are inside the relatively large

Fig. 1. A photo of a needle sparger used in a slurry bubble column with one-third of the needles in operation. By using long needles instead of holes, a much higher pressure drop is achieved, which leads to a much more uniform bubble size and consequently a lowered E_L [31].

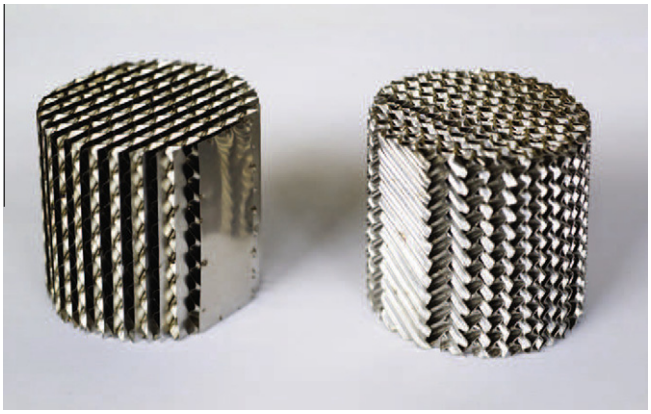

Fig. 2. Photos of cross-flow structure packings used in a fixed bed reactors. By forcing the gas–liquid mixture in diagonal pathways, a much more effective radial heat transfer is obtained than in a randomly packed bed and consequently more uniform temperature profile [5].

catalyst particles (d_p = 2 mm) [6]. We take internal transport limitations into account by calculating the catalyst effectiveness factor (typically <1) from a reaction–diffusion perspective [26], which can vary with the reactor coordinate.

In the case of the multi-tubular FB reactor it is sufficient to model one single tube, since it is reasonable to assume the same behavior for each tube. Fig. 3 shows a schematic representation of the model for both SBC and FB.

The mathematical model for mass and heat transfer in the SBC and FB is presented in Table 1 and operating conditions [6,27,28] have been summarized in Table 2.

We describe the FTS using the rate expression of Yates and Satterfield [29]:

$$R_{CO} = F\nu_{CO}\frac{aP_{CO}P_{H_2}}{(1+bP_{CO})^2} \quad (2)$$

in which:

$$a = a_0 \exp\left[4494.41\left(\frac{1}{493.15}-\frac{1}{T}\right)\right] \quad (3)$$

$$b = b_0 \exp\left[-8236\left(\frac{1}{493.15}-\frac{1}{T}\right)\right] \quad (4)$$

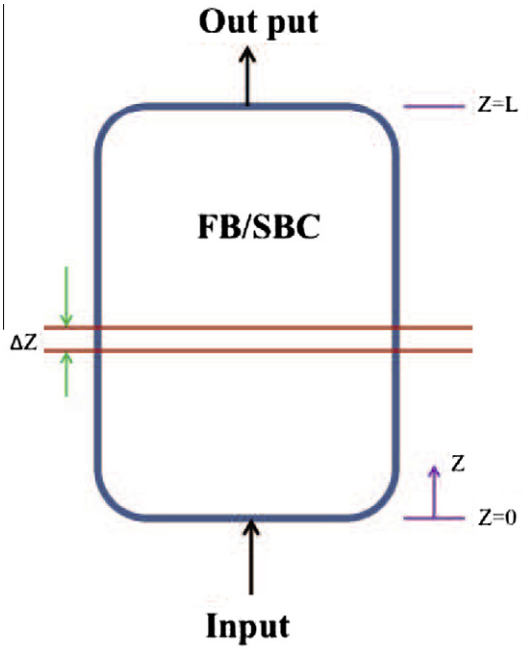

Fig. 3. Schematic representation of a slurry bubble column and a fixed bed reactor model. *Note:* the fixed bed reactor operation is co-current, top down.

where a_0 = 8.8533 × 10^{-3} mol/s kg_{cat} bar^2, b_0 = 2.226 1/bar, $\nu_{CO} = -1$ and $\nu_{H_2} = -2$. We introduce a multiplication factor F = 3 to account for improvements in FTS-catalyst activity [30] since the publication of this rate expression.

4. Results and discussions

By solving the coupled sets of design equations the performance of both reactors are determined at steady state conditions. In both reactor types the probability factor of hydrocarbon chain growth, α, is considered to be constant (α = 0.9) which is a simplification for the FB [26]. The α determines the C_{5+} selectivity, which can be calculated through: $S_{C5+} = 1 - \sum_{n=1}^{4} n(1-\alpha)^2\alpha^{n-1}$. Since α is assumed constant value, we can calculate the S_{C5+} value immediately, which is 0.92. In the following sections, we will calculate the

Table 1
Mathematical model for mass and heat balance in a slurry bubble column and fixed bed. In calculation i = CO or H_2 and 'nr' is number of independent reactions.

Balances	Slurry bubble column	Fixed bed
Mass balance for ith component in large bubbles:		
$\frac{\partial}{\partial z}\left(\varepsilon_{large}E_{g,large}\frac{\partial C_{i,g,large}}{\partial z}\right)-\frac{\partial}{\partial z}[(U_{sg}-U_{df})C_{i,g,large}]$	$E_{g,large}=E_{g,large,SB}$ [27]	$E_{g,large}=0$
$-k_{L,i,large}a_{large}\left(C^*_{i,large}-C_{i,L}\right)=0$	$k_{L,i,large}=k_{L,i,large,SB}$ [20]	$k_{L,i,large}=\infty$
$C^*_{i,large}=C_{i,g,large}/m_i$		$C^*_{i,large}=C_{i,L}$
Mass balance for ith component in small bubbles:		
$\frac{\partial}{\partial z}\left(\varepsilon_{small}E_{g,small}\frac{\partial C_{i,g,small}}{\partial z}\right)-\frac{\partial}{\partial z}(U_{df}C_{i,g,small})$	$E_{g,small}=E_L$ [27]	$E_{g,small}=0$
$-k_{L,i,small}a_{small}(C^*_{i,small}-C_{i,L})=0$	$k_{L,i,small}=k_{L,i,small,SB}$ [20]	$k_{L,i,small}=\infty$
$C^*_{i,small}=C_{i,g,small}/m_i$		$C^*_{i,small}=C_{i,L}$
Mass balance for ith component in liquid phase:		
$\frac{\partial}{\partial z}\left(\varepsilon_L E_L\frac{\partial C_{i,L}}{\partial z}\right)-\frac{\partial}{\partial z}(U_{ss}C_{i,L})$	$E_L=E_{L,SB}$	$E_L=0$
$+k_{L,i,large}a_{large}\left(C^*_{i,large}-C_{i,L}\right)$		$C_s\varepsilon_L=\varepsilon_{bed}$
$+k_{L,i,small}a_{small}(C^*_{i,small}-C_{i,L})$		
$-C_s\varepsilon_L\rho_p\sum_{j=1}^{nr}R_i=0$		
Heat balance is derived as:		
$\frac{\partial}{\partial z}\left(\varepsilon_L\lambda_{ax}\frac{\partial T}{\partial z}\right)-U_{ss}\rho_s C_{ps}\frac{\partial T}{\partial z}-\alpha_{eff}a_w(T-T_c)$	$\lambda_{ax}=\lambda_{ax,SB}$ [27]	$\lambda_{ax}=0$
$+C_s\varepsilon_L\sum_{j=1}^{nr}(-\Delta H_{Ri})R_i=0$	$\alpha_{eff}=\alpha_{eff,SB}$ [21]	$\alpha_{eff}=U_{ov}$
	$\alpha_w=\alpha_{w,SB}$	$\alpha_w=4/d_{tube}$

Table 2
Dimensions and operating conditions.

Dimensions	SBC	FB
Diameter (m)	7.5	0.05
Height (m)	30.0	10.0
Operating conditions		
Reactor pressure (MPa)	3.0	3.0
Inlet temperature of syngas (K)	498	Varies
Area of the heat transfer (m^2/m^3 reactor)	10.0	80.0
Slurry velocity (m/s)	0.01	–
Liquid velocity (m/s)	–	0.01
Catalyst diameter (mm)	0.05	2.0
Catalyst density (kg/m^3)	1500	1500
Catalyst hold-up (–)	0.25	0.6

conversion for the different cases. Combined with the C_{5+} selectivity, this gives us the productivity for the different cases.

4.1. Slurry bubble column reactors

Guided by the previous studies [12,22], we characterize to what extent the reducing axial dispersion by structuring affects the syngas conversion. The different cases we have considered for the sensitivity analysis in a SBC have been summarized in Table 3a. We chose a base case (case 1, unstructured, backmixing properties following Eq. (1)) superficial gas velocity of 0.3 m/s and compared the C_{5+} productivity to a reactor that was operated with reduced backmixing properties as a consequence of structuring (case 2, structured reactor, 75% reduced backmixing). The same production sensitivity analysis was performed for an increased superficial gas velocity of 0.4 m/s – case 3 (unstructured, backmixing effects according to Eq. (1)) and case 4 (structured reactor, 75% reduced backmixing). The results show that in a SBC a 75% decrease in the liquid axial dispersion coefficient both from case 1 to case 2

Table 3
(a) Different cases in slurry bubble column model (d_p = 50 μm). *Note:* In case 1 and 2 the $E_{L,SB}$ was calculated using Eq. (4). (b) Different cases in fixed bed model (U_{sg} = 0.4 m/s).

Case	U_{sg} (m/s)	$E_{L,SB}$ (m^2/s)
(a) SBC		
1	0.3	7.77
2	0.3	1.95
3	0.4	8.52
4	0.4	2.12
Case (b) FB	d_p (mm)	U_{ov} ($W/m^2/K$)
1	2.0	400
2	1.0	400
3	2.0	1000
4	1.0	1000

and from case 3 to case 4 yields a higher final syngas conversion (see Fig. 4). The backmixing causes the differences in the syngas concentration in different heights of the reactor and consequently the lower conversion in the lower part of the reactor than in the higher part. Increasing the superficial gas velocity (case 1 to case 3 and case 2 to case 4) lowers the conversion, but increases the productivity (see Table 4).

4.2. Fixed bed reactors

Previous studies on structuring the FB reactors done by Pangarkar et al. [1,3,4] and Vervloet et al. [5] on cross-flow structured packings show that using such structures improve the overall heat transfer (U_{ov}) performance of the FB from 400 (W/m^2 K) (randomly packed bed, cases 1 and 3) to 1000 (W/m^2 K) (structured packing, cases 2 and 4). This catalyst support structure allows for a shorter catalyst diffusion length (d_p), which we will also exploit in our modelling analysis. We decrease the particle diameter, d_p in case 2 and 4 from typically 2.0 mm to 1.0 mm to study the influence of the diffusion length. Table 3b contains the four cases studied for the FB reactor. For the temperature control in the FB two criteria have been imposed: (1) we consider a maximum allowed temperature of 510 K, both for the selectivity and safety (runaway) issues and (2) the average bed temperature is

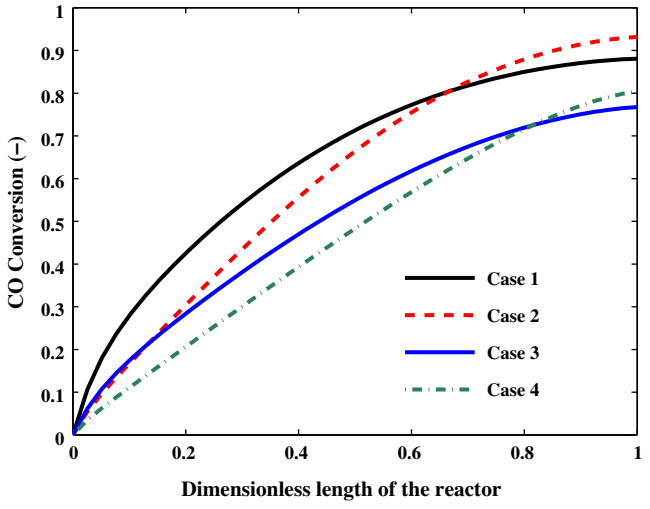

Fig. 4. CO conversion versus dimensionless reactor length for different values of superficial gas velocities and liquid axial dispersion coefficient in a slurry bubble column with D_T = 7.5 m and H = 30 m. *Note:* for different cases see Table 3a.

Table 4
Productivity of the reactors.

Productivity	SBC				FB			
	Case 1	Case 2	Case 3	Case 4	Case 1	Case 2	Case 3	Case 4
STY_{C5+}(kg/kg$_{cat}$/h)	0.263	0.278	0.307	0.320	0.288	0.353	0.279	0.408
STY'_{C5+} (kg/m$^3_{G+L+cat}$/h)	99	104	115	120	259	318	251	367
STY''_{C5+} (kg/m$^3_{reactor}$/h)	97	102	112	118	161	197	156	228

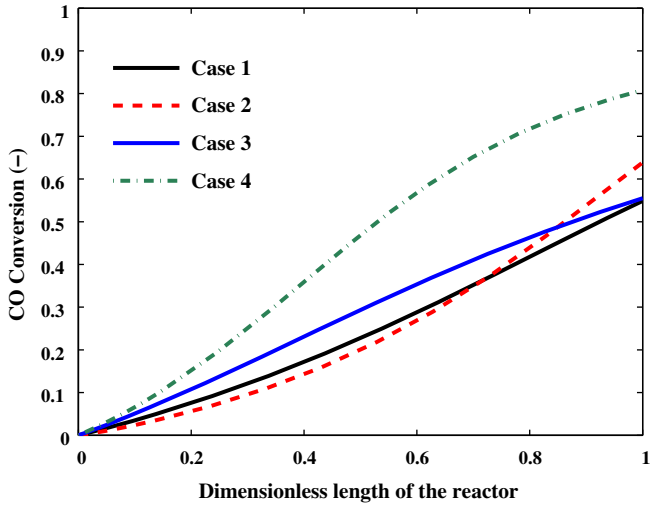

Fig. 5. CO conversion versus dimensionless reactor length for different values of catalyst diameter and overall heat transfer values in a fixed bed reactor with $D_{T,FB}$ = 0.05 m and H_{FB} = 10 m. *Note:* for different cases see Table 3b.

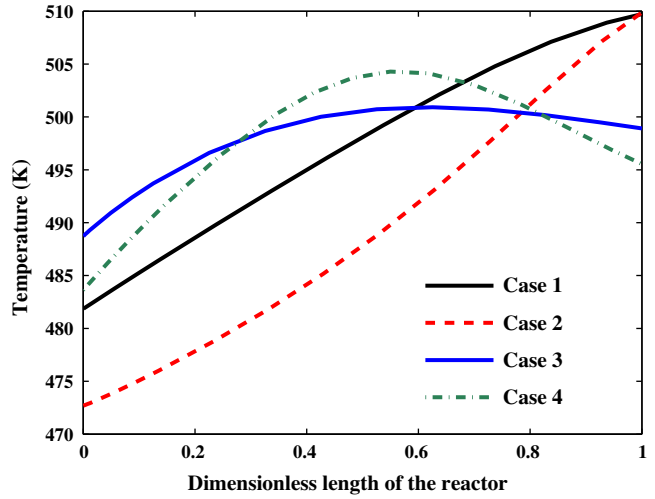

Fig. 6. Temperature profile in the fixed bed reactor for different values of catalyst diameter and overall heat transfer values in a fixed bed reactor with $D_{T,FB}$ = 0.05 m and H = 10 m. Note: for different cases see Table 3b.

as close to 498 K as possible satisfying the first restriction – by varying the inlet temperature ($T_{in} = T_c$).

Fig. 5 shows the conversion profiles in the fixed bed reactor for cases 1–4. The results indicate that a decrease in the particle diameter from 2.0 mm to 1.0 mm (case 3) or an improvement in the heat transfer (case 2) only marginally increase the syngas conversion compared to the base case. However, when both parameters are varied (case 4) a significant improvement is found. To explain this, we investigate the axial temperature profiles of the FB (Fig. 6).

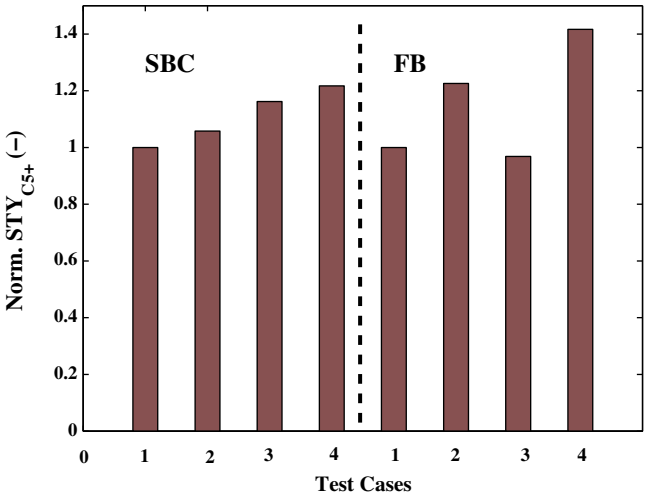

Fig. 7. Normalized space time yield of a SBC and a FB reactor in an intensified operation relative to the case 1 for each reactor type.

Cases 1 and 2 are temperature limited as they reach the 510 K constraint, due to limited heat removal. Because of significant heating of the fluids with the axial reactor coordinate a relatively low inlet and cooling temperature have to be chosen. This leads to a lower than desired average reactor temperature, and therefore limits the overall productivity. Cases 3 and 4 show much flatter axial temperature profiles, due to the improved heat transfer coefficient, that are not bound by the upper temperature limit. The relatively flat temperature profiles allow for a higher inlet and cooling temperature to reach the desired average bed temperature, without violating the maximum temperature constraint.

4.3. Opportunities for process intensification for both reactor types

In this section, we will compare the two reactor types side by side. It should be noted that we did not further optimize the reactor performance by varying the flow rates, the syngas composition, or separate optimization of the cooling and inlet temperature, which may alter the reactor performance to a certain extent.

Fig. 7 gives the normalized *STY* relative to the base case. Reducing the liquid dispersion and increasing the gas velocity increases the *STY* of C_{5+} for a SBC, while decreasing the diffusion length and increasing the heat transfer increases the *STY* for the FB. The results show that the FB reactor has a potential of increasing the STY of C_{5+} with over 40% and SBC over 20%. We emphasize that the conversion in the regular (non-structured) SBC is already higher than the FB (88% versus 53% for the base cases), making the room for improvement is smaller in case of a SBC. In industry, FBs for Fischer–Tropsch Synthesis are typically operated in series.

Table 4 gives the space time yield (*STY*) of C_{5+} (the targeted product fraction) for all the four cases in both SBC and FB reactors. The table shows that hydrocarbon production per unit of catalyst mass is roughly equal for both reactor types. However, reactor

volume without and with considering the cooling volume, STY' and STY'', in all four cases is considerably higher for the FB than for the SBC. The productivity of C_{5+} per reactor volume considering the cooling volume, is for a FB is about two times that of for a SBC.

Instead of increasing the conversion for a given reactor configuration, one can also consider to reduce the reactor volume at keeping the conversion constant. For the FB comparing case 4 with the base case in Fig. 5 shows that we can reduce the reactor volume with 40% while keeping the same conversion as in the base case. The improved heat transfer (flatter temperature profile) can also be used to increase the tube diameter, and thus reducing the number of tubes. This will mean a reduction of the capital investment in case of the multi-tubular FB reactor. For the SBC we consider case 2 and the base case. For plug flow with axial dispersion, the conversion at a fixed axial position varies when the reactor length is changed; this makes it necessary to perform an additional simulation. We calculated which reactor height is needed to reach 88% conversion (base case) while the $E_L = 1.95\ m^2/s$ (case 2). The results of the simulation show that the reactor height can be reduced by 14%.

5. Conclusions

Using a simple 1-D model, we studied the intensification of Fischer–Tropsch Synthesis in two different catalytic reactors: a slurry bubble column and a fixed bed. We compared four different cases for each of these reactors and varied main parameters which can improve the performance of the reactors.

- Our model shows that by structuring both three-phase catalytic reactors can be intensified.
- In a slurry bubble column reactor with a conversion of 88% as the base case, a 75% decrease in the liquid axial dispersion coefficient enhances the productivity by 20%.
- In a fixed bed reactor with a conversion of 53% as the base case, the productivity can be improved by more than 40% when the heat transfer coefficient is improved with a factor 2.5 and the diffusion length in the catalyst particles is decreased with a factor 2.
- In both reactor types structuring can also be used to reduce reactor volume rather than increasing conversion.

References

[1] K. Pangarkar, T.J. Schildhauer, J.R. van Ommen, J. Nijenhuis, F. Kapteijn, J.A. Moulijn, Structured packings for multiphase catalytic reactors, Ind. Eng. Chem. Res. 47 (2008) 3720–3751.
[2] M.T. Kreutzer, F. Kapteijn, J.A. Moulijn, Fast gas–liquid–solid reactions in monoliths: a case study of nitro-aromatic hydrogenation, Catal. Today 105 (2005) 421–428.
[3] K. Pangarkar, T.J. Schildhauer, J.R. van Ommen, J. Nijenhuis, J.A. Moulijn, F. Kapteijn, Experimental and numerical comparison of structured packings with a randomly packed bed reactor for Fischer–Tropsch synthesis, Catal. Today 147 (Supplement) (2009) S2–S9.
[4] K. Pangarkar, T.J. Schildhauer, J.R. van Ommen, J. Nijenhuis, J.A. Moulijn, F. Kapteijn, Heat transport in structured packings with co-current downflow of gas and liquid, Chem. Eng. Sci. 65 (2010) 420–426.
[5] D. Vervloet, M. Kamali, J.J.J. Gillissen, J. Nijenhuis, H.E.A. van den Akker, F. Kapteijn, J.R. van Ommen, Intensification of co-current gas–liquid reactors using structured catalytic packings: a multiscale approach, Catal. Today 147 (Supplement) (2009) S138–S143.
[6] R. Guettel, T. Turek, Comparison of different reactor types for low temperature Fischer–Tropsch synthesis: a simulation study, Chem. Eng. Sci. 64 (2009) 955–964.
[7] C.P. Stemmet, M. Meeuwse, J. van der Schaaf, B.F.M. Kuster, J.C. Schouten, Gas–liquid mass transfer and axial dispersion in solid foam packings, Chem. Eng. Sci. 62 (2007) 5444–5450.
[8] P. Heidebrecht, M. Pfafferodt, K. Sundmacher, Multiscale modelling strategy for structured catalytic reactors, Chem. Eng. Sci. 66 (2011) 4389–4402.
[9] N. Hooshyar, P.J. Hamersma, R.F. Mudde, J.R. van Ommen, Intensified operation of slurry bubble columns using structured gas injection, Can. J. Chem. Eng. 88 (2010) 533–542.
[10] J. Ellenberger, R. Krishna, Intensification of slurry bubble columns by vibration excitement, Can. J. Chem. Eng. 81 (2003) 655–659.
[11] A. Lakota, M. Jazbec, J. Levee, Impact of structured packing on bubble column mass transfer charasteristics: part 1. Backmixing in the liquid phase, Acta Chim. Slov. 48 (2001) 453–468.
[12] A. Dreher, R. Krishna, Liquid-phase backmixing in bubble columns, structured by introduction of partition plates, Catal. Today 69 (2001) 165–170.
[13] D.I. Enache, G.J. Hutchings, S.H. Taylor, S. Raymahasay, J.M. Winterbottom, M.D. Mantle, A.J. Sederman, L.F. Gladden, C. Chatwin, K.T. Symonds, E.H. Stitt, Multiphase hydrogenation of resorcinol in structured and heat exchange reactor systems: influence of the catalyst and the reactor configuration, Catal. Today 128 (2007) 26–35.
[14] F. Kapteijn, J.J. Heiszwolf, T.A. Nijenhuis, J.A. Moulijn, Monoliths in multiphase catalytic processes – aspects and prospects, CATTECH 3 (1999) 24–41.
[15] A. Cybulski, J.A. Moulijn, Structured Catalysts and Reactors, Chemical Industries, Taylor & Francis, 2006.
[16] T.A. Nijhuis, M.T. Kreutzer, A.C.J. Romijn, F. Kapteijn, J.A. Moulijnk, Monolithic catalysts as more efficient three-phase reactors, Catal. Today 66 (2001) 157–165.
[17] J.R. van Ommen, J. Nijenhuis, C.M. van den Bleek, M.-O. Coppens, Four ways to introduce structure in fluidized bed reactors, Ind. Eng. Chem. Res. 46 (2007) 4236–4244.
[18] J. Ellenberger, J. van Baten, R. Krishna, Intensification of bubble columns by vibration excitement, Catal. Today 79–80 (2003) 181–188.
[19] N. Hooshyar, P.J. Hamersma, R.F. Mudde, J.R. van Ommen, Gas fraction and bubble dynamics in structured slurry bubble columns, Ind. Eng. Chem. Res. 49 (2010) 10689–10697.
[20] C. Maretto, R. Krishna, Modelling of a bubble column slurry reactor for Fischer–Tropsch synthesis, Catal. Today 52 (1999) 279–289.
[21] W.D. Deckwer, Y. Serpemen, M. Ralek, B. Schmidt, Modeling the Fischer–Tropsch synthesis in the slurry phase, Ind. Eng. Chem. Proc. Des. Dev. 21 (1982) 231–241.
[22] Z.-M. Cheng, Y. Wu, Z.-B. Huang, Backmixing reduction of a bubble column by interruption of the global liquid circulation, Ind. Eng. Chem. Res. 48 (2009) 6558–6563.
[23] G.F. Froment, K.B. Bischoff, Chemical Reactor Analysis and Design, Wiley, 1979.
[24] A. Jess, C. Kern, Modeling of multi-tubular reactors for Fischer–Tropsch synthesis, Chem. Eng. Technol. 32 (2009) 1164–1175.
[25] N. Hooshyar, S. Fatemi, M. Rahmani, Mathematical modeling of Fischer–Tropsch synthesis in an industrial slurry bubble column, Int. J. Chem. React. Eng. 7 (2009).
[26] D. Vervloet, F. Kapteijn, J. Nijenhuis, J.R. van Ommen, Fischer–Tropsch reaction–diffusion in a cobalt catalyst particle: Aspects of activity and selectivity for a variable chain growth probability, Catal. Sci. Technol. 2 (2012) 1221–1233.
[27] J.W.A. De Swart, R. Krishna, Simulation of the transient and steady state behaviour of a bubble column slurry reactor for Fischer–Tropsch synthesis, Chem. Eng. Process 41 (2002) 35–47.
[28] S.T. Sie, R. Krishna, Fundamentals and selection of advanced Fischer–Tropsch reactors, Appl. Catal. A – Gen. 186 (1999) 55–70.
[29] I.C. Yates, C.N. Satterfield, Intrinsic kinetics of the Fischer–Tropsch synthesis on a cobalt catalyst, Energy Fuels 5 (1991) 168–173.
[30] A. Steynberg, M. Dry, B. Davis, B. Breman, Fischer–Tropsch reactors, Stud. Surf. Sci. Catal. 152 (2004) 64–195.
[31] R.F. Mudde, W.K. Harteveld, H.E.A. van den Akker, Uniform flow in bubble columns, Ind. Eng. Chem. Res. 48 (2009) 148–158.

Paper II

Intensified operation of slurry bubble columns using structured gas injection

Has been published in the Canadian Journal of Chemical Engineering.

INTENSIFIED OPERATION OF SLURRY BUBBLE COLUMNS USING STRUCTURED GAS INJECTION

Nasim Hooshyar,* Peter J. Hamersma, Robert F. Mudde and J. Ruud van Ommen

Delft University of Technology, Julianalaan 136, 2628 BL Delft, the Netherlands

We investigate uniform gas injection using a needle sparger as a structuring methodology to reduce backmixing in slurry bubble columns. Using optical probes, we determined the gas fraction and the bubble behaviour in 2D and 3D slurry bubble columns with a uniform gas injection. Experimental results for air–water–glass beads ($d_s = 108\ \mu m$, $U_{sg} = 0$–0.10 m/s) indicate that a strong reduction in the vortical structures has been achieved and the homogeneous flow regime can be extended beyond 30% gas fraction. Increasing the solids concentration decreases the gas fraction and widens the bubble velocity distribution. Furthermore, we show by modelling that the reduced backmixing leads to a major improvement of the conversion in case of Fischer–Tropsch synthesis.

L'injection uniforme de gaz est étudiée utilisant une aiguille d'aération en tant que méthodologie structurante pour réduire le mélange de retour dans les colonnes à bulles en suspension. Utilisant les sondes optiques, nous avons déterminé la fraction de gaz et le comportement des bulles dans des colonnes à bulles 2D et 3D avec une injection uniforme de gaz. Les résultats expérimentaux pour des billes air-eau-verre ($d_s = 108\ \mu m$, $U_{sg} = 0$–0.10 m/s) indiquent qu'une réduction importante des structures turbulentes a été réalisée et le régime d'écoulement homogène peut être étendu au delà de la fraction de gaz de 30%. L'augmentation de la concentration des solides diminue la fraction de gaz et élargit la distribution de vitesse des bulles. En outre, nous démontrons par la modélisation que la réduction du mélange au retour entraîne une amélioration significative de la conversion dans le cas de synthèse Fischer-Tropsch.

Keywords: structured slurry bubble column, hydrodynamics, axial dispersion, optical probe

INTRODUCTION

Slurry bubble column reactors (SBCRs) are widely applied in chemical and biochemical processes. However, the design and scale-up are difficult due to the complexity of the hydrodynamic behaviour of these three-phase systems.

Depending on the superficial gas velocity, the hydrodynamics in SBCRs can be characterised by two different flow regimes, namely, the homogeneous and heterogeneous regime. The homogeneous flow regime exists at low superficial gas velocities and is characterised by a bubbly flow without significant backmixing of the liquid phase and almost uniform sized bubbles with a narrow distribution (Shah et al., 1982; Krishna et al., 1999a; Mudde et al., 2009). With increasing superficial gas velocity the homogeneous regime becomes unstable and changes to the heterogeneous flow regime. In the heterogeneous flow regime there is strong interaction between gas bubbles. At high gas velocities, continuous breakup and coalescence of bubbles is observed. This is the so-called "churn-turbulent" regime, which is a part of heterogeneous flow (Mudde et al., 2009), where the larger gas bubbles move in a plug-flow manner and large-scale liquid recirculation is present. The small gas bubbles are entrained within the liquid re-circulation. In this way, backmixing takes places both in the liquid and the gas phase. The hydrodynamic behaviour, heat and mass transfer, and mixing behaviour are quite different between the homogeneous and heterogeneous regimes. The transition from the homogeneous flow regime into the heterogeneous regime occurs at the transition velocity, $U_{sg,trans}$. The value of this transition velocity, $U_{sg,trans}$ depends on several transport properties and increases with higher pressure (van der Schaaf et al., 2007) and decreases with higher solids concentration (Krishna, 2000). A common method to find the change from the homogeneous to the heterogeneous regime is to determine the inflection point in a gas fraction versus superficial gas velocity plot (Shah et al., 1982; Chilekar et al., 2005; Ribeiro and Lage, 2005; Mudde et al., 2009).

*Author to whom correspondence may be addressed.
E-mail address: n.hooshyar@tudelft.nl
Can. J. Chem. Eng. 88:533–542, 2010

DOI 10.1002/cjce.20338
Published online 17 June 2010 in Wiley InterScience (www.interscience.wiley.com)

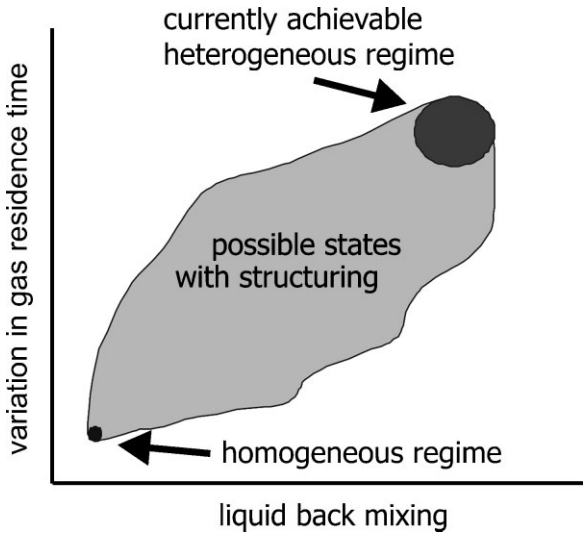

Figure 1. Graphical representation of extended operation modes.

To obtain a sufficiently high throughput, many industrial columns are operated at high superficial gas velocities, and are therefore in the heterogeneous flow regime. This has the advantage of high mass transfer and good mixing. However, the degree of mixing cannot be controlled; this is one of the disadvantages of working in this flow regime. For the turbulent flow regime, the characteristics of the bubbles will be controlled by the liquid circulation and turbulence level, and the effect of gas distribution will be less than in the bubbly flow regime (Drahoš et al., 1992). The axial dispersion model (ADM) can be used to describe the characteristics of the gas, liquid, and solid catalysts between the limits of plug-flow and complete backmixing behaviour in these kinds of reactors. Yang et al. (1992) studied the liquid backmixing in a bubble column and observed that the axial dispersion coefficients increased with increasing column diameter and superficial gas velocity.

The main purpose of our approach is to improve the conversion and selectivity in SBCRs by developing a methodology for controlling these systems in such a way that a desired flow pattern is imposed on the system. The idea is to introduce dynamic structuring in slurry bubble columns allowing for modes of operation that cannot be achieved with the current steady-state operation (see Figure 1). A similar approach has been shown by our group for gas–solid fluidized beds (van Ommen et al., 2007).

To reach this goal there is a need to use proper measurement techniques to assess the hydrodynamics. We have started our experiments in a 2D and 3D column equipped with a needle sparger using four-point optical probes as a measurement method but is not applicable at an industrial scale. Therefore, we will additionally use high-frequency pressure probes in later work. The signals from these probes are more difficult to interpret but have the advantage that the technique is very robust and can be used in industrial applications (Villa et al., 2003; van Ommen and Mudde, 2008).

The present paper presents experimental results using a special needle sparger, allowing very uniform inflow of gas. We investigate the extent of the homogeneous regime as a function of the solids volume fraction. Moreover, we investigate via modelling the increase of the conversion in Fischer–Tropsch synthesis when reducing the backmixing.

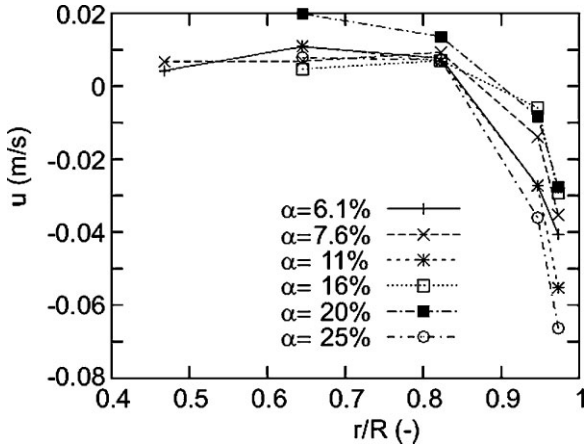

Figure 2. Mean axial liquid velocity profile for various gas fractions for homogeneous flow in a bubble column at different gas fractions (Mudde et al., 2009).

STRUCTURES IN SLURRY BUBBLE COLUMN

Flow Pattern

Generally, the gas phase in slurry bubble columns is not distributed uniformly over the cross-section of the column: there is a larger gas fraction in the central part of the column than close to the wall. Consequently, an internal circulation is induced with liquid flowing upwards in the centre and downwards close to the wall (Nevers, 1968; Groen et al., 1996).

Yang et al. (1986) studied the flow pattern in bubble columns and reported that in the inner region around the column axis a so-called bubble-street is formed, with liquid flowing upward with maximum velocity near the column axis, whereas in the region near the reactor wall the liquid flows downwards. Between these two regions there is the shear zone, where the flow direction changes and the averaged velocity of the liquid becomes zero. The radial position of this inversion of flow depends on the properties of the gas/liquid system and the operating conditions, and it can be used to characterise liquid velocity profiles. Yang et al. (1986) found that the mean value for the inversion point in liquid flow in a bubble column is $r/R = 0.70$–0.73 for low viscosity fluids. In liquids of high viscosity, the inversion point is nearer to the central axis of the column; the shape of the liquid velocity profile in these liquids is different too. Mudde et al. (2009) have shown that by applying a very even gas supply obtained by a special needle sparger, the inversion point could be shifted to $r/R > 0.9$, which represents a very strong homogeneity (Figure 2).

Bubble Dynamics

The bubble size distribution and the bubble rise velocity play a key role in SBCR design; many studies have focused on these descriptors of the bubble dynamics. Devices such as a four-point optical probe (Guet et al., 2003; Xue et al., 2003, 2008b; Mudde et al., 2009) have been used to measure the bubble size and rise velocity as well as local hydrodynamic parameters. The effects of superficial gas velocity, solids concentration, liquid viscosity, different injection systems, and also different operational pressures and temperatures have been investigated by various researchers (Shah et al., 1982; Heijnen and van't Riet, 1984; Yang et al., 1986; Smith et al., 1995; Chilekar et al., 2005; Kantarci et al., 2005; Ribeiro and Lage, 2005; Behkish et al., 2007; Zhang et al., 2008; Xue et al., 2008a).

Previous studies have shown that at low superficial gas velocities the bubbles are small and uniform (e.g., Wang et al., 2007) and that increasing the gas fraction increases the bubble size (e.g., Kantarci et al., 2005). A further increase results in bubble size enhancement beyond a critical size in which uniform flow looses its stability (Mudde et al., 2009). At high superficial gas velocities, coalescence and breakup cause a wide range of bubble sizes. Chilekar et al. (2005) observed that the average bubble size in the transition from homogeneous to heterogeneous increases rapidly with increasing superficial gas velocity due to coalescence, and that for further increasing gas velocity the increase of bubble size becomes slower.

It was reported that an increase in solids concentration and liquid viscosity increases the bubble size (Ribeiro and Lage, 2005) and a reduction in the surface tension decreases the bubble size (Kantarci et al., 2005). Behkish et al. (2007) observed that at any given solids concentration, increasing pressure decreases the bubble size.

Zhang et al. (2008) studied the bubble rise velocity in a SBCR and reported increasing bubble rise velocity with increasing superficial gas velocity through the column. Xue et al. (2008a) reported that at a superficial velocity of 2 cm/s, all bubbles have an upward motion in the column. In the churn-turbulent regime the bubble rise velocity is much more complex (Wang et al., 2007), due to coalescence, breakup, and liquid circulations patterns.

Different Approaches for Structuring

The aim of looking for structuring of the flow in SBCRs is to decrease the liquid axial dispersion. This will decrease the deviation from plug flow and will increase the conversion and selectivity. In this section, we give a brief literature review of the various approaches that have been investigated to achieve this goal.

Ellenberger and Krishna (2002, 2003b) studied vibrated bubble columns with a 12-capillary gas inlet device and showed that the application of low-frequency vibrations, in the 40–120 Hz range, to the liquid phase of an air–water bubble column causes the formation of smaller bubbles. They claim that the application of vibration to the liquid phase helps to overcome the surface tension forces and therefore breakup of the bubbles will happen. Vibrations delay the transition to the heterogeneous flow regime and lead to a more uniform bubble size and radial spreading of the bubbles. Another effect of the vibration is increasing the gas fraction. Ellenberger and Krishna (2002, 2003b) show that the higher the vibration frequency, the higher the gas fraction, and that the higher the vibration amplitude, the higher the gas fraction. They also reported the enhancement in $k_L a$ by a factor of 2 or more. Their results suggest that the $k_L a$ improvement is a consequence of both increase in interfacial area and higher value of k_L. The physical reason for higher k_L is that the gas bubbles and liquid oscillate at different velocities as a result of the added mass force (de Vries et al., 2002), which leads to an increase in surface renewal.

Knopf et al. (2006a,b); and Waghmare et al. (2009) also subjected the liquid phase of a batch bubble column to low frequencies (10–30 Hz) and measured the gas fraction, mass transfer, and bubble size distribution at both low and jetting gas rates. Their results showed that at low gas flow rates (up to 0.083 cm/s), liquid and gas phases inside the injector undergo expulsion and that suck-back of liquid into the injector causes bubble breakage inside the injector. For higher superficial gas velocities, the large momentum of the gas which flowed through the injector could overcome the expulsion and suck-back and the larger sized bubbles formed near the injector. As bubbles moved through the column, the turbulence or shear forces induced started to break the bubbles up and smaller sized bubbles were formed. When the rate of bubble breakage and coalescence became equal, the bubble size distribution reached a constant shape. Similar to Ellenberger and Krishna (2003a); Knopf et al. (2006a,b); and Waghmare et al. (2009) reported that application of vibrations delays the transition from homogeneous to heterogeneous flow. Although the results at lab-scale are promising, applying vibration to large-scale reactors will probably yield serious practical problems.

There are other strategies that have been reported in literature to structure the flow and thereby decrease the backmixing. The impact of structured packings on mass transfer of bubble columns was investigated by Lakota et al. (2001). They measured the volumetric mass transfer coefficient in a system of tap water and oxygen and their results indicate that using a polyethylene structured packing (Sulzer SMV 16) reduced the axial dispersion coefficient in the liquid (E_L) by about 50% at low gas velocity but only 20% at high gas velocity. They showed that E_L is affected by both liquid and gas superficial velocity in a packed system, whereas in an unpacked system only the superficial gas velocity affects E_L (Baird and Rice, 1975; Shah et al., 1982).

Urseanu et al. (2001) measured the gas fraction and axial dispersion coefficient in structured bubble columns which consist of two parts of a structured packed section containing KATAPAK-S elements in the lower part and an unstructured bubble column section in the upper part. They showed that the presence of structures decreases the backmixing of the liquid phase, and that the superficial gas velocity does not have a significant effect on the axial dispersion in the structured part.

Maretto and Krishna (2001) modelled and optimized a multistage bubble column slurry reactor for Fischer–Tropsch synthesis. They divided the column into four stages by introducing sieve plates as "baffles," approaching plug flow conditions instead of well-mixed. As a consequence, higher syngas conversion and higher productivity were achieved.

Dreher and Krishna (2001) applied one or two partition plates in their bubble columns with the aim of reduction of liquid backmixing in bubble columns. They made a comparison with previous work (Krishna et al., 1999b, 2000a,b). Experimental studies on backmixing in the liquid phase have shown an increasing axial dispersion coefficient with increasing column diameter, D_T, in empty bubble columns without partitions.

MODELLING AND SIMULATION

One of the most important applications of SBCRs is Fischer–Tropsch synthesis; we will use this application to illustrate the benefit of structuring. Application of SBCRs for Fischer–Tropsch has several advantages such as high mass transfer and catalyst efficiency, relatively low pressure drop and operation in near-isothermal conditions (Maretto and Krishna, 1999). This works presents the results of mathematical modelling of the Fischer–Tropsch process in a large-scale SBCR to show the sensitivity to the axial dispersion coefficient. A 1D model was used to describe the system in an unsteady state mode of operation. In this reactor, heat is removed by internal tubes; the volume of these tubes is small in comparison to the reactor volume. Such a model with first-order kinetics to describe the Fischer–Tropsch reaction was published by de Swart and Krishna (2002), and with a more realistic Langmuir–Hinshelwood kinetic model (Yates and Satterfield, 1991) by Hooshyar et al. (2009).

Table 1. Mathematical model for mass and heat balances in a SBCR (Hooshyar et al., 2009)

Mass balance for *i*th component in large bubbles is:

$$\varepsilon_b \frac{\partial C_{i,g,large}}{\partial t} = \frac{\partial}{\partial z}\left(\varepsilon_b E_{g,large} \frac{\partial C_{i,g,large}}{\partial z}\right) - \frac{\partial}{\partial z}[(U_{sg} - U_{df})C_{i,g,large}] - k_{L,i,large} a_{large}(C^*_{i,large} - C_{i,L})$$

$$C^*_{i,large} = C_{i,g,large}/m_i$$

Mass balance for *i*th component in small bubbles is:

$$\varepsilon_{small} \frac{\partial C_{i,g,small}}{\partial t} = \frac{\partial}{\partial z}\left(\varepsilon_{small} E_{g,small} \frac{\partial C_{i,g,small}}{\partial z}\right) - \frac{\partial}{\partial z}(U_{df} C_{i,g,small}) - k_{L,i,small} a_{small}(C^*_{i,small} - C_{i,L})$$

$$C^*_{i,small} = C_{i,g,small}/m_i$$

Mass balance for *i*th component in liquid phase is:

$$\varepsilon_L \frac{\partial C_{i,L}}{\partial t} = \frac{\partial}{\partial z}\left(\varepsilon_L E_L \frac{\partial C_{i,L}}{\partial z}\right) - \frac{\partial}{\partial z}(U_{ss} C_{i,L}) + k_{L,i,large} a_{large}(C^*_{i,large} - C_{i,L}) + k_{L,i,small} a_{small}(C^*_{i,small} - C_{i,L}) - C_s \varepsilon_L \rho_p \sum_{j=1}^{nr} \upsilon_{ij} R_j$$

Heat balance is derived as:

$$\rho_s C_{ps} \varepsilon_L \frac{\partial T}{\partial t} = \frac{\partial}{\partial z}\left(\varepsilon_L \lambda_{ax} \frac{\partial T}{\partial z}\right) - U_{ss} \rho_s C_{ps} \frac{\partial T}{\partial z} - \alpha_{eff} a_w (T - T_c) + C_s \varepsilon_L \sum_{j=1}^{nr} (-\Delta H_{Ri}) R_j$$

The mathematical model for mass and heat transfer in the SBCR is presented in Table 1 and operating conditions have been summarised in Table 2.

Figure 3 shows the dimensionless hydrogen concentration in both the liquid and gas phase and the conversion as a function of the axial position in the reactor. The previous results (Hooshyar et al., 2009) showed that after 7 min the concentrations of synthesis gas in both the gas and liquid phase reached a steady mode. The modelling results presented in this paper are obtained after $t = 3$ h to ensure steady state. Figure 3 illustrates that the concentration of H_2 in the small bubbles behaves rather similarly to the H_2 concentration in the liquid phase as a result of the backmixing ($E_{g,small} = E_L$). The H_2 concentration in the large bubbles, for which less backmixing has been assumed ($E_{g,large} = 0.03\ m^2/s$), is higher in the lower part of the reactor.

The axial dispersion coefficient of the liquid phase is calculated using the relation proposed by Deckwer et al. (1982):

$$E_L = 0.768 U_{sg0}^{0.32} D_T^{1.34} \quad (1)$$

Figure 4 shows the syngas conversion as a function of the axial position in the reactor. The magnitude of the liquid axial dispersion coefficient, E_L, for a column with inner diameter of 7.5 m and inlet superficial gas velocity of 0.1 m/s was $5.5\ m^2/s$ for a SBCR and shows a large deviation from plug flow (Levenspiel, 1993). Figure 4 shows that a decrease in axial dispersion coefficient will increase the syngas conversion at the top half of the reactor. With high axial dispersion, in which the reactor is well mixed: this will lead to a higher local conversion in the bottom part of the column—the product is returned to the bottom—but a lower overall conversion. Decreasing axial dispersion shifts the behaviour of the reactor to plug flow. The figure clearly shows that it is advantageous to decrease the axial dispersion. This provides the motivation for our research: can we reduce the axial mixing by imposing dynamic structure to the slurry bubble column? We have chosen dynamic structuring as it might provide a flexible way of operating slurry bubble columns.

Table 2. Operating conditions (de Swart and Krishna, 2002)

Operating conditions	Value	Dimension
Reactor pressure (P)	3.0	MPa
Reactor diameter (D_T)	7.5	m
Reactor height (H)	30.0	m
Inlet temperature of syngas (T_i)	501	K
Temperature of coolant (T_c)	501	K
Area for heat transfer (a_w)	10	m^2 (m^3 reactor)$^{-1}$
Superficial inlet gas velocity (U_{sg0})	0.1	m/s
Slurry velocity (U_{ss})	0.01	m/s

EXPERIMENTAL

Set-Up

Our group has used a special needle sparger to inject gas into a bubble column in a very even way (Harteveld, 2005; Mudde et al., 2009). The high-pressure drop over the needles results in an effective decoupling of the gas supply system and the bubbles formed at the outlet of the needle. This results in the formation of mono-sized bubbles and a very uniform bubble size distribution in the entire bottom region of the column (see Figure 5). In this work, we apply this sparger also to *slurry* bubble columns.

Our experiments are carried out in both a 2D and 3D set-up. The 2D column (width × depth × height = 240 mm × 40 mm × 1000 mm) consists of a gas injection system with 95 needles each with an inner diameter of 0.8 mm. The needles are placed in a triangular pattern with a pitch of 6 mm. The 3D set-up

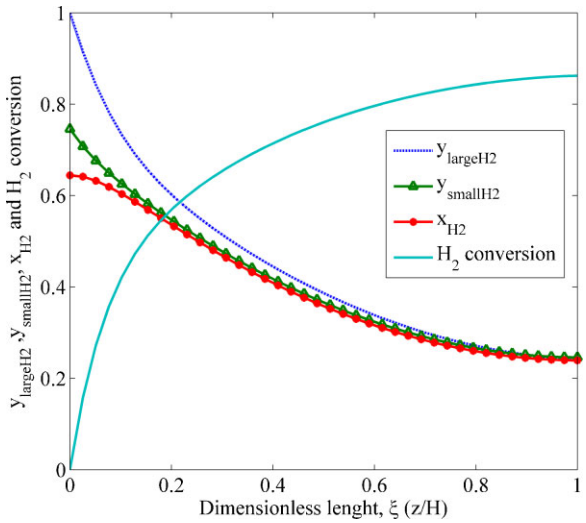

Figure 3. Dimensionless hydrogen concentration and conversion profile in a slurry bubble column reactor under steady-state condition with: $D_T = 7.5$ m, $H = 30$ m, and $U_{sg0} = 0.1$ m/s (Hooshyar et al., 2009).

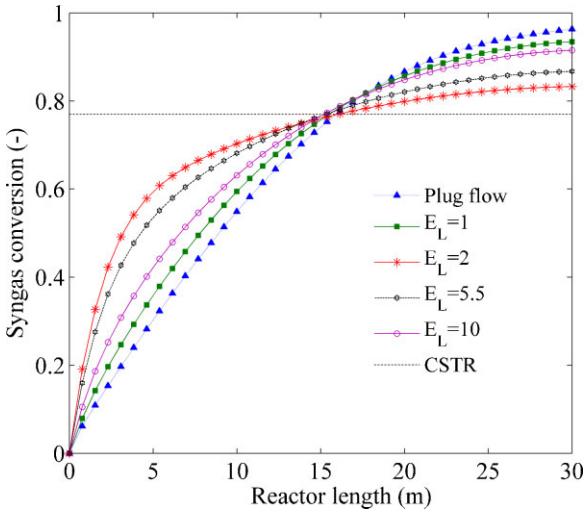

Figure 4. Syngas conversion versus reactor length for different values of the liquid axial dispersion coefficient in a slurry bubble column reactor with $D_T = 7.5$ m, $H = 30$ m, $U_{sg0} = 0.1$ m/s. Note that E_L dimension is in m^2/s.

has an inner diameter of 150 mm and is equipped with a needle sparger with 559 needles of which the upper tip is located 5 mm above the column bottom. The needles are grouped in 11 groups; this arrangement gives the possibility to control the gas flow through the needles and achieve a very homogeneous flow over the entire column cross-section. A schematic diagram of the column is shown in Figure 6.

The columns are filled with water as the liquid phase and air is injected from the bottom. Glass beads with a mean diameter of 108 μm and a density of 2500 kg/m^3 are used as solid phase in our studies.

Measurement Technique

Optical probes are used to measure the gas fraction and bubble dynamics. The probes in our study are working on the principle of the difference in light refraction between probe material (glass or plastic), water, and air. The local gas fraction and bubble dynamics are obtained by analysing and processing the response from the probes. Gas fraction profiles are measured by using a single-point optical probe and bubble velocity and size are measured by a four-point probe (Xue et al., 2003; Harteveld, 2005; Mudde et al., 2009). The single-point probe increases the accuracy of the gas fraction measurement.

Figure 5. Bubble formation by a needle sparger in a bubble column with one-third of the needles in operation (Mudde et al., 2009).

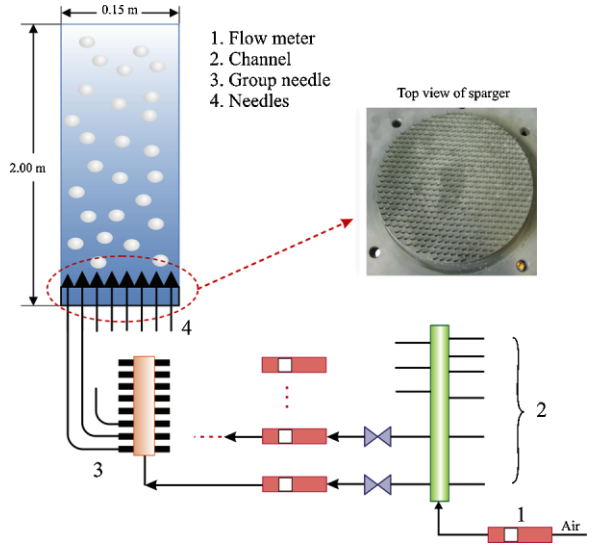

Figure 6. Schematic diagram of the experimental set-up.

Figure 7 shows the four-point probe configuration, with $\Delta S = 1.7$ mm and $d_p = 0.6$ mm. Tips (T_1, T_2, and T_3) are in a horizontal plane, while the central tip T_C is located a distance ΔS from this plane. Probes (250 μm diameter) are glued together and placed vertically in the column to detect the bubbles.

For gas fraction measurements, the recorded time series are converted to binaries via a threshold value, th_α. The threshold value is set at 10% of the difference between the voltage value of the tip in the air (s_a) and that in the water (s_w) (Mudde et al., 2009):

$$b(t_j) = \begin{cases} 1, & \text{if } s(t_j) > \text{th}_\alpha = 0.1(s_a - s_w) + s_w \\ 0, & \text{else} \end{cases} \quad (2)$$

The local gas fraction is obtained as follows:

$$\alpha = \frac{\sum_{j=1}^{N} b(t_j) \cdot \Delta t_s}{N \Delta t_s} \quad (3)$$

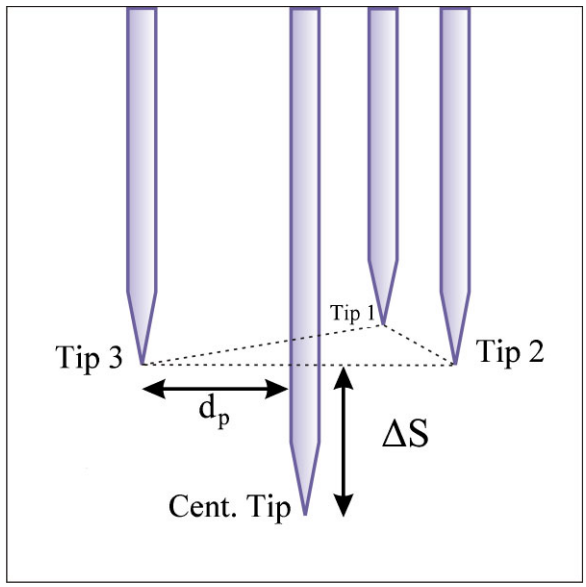

Figure 7. Configuration of the four-point optical probe.

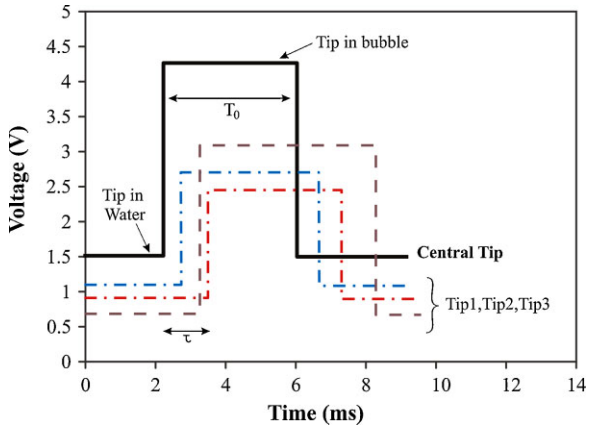

Figure 8. Schematic response of the piercing single bubble. The noise is not considered.

in which N is the total number of samples and Δt_s is the sample time. Figure 8 schematically shows the signal of a single bubble passing the four-point probe.

The bubble velocity is calculated from:

$$U_b = \frac{\Delta S}{\tau} \tag{4}$$

and the bubble chord length from:

$$L_b = U_b T_0 \tag{5}$$

where τ is the average of the times of flight of a bubble from the central tip to the other tips (T_i, $i = 1, 2, 3$) and T_0 is the time of the central probe in the bubble (Mudde and Saito, 2001).

RESULTS AND DISCUSSION

At low superficial gas velocities the flow regime is homogeneous and the gas fraction increases linearly with increasing superficial gas velocity. The transition from homogeneous flow regime to heterogeneous flow regime occurs at $U_{sg,trans}$. Figure 9 shows a comparison of overall void fractions obtained with measuring the height of the bubbly mixtures, a porous plate sparger, and perforated plates with two different orifice sizes. In these measurements, the measurement errors are about 5% of the value of the gas fraction. Using the needle sparger gives the transition velocity of 0.059 m/s, which is higher than for the other spargers. At $U_{sg,trans} > 0.059$ m/s, large dynamic structures are observed in the top of the 3D column with the needle sparger. Figure 9 also shows that with the needle sparger much higher gas loadings can be achieved at high velocities. It shows that by structuring the flow we can extend the homogeneous flow regime. The difference is explained by the very uniform gas injection and a narrow bubble size distribution for the needle sparger.

Measuring the radial gas fraction profile (in $r/R = 0.93$, 0.67, 0.4, and 0.13) in a 3D bubble column (with the needle sparger) with single point glass fibres shows that at a gas velocity <0.06 m/s, the gas fraction in the cross-section of the column is very flat. This illustrates that vortical structures and backmixing are absent and a uniform flow exists in the column. At higher gas velocity the wall region has the lowest gas fraction (see Figure 10). It supports the visual observation of a downward motion of the liquid, driving bubbles away from the wall. Note that bubbles which are going downward have a smaller probability of being

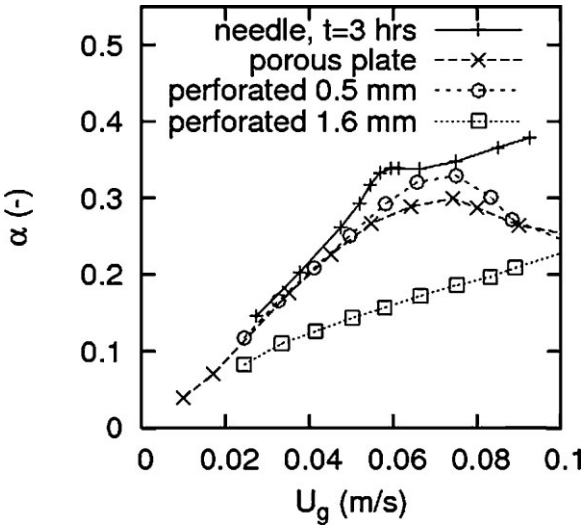

Figure 9. Comparison of gas fraction in bubble columns with different gas spargers (Harteveld, 2005).

pierced by the probe. Figure 10 shows that near the centre of the column the gas fraction still increases with U_{sg}.

We also investigate the effects of solids concentration on the gas fraction and bubble velocity and size using a four-point optical probe. Our results indicate that adding glass beads to an air–water system decreases the local gas fraction. The 15% reduction in the gas fraction in the heterogeneous flow regime is clear in Figure 11. Visual observations support the results from the optical probe: the presence of solids has more effect at higher superficial gas velocities due to enhanced liquid circulation and formation of some larger bubbles in the system. It should be noted that C_s is the solids volume fraction in gas-free slurry.

Figure 12 shows that increasing the solids concentration increases the average bubble chord.

Bubble velocity measurements at $U_{sg} = 0.044$ m/s show that an increase in solids concentration to 10% shifts the average bubble velocity from 0.22 to 0.30 m/s. Moreover, a wider range of bubble velocities appears in the column (see Figure 13).

Figure 14 shows the bubble chord length distribution at $U_{sg} = 0.044$ m/s measured by the optical probe. This graph shows that the average bubble chord length shifts from 2.6 to 2.9 mm when the solids concentration increases to 10%. Assuming a con-

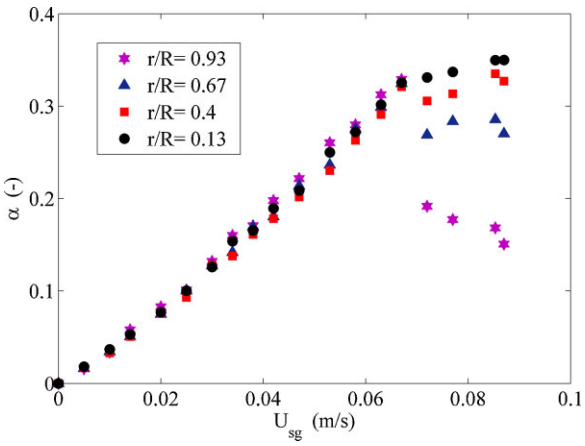

Figure 10. Local radial gas fraction for an air–water system in the 3D column with the needle sparger.

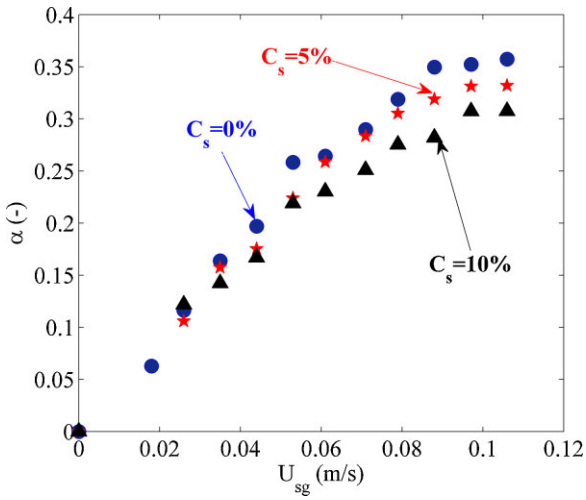

Figure 11. Effect of solids concentration (volume %) on gas volume fraction in the centre of the 2D column with the needle sparger.

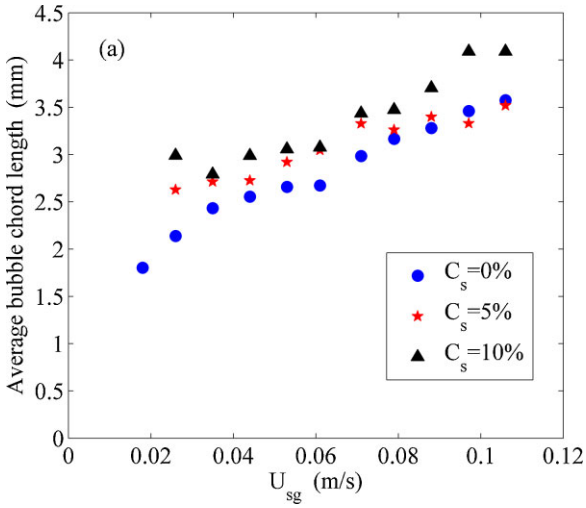

Figure 12. Effect of solids concentration (volume %) on the average bubble chord length in the centre of the 2D column with the needle sparger.

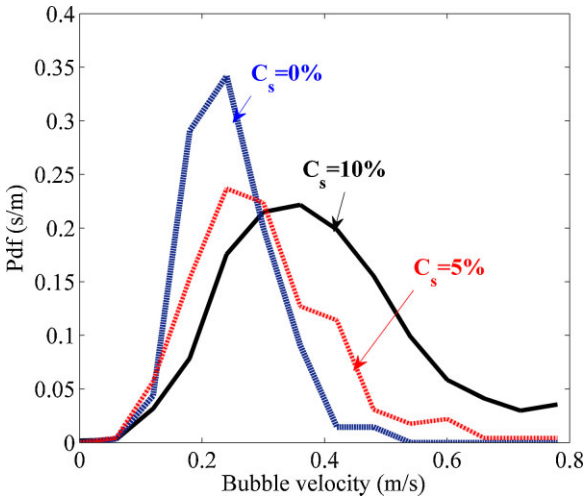

Figure 13. Effect of solids concentration (volume %) on bubble velocity in the centre of a 2D column with the needle sparger ($U_{sg} = 0.044$ m/s).

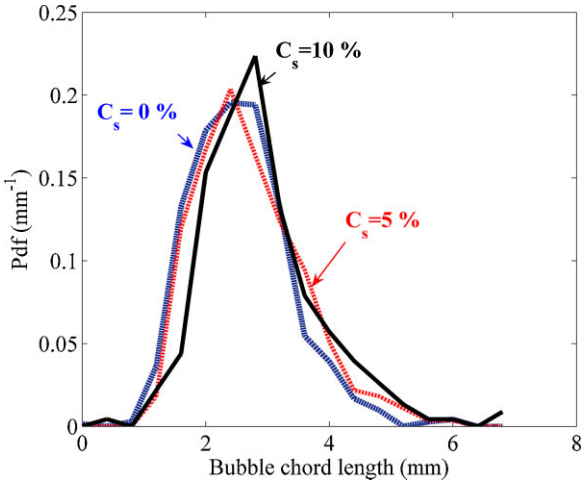

Figure 14. Effect of solids concentration (volume %) on bubble chord length distribution in 2D column with the needle sparger ($U_{sg} = 0.044$ m/s).

stant drag coefficient, C_D, for the system and neglecting the liquid velocity, we expect from a force balance that the 16% increase in the bubble chord length due to the addition of solids would increase the velocity of the bubble by a factor of 1.1 ($U_b \propto \sqrt{L_b}$). Our measurements show that at a solids concentration of 10%, the average bubble velocity increased to 1.36 times the average bubble velocity in an air–water system. A comparison between theory and experimental results shows that the drag coefficient and Reynolds number are not constant and have changed. The drag coefficient is a function of geometry and Reynolds number, and therefore of the physical properties of the liquid phase. A change in the physical properties of the slurry phase not only affects the size and velocity of the bubbles but also the drag coefficient.

Furthermore, our visual observations indicate that adding solids to the system increases the liquid circulation and although some large bubbles form, there are still many small bubbles present in the column. We can conclude that the increase in bubble velocity is not only due to the appearance of larger bubbles, but also to liquid circulation. In future work, we will study the effect of liquid circulation patterns more in detail.

Figure 14 shows that the presence of solids hardly affects the width of the bubble size distribution; it only shifts the entire distribution to slightly larger bubbles. This is probably the effect of the needle sparger which injects small bubbles of a constant size.

CONCLUSIONS

Previous studies show that structuring of slurry bubble columns via application of special spargers, inducing vibration to the liquid, or using structured packings helps to control the flow behaviour and to decrease the axial dispersion. Of these methods, vibration will be the most complicated one to apply to large-scale reactors.

Axial dispersion in the liquid phase depends on various parameters such as reactor geometry and superficial gas velocity. From the modelling results we observed a higher conversion in the Fischer–Tropsch synthesis for a system with a smaller axial dispersion coefficient, that is, in our model a decrease in axial dispersion coefficient by 82% gives an increase in conversion of 7.7%. We are looking for a methodology to control the system in such a way that a desired flow pattern is imposed on the system in order

to obtain lower axial dispersion. Using a needle sparger for gas injection gives us the possibility to control the local flow rate and generate uniform flow without any large-scale structures over the entire of the column for higher superficial gas velocities.

Using optical probes, we have shown that the use of a more structured system in a 2D and 3D column results in a shift of the transition point to higher superficial gas velocities. Furthermore, for superficial gas velocities above the transition point the gas fraction still increases continuously. With the aid of a four-point optical probe we showed that the bubble velocity distribution in a three-phase slurry system is strongly affected by the presence of the solids: the distribution becomes wider and its average occurs at higher bubble velocities. Adding 10% solids to the system affects the physical properties of the slurry phase and enhances the bubble rise velocity. Moreover, we showed that the bubble size stays rather constant. The increase in average bubble velocity is not only due to the changes in the physical properties of the system but also liquid circulation contributes which will be studied in future work.

NOMENCLATURE

a_{large}	gas–liquid specific area for large bubbles (m^2/m^3)
a_{small}	gas–liquid specific area for small bubbles (m^2/m^3)
a_w	cooling tube specific external surface area referred to the total reactor volume (m^2/m^3)
B	binary value
C_D	drag coefficient
$C_{i,g0}$	concentration of i in the gas phase at reactor inlet (mol/m^3)
$C_{i,g,small}$	concentration of i in small bubbles (mol/m^3)
$C_{i,g,large}$	concentration of i in large bubbles (mol/m^3)
$C_{i,L}$	concentration of i in liquid (mol/m^3)
$C_{P,s}$	heat capacity of the slurry (J/kg K)
C_s	solids volume fraction in gas free slurry
d_p	radial distance between central tip and other tips (m)
d_s	solid average diameter (m)
D_T	column diameter (m)
$E_{g,\text{large}}$	axial dispersion coefficient of the large bubbles (m^2/s)
$E_{g,\text{small}}$	axial dispersion coefficient of the small bubbles (m^2/s)
E_L	axial dispersion coefficient of the liquid phase (m^2/s)
H	reactor height (m)
$k_{L,i,small}$	volume mass transfer coefficient of i with small bubbles (L/s)
$k_{L,i,large}$	volume mass transfer coefficient of i with large bubbles (L/s)
L_B	bubble chord length (m)
m_i	Henry's coefficient
N	number of samples
nr	number of independent reaction
ns	number of species
P	total pressure (Pa)
r	radial position (m)
R	column radius (m)
s_s	output value of the tip in air (V)
s_w	output value of the tip in water (V)
$\triangle S$	axial distance between central tip and other tips (m)
t	time (s)
$\triangle t_s$	sample time (s)
th_α	threshold value
T	temperature (K)
T_c	cooling temperature (K)
T_i, $i=0, 1, 2, 3$	time interval that tip i spend in the bubble (s)
U_b	bubble velocity (m/s)
U_{df}	superficial velocity of gas through the dense phase (m/s)
U_{ex}	liquid exchange velocity (m/s)
U_{sg}	superficial gas velocity (m/s)
$(U_{sg}-U_{df})$	superficial gas velocity through the dilute phase (m/s)
U_{ss}	superficial slurry velocity (m/s)
x_i	dimensionless i concentration in liquid phase
X_i	conversion of i
$y_{i,large}$	dimensionless i concentration in large bubbles
$y_{i,small}$	dimensionless i concentration in small bubbles
Z	height above the gas distributor (m)

Greek Symbols

α	gas fraction
α_{eff}	slurry to internal coil wall conversion heat transfer coefficient (W/m^2 K)
ε_b	holdup in large bubbles
ε_L	liquid holdup
$\varepsilon_{\text{small}}$	holdup in small bubbles
λ_{ax}	effective axial heat conductivity of the liquid–solid suspension (W/m K)
ξ	axial coordinate, z/H
ρ_g	gas density (kg/m^3)
ρ_L	liquid density (kg/m^3)
ρ_P	particle density (kg/m^3)
ρ_s	slurry density (kg/m^3)
τ	average time (s)
Φ	inversion point

REFERENCES

Baird, M. H. I. and R. G. Rice, "Axial Dispersion in Large Unbaffled Columns," Chem. Eng. J. **9**, 171–174 (1975).

Behkish, A., R. Lemoine, L. Sehabiague, R. Qukaci and B. I. Morsi, "Gas Holdup and Bubble Size Behavior in a Large-Scale Slurry Bubble Column Reactor Operating With an Organic Liquid under Elevated Pressures and Temperatures," Chem. Eng. J. **128**, 69–84 (2007).

Chilekar, V. P., M. J. F. Warnier, J. Van Der Schaaf, B. F. M. Kuster, J. C. Schouten and J. R. van Ommen, "Bubble Size Estimation in Slurry Bubble Columns from Pressure Fluctuations," AIChE J. **51**, 1924–1937 (2005).

de Swart, J. W. A. and R. Krishna, "Simulation of the Transient and Steady State Behaviour of a Bubble Column Slurry Reactor for Fischer-Tropsch Synthesis," Chem. Eng. Process. **41**, 35–47 (2002).

de Vries, J., S. Luther and D. Lohse, "Induced Bubble Shape Oscillations and Their Impact on the Rise Velocity," Eur. Phys. J. B **29**, 503–509 (2002).

Deckwer, W. D., Y. Serpemen, M. Ralek and B. Schmidt, "Modeling the Fischer-Tropsch Synthesis in the Slurry Phase," Ind. Eng. Chem. Process. Des. Dev. **21**, 231–241 (1982).

Drahoš, J., J. Zahradník, M. Fialová and F. Bradka, "Identification and Modelling of Liquid Flow Structures in Bubble Column Reactors," Chem. Eng. Sci. **47**, 3313–3320 (1992).

Dreher, A. J. and R. Krishna, "Liquid-Phase Backmixing in Bubble Columns, Structured by Introduction of Partition Plates," Catal. Today **69**, 165–170 (2001).

Ellenberger, J. and R. Krishna, "Improving Mass Transfer in Gas-Liquid Dispersions by Vibration Excitement," Chem. Eng. Sci. **57**, 4809–4815 (2002).

Ellenberger, J. and R. Krishna, "Intensification of Slurry Bubble Columns by Vibration Excitement," Can. J. Chem. Eng. **81**(3-4), 655–659 (2003a).

Ellenberger, J. and R. Krishna, "Shaken, Not Stirred, Bubble Column Reactors: Enhancement of Mass Transfer by Vibration Excitement," Chem. Eng. Sci. **58**, 705–710 (2003b).

Groen, J. S., R. G. C. Oldemam, R. F. Mudde and H. E. A. van den Akker, "Coherent Structures and Axial Dispersion in Bubble Column Reactors," Chem. Eng. Sci. **51**, 2511–2520 (1996).

Guet, S., R. V. Fortunati, R. F. Mudde and G. Ooms, "Bubble Velocity and Size Measurement With a Four-Point Optical Fiber Probe," Part. Part. Syst. Charact. **20**, 219–230 (2003).

Harteveld, W. K., "Bubble Columns: Structures or Stability?" PhD Thesis, Delft, the Netherlands (2005).

Heijnen, J. J. and K. van't Riet, "Mass Transfer, Mixing and Heat Transfer Phenomena in Low Viscosity Bubble Column Reactors," Chem. Eng. J. **28**, B21–B42 (1984).

Hooshyar, N., S. H. Fatmei and M. Rahmani, "Mathematical Modeling of Fischer-Tropsch in Industrial Slurry Bubble Columns," Int. J. Chem. React. Eng. **7**, A23 (2009).

Kantarci, N., F. Borak and K. O. Ulgen, "Bubble Column Reactors," Process Biochem. **40**, 2263–2283 (2005).

Knopf, F. C., J. Ma, R. G. Rice and D. Nikitopoulos, "Pulsing to Improve Bubble Column Performance: I. Low Gas Rates," AIChE J. **52**, 1103–1115 (2006a).

Knopf, F. C., Y. Waghmare, J. Ma and R. G. Rice, "Pulsing to Improve Bubble Column Performance: II. Jetting Gas Rates," AIChE J. **52**, 1116–1126 (2006b).

Krishna, R., "A Scale-Up Strategy for a Commercial Scale Bubble Column Slurry Reactor for Fischer-Tropsch Synthesis," Oil Gas Sci. Tech. **55**(4), 359–393 (2000).

Krishna, R., J. Ellenberger and C. Maretto, "Flow Regime Transition in Bubble Columns," Int. Commun. Heat Mass Trans. **26**, 467–475 (1999a).

Krishna, R., M. I. Urseanu, J. M. van Baten and J. Ellenberger, "Influence of Scale on the Hydrodynamics of Bubble Columns Operating in the Churn-Turbulent Regime: Experiments vs. Eulerian Simulations," Chem. Eng. Sci. **54**, 4903–4911 (1999b).

Krishna, R., M. I. Urseanu, J. M. van Baten and J. Ellenberger, "Liquid Phase Dispersion in Bubble Columns Operating in the Churn-Turbulent Flow Regime," Chem. Eng. J. **78**, 43–51 (2000a).

Krishna, R., J. M. van Baten and M. I. Urseanu, "Three-Phase Eulerian Simulations of Bubble Column Reactors Operating in the Churn-Turbulent Regime: A Scale Up Strategy," Chem. Eng. Sci. **55**, 3275–3286 (2000b).

Lakota, A., M. Jazbec and J. Levee, "Impact of Structured Packing on Bubble Column Mass Transfer Characteristics: Part 1. Backmixing in the Liquid Phase," Acta Chim. Slov. **48**, 453–468 (2001).

Levenspiel, O., "The Chemical Reactor Omnibook," OSU Book Stores, Inc., Corvallis, OR (1993).

Maretto, C. and R. Krishna, "Modelling of a Bubble Column Slurry Reactor for Fischer-Tropsch Synthesis," Catal. Today **52**, 279–289 (1999).

Maretto, C. and R. Krishna, "Design and Optimisation of a Multi-Stage Bubble Column Slurry Reactor for Fischer-Tropsch Synthesis," Catal. Today **66**, 241–248 (2001).

Mudde, R. F. and T. Saito, "Hydrodynamical Similarities between Bubble Column and Bubbly Pipe Flow," J. Fluid Mech. **437**, 203–228 (2001).

Mudde, R. F., W. K. Harteveld and H. E. A. van den Akker, "Uniform Flow in Bubble Columns," Ind. Eng. Chem. Res. **48**, 148–158 (2009).

Nevers, N. D., "Bubble Driven Fluid Circulations," AIChE J. **14**, 222–226 (1968).

Ribeiro, C. P. Jr. and P. L. C. Lage, "Gas-Liquid Direct-Contact Evaporation: A review," Chem. Eng. Technol. **28**, 1081–1107 (2005).

Shah, Y. T., B. G. Kelkar, S. P. Godbole and W. D. Deckwer, "Design Parameters Estimations for Bubble Column Reactors," AIChE J. **28**, 353–379 (1982).

Smith, G. B., B. R. Gamblin and D. Newton, "X-Ray Imaging of Slurry Bubble Column Reactors: The Effects of System Pressure and Scale," Chem. Eng. Res. Des. **73**, 632–636 (1995).

Urseanu, M. I., J. Ellenberger and R. Krishna, "A Structured Catalytic Bubble Column Reactor: Hydrodynamics and Mixing Studies," Catal. Today **69**, 105–113 (2001).

van der Schaaf, J., V. P. Chilekar, J. R. van Ommen, B. F. M. Kuster, J. Tinge and J. C. Schouten, "Effect of Particle Lyophobicity in Slurry Bubble Columns at Elevated Pressures," Chem. Eng. Sci. **62**(18–20), 5533–5537 (2007).

van Ommen, J. R. and R. F. Mudde, "Measuring the Gas-Solids Distribution in Fluidized Beds—A Review," Int. J. Chem. React. Eng. **6**, R3 (2008).

van Ommen, J. R., J. Nijenhuis, C. M. van den Bleek and M. O. Coppens, "Four Ways to Introduce Structure in Fluidized Bed Reactors," Ind. Eng. Chem. Res. **46**, 4236–4244 (2007).

Villa, J., J. R. van Ommen and C. M. van den Bleek, "Early Detection of Foam Formation in Bubble Columns by Attractor Comparison," AIChE J. **49**, 2442–2444 (2003).

Waghmare, Y. G., C. A. Dorao, H. A. Jakobsen, F. C. Knopf and R. G. Rice, "Bubble Size Distribution for a Bubble Column Reactor Undergoing Forced Oscillations," Ind. Eng. Chem. Res. **48**, 1786–1796 (2009).

Wang, T., J. Wang and Y. Jin, "Slurry Reactors for Gas-to-Liquid Processes: A Review," Ind. Eng. Chem. Res. **46**, 5824–5847 (2007).

Xue, J., M. Al-Dahhan, M. P. Dudukovic and R. F. Mudde, "Bubble Dynamics Measurements Using Four-Point Optical Probe," Can. J. Chem. Eng. **81**(3-4), 375–381 (2003).

Xue, J., M. Al-Dahhan, M. P. Dudukovic and R. F. Mudde, "Bubble Velocity, Size, and Interfacial Area Measurements in a Bubble Column by Four-Point Optical Probe," AIChE J. **54**, 350–363 (2008a).

Xue, J., M. Al-Dahhan, M. P. Dudukovic and R. F. Mudde, "Four-Point Optical Probe for Measurement of Bubble Dynamics: Validation of the Technique," Flow Meas. Inst. **19**, 293–300 (2008b).

Yang, Z., U. Rustemeyer, R. Buchholz and U. Onken, "Profile of Liquid Flow in Bubble Columns," Chem. Eng. Commun. **49**, 51–67 (1986).

Yang, Y. B., N. Devanathan and M. P. Dudukovic, "Liquid Backmixing in Bubble Columns," Chem. Eng. Sci. **47**, 2859–2864 (1992).
Yates, I. C. and C. N. Satterfield, "Intrinsic Kinetics of the Fischer-Tropsch Synthesis on a Cobalt Catalyst," Energy Fuels **5**, 168–173 (1991).
Zhang, L. J., T. Li, W. Y. Ying and D. Y. Fang, "Experimental Study on Bubble Rising and Descending Velocity Distribution in a Slurry Bubble Column Reactor," Chem. Eng. Technol. **31**, 1362–1368 (2008).

Manuscript received November 28, 2009; revised manuscript received February 2, 2010; accepted for publication February 4, 2010

Paper III

Gas fraction and bubble dynamics in structured slurry bubble columns

Has been published in Industrial and Engineering Chemistry Research.

Gas Fraction and Bubble Dynamics in Structured Slurry Bubble Columns

Nasim Hooshyar,*,† Peter J. Hamersma,† Robert F. Mudde,‡ and J. Ruud van Ommen†

Chemical Engineering Department, Delft University of Technology, Julianalaan 136, 2628 BL Delft, The Netherlands, and Kramers Laboratorium voor Fysische Technologie, Delft University of Technology, Pr. Bernardlaan 6, 2628 BW Delft, The Netherlands

With the aim of structuring the flow and reducing backmixing in slurry bubble columns, we investigate the effect of needle spargers in three-phase systems. We apply optical probes in a 2D and 3D column to measure the bubble dynamics and gas fraction. Experimental results for air−water−glass beads show that an increase in solids volume fraction (1) decreases the gas fraction, (2) shifts the transition point from homogeneous to heterogeneous flow to a lower gas velocity, (3) increases the mean bubble velocity by 60−100% in the range of superficial gas velocities from 0.02 to 0.1 m/s, and (4) has only a limited effect on the bubble size distribution. Fitting our experimental data to the Richardson and Zaki and Garnier models shows that we cannot use the model coefficients they report in their papers. However, fitting our data results in realistic values for the terminal bubble velocity in a swarm. By using needle spargers, giving a very uniform gas supply, a first step toward structuring the hydrodynamics of slurry bubble columns has been taken.

1. Introduction

Many important reactions in the chemical industry concern both gases and liquids, while the reaction is catalyzed by a solid catalyst. The reactors used for these processes can roughly be divided in systems with mobile catalyst particles (often a slurry system) and systems with an immobilized catalyst. Typical problems in slurry systems are backmixing and solid separation, while fixed catalyst systems commonly show problems such as maldistribution and temperature gradients. Structuring the reaction environment is an attractive way to tackle the disadvantages of the current multiphase reactors. Structuring introduces extra degrees of freedom, allowing decoupling of conflicting design objectives and the possibility to optimize them independently. Although structuring is more commonly proposed for systems with a fixed catalyst structure,[1,2] it is also possible for reactors with a mobile catalyst, both for gas−solid[3] and gas−liquid−solid systems.[4]

To impose a structure on the hydrodynamics in a bubble column or slurry bubble column, several approaches are possible. In this paper, we will focus on structuring by manipulating the gas phase. In this case, two approaches are possible: temporal manipulation and spatial manipulation of the gas supply to come to structured hydrodynamics. The first approach—varying the gas supply in time—can in principle be done using feedback control. For example, it has been shown that it is possible to change the chaotic motion of a single train of gas bubbles rising in a liquid into a self-stabilized periodic motion by controlling the gas supply to the injector, keeping the average gas supply constant.[5] In practice, however, it is far from straightforward to measure the relevant properties in a bubble column or slurry bubble column and use this information for feedback control. The alternative approach is to apply "open-loop control": oscillating the gas supply without a feedback mechanism. To our best knowledge, this has not been tried yet, but other researchers have oscillated or vibrated the liquid or the whole system.[6−10] The influence of the sparger design on the hydrodynamics has been studied in various papers (see, e.g., the work of Kulkarni et al.,[11] Hebrard et al.,[12] and Thorat[13]). Harteveld and co-workers[14,15] studied a needle sparger, leading to bubble injection with a very homogeneous nature, regular both in time and space. Using this sparger, they were able to extend the more regular structure of the homogeneous regime in bubble columns to higher velocities than attainable for regular spargers. In this paper, we will demonstrate that this is also feasible for *slurry* bubble columns. Moreover, we will investigate the phenomena that play a role in the extension of the homogeneous regime.

2. Experimental Setup

The experiments are carried out in columns equipped with a special needle sparger to inject gas into the system in a very even way; our group has applied these spargers previously to bubble columns.[14,15] The high pressure drop over the needles results in an effective decoupling of the gas supply system and the bubbles formed at the outlet of the needle. This results in the formation of monosized bubbles and a very uniform bubble size distribution in the entire bottom region of the column. In this work, we apply this sparger to *slurry* bubble columns.

Our experiments are carried out in both a 2D and 3D setup. The 2D column (width × depth × height = 240 × 40 × 1000 mm) consists of a gas injection system with 95 needles, each with an inner diameter of 0.8 mm. The needles are placed in a triangular pattern with a pitch of 6 mm, and the upper tip is located 5 mm above the column bottom. The 3D setup is a cylindrical column with an inner diameter of 150 mm and is equipped with a needle sparger with 559 needles, of which the upper tip is located 5 mm above the column bottom. The needles are divided in eleven groups; this arrangement gives the possibility to control the gas flow through the needles and achieve a very homogeneous flow over the entire column cross section. A schematic diagram of the column is shown in Figure 1.

Water is used as the liquid phase, and air is used as the gas phase. Glass beads with a density of 2500 kg/m^3 are used as the solid phase in our studies. The range of the superficial gas velocities that have been applied is given in Table 1. This table

* Corresponding Author: E-mail address: n.hooshyar@tudelft.nl, Tel: +31 15 278 4753; Fax: +31 15 278 5006.

† Chemical Engineering Department, Delft University of Technology.

‡ Kramers Laboratorium voor Fysische Technologie, Delft University of Technology.

10.1021/ie100528c
Published on Web 10/06/2010

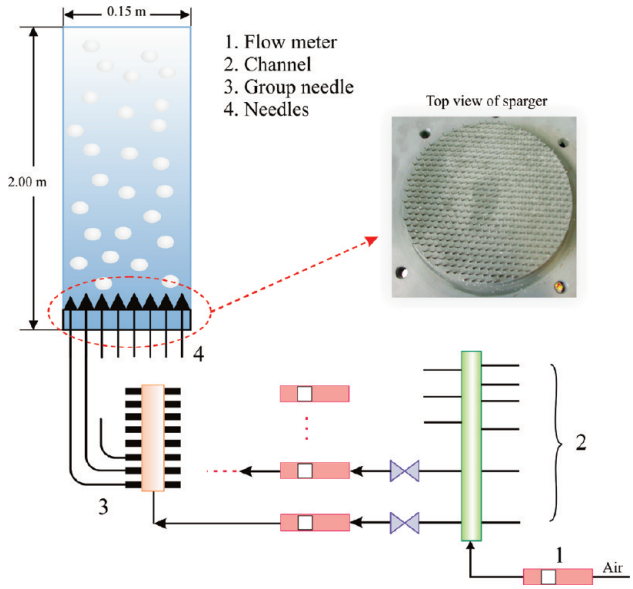

Figure 1. Schematic diagram of the 3D setup.[4]

Table 1. Range of Operating Parameters for the Gas Fraction and Bubble Dynamics Study

parameter	2D column	3D column
range of superficial gas velocity, U_{sg} (m/s)	0−0.10	0−0.106
solids mean size, d_s (μm)	108	78
range of solids volume fraction, C_s (%)	0−10	0−20

also shows the size and the volume fractions of the glass beads that have been used.

3. Experimental Technique

Optical probes are used to measure the gas fraction and bubble dynamics. The probes in our study are working on the principle of the difference in light refraction between probe material (plastic), water, and air. The local gas fraction and bubble dynamics are obtained by analyzing and processing the response from the probes.

Gas fraction profiles are measured by using a single-point optical probe, and bubble velocity and size are measured by a four-point probe.[14−16] The single-point probe increases the accuracy of the gas fraction measurement.

Various types of optical probes have been used in different studies for gas fraction and/or bubble dynamics measurements.[15,17−22] The most important difference between these probes is the number of the tips used. Single- or two-point probes are only suited for detecting bubbles that are rising in one direction. In the case of bubble columns, bubbles are moving in different directions. With the application of four-point probes,

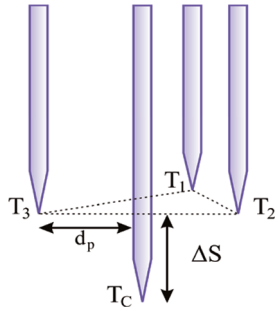

Figure 2. Four-point probe configuration: T_1 refers to tip one, T_2 refers to tip two, and T_3 refers to tip three.[4]

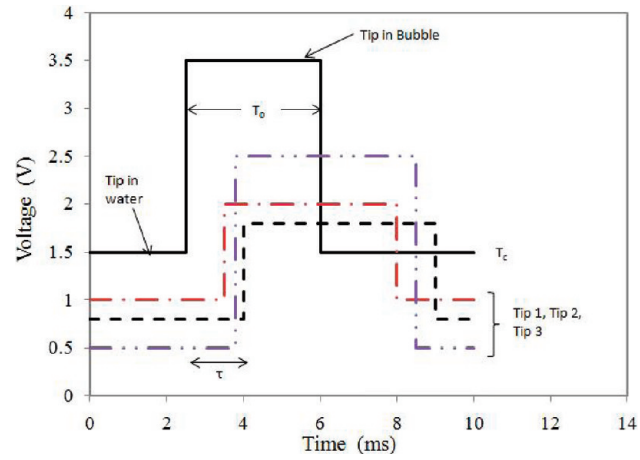

Figure 3. Schematic of the signals of a single bubble passing the four-point probe.[4]

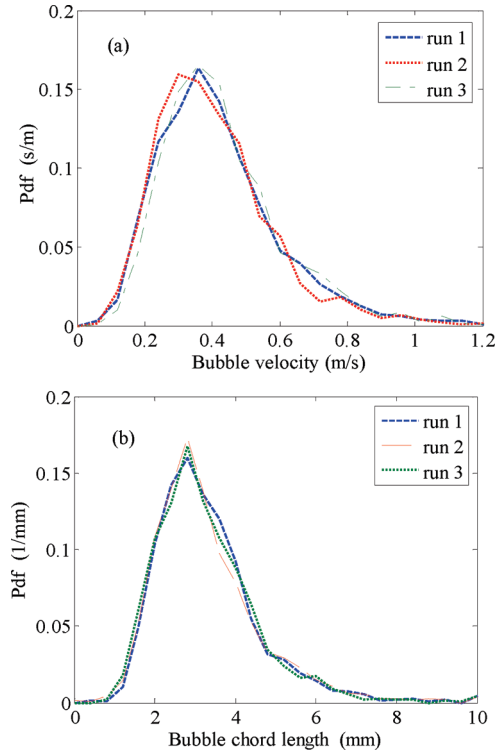

Figure 4. Reproducibility check for bubble velocity and bubble chord length, $U_{sg} = 0.088$ m/s in the 2D column. In run 1: $\langle U_b \rangle = 0.422$ m/s, $\langle L_b \rangle = 3.34$ mm; in run 2: $\langle U_b \rangle = 0.408$ m/s, $\langle L_b \rangle = 3.316$ mm; in run 3: $\langle U_b \rangle = 0.434$ m/s, $\langle L_b \rangle = 3.28$ mm.

it is possible to distinguish the signals from the bubbles with movement deviating from the probe axial direction.[14]

Figure 2 shows the four-point probe configuration, with $\Delta S = 1.7$ mm and $d_p = 0.6$ mm. Tips T_1, T_2, and T_3 form an equilateral triangle in a horizontal plane, while the central tip C is located a distance ΔS from this plane. The fibers (250 μm diameter) are glued together and placed vertically, facing downward, in the column to detect the bubbles.

3.1. Signal Analysis. For gas fraction measurements, the recorded time-series are converted to binaries via a threshold value, th_α. The threshold value is set at 10% of the difference between the voltage value of the tip in the air (s_a) and that in the water (s_w):[15]

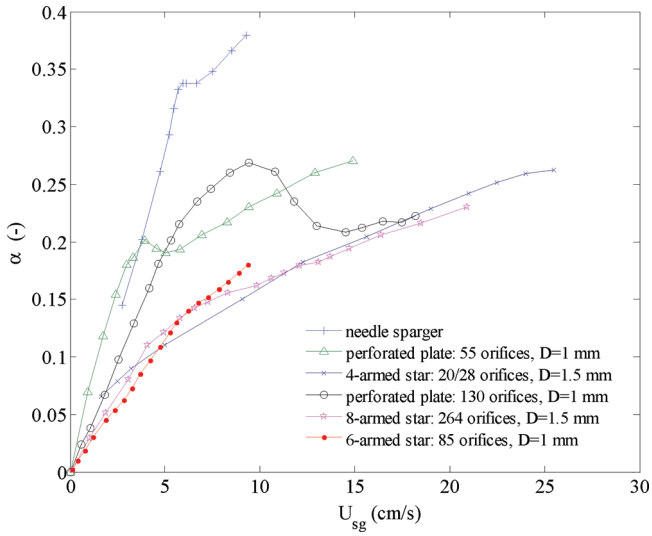

Figure 5. Comparison of the overall gas fraction in bubble columns with different gas injection systems: for the needle sparger, see Mudde et al.;[15] for the perforated plate with 55 orifice, see Jamialahmadi and Muller-Steinhagen;[24] for the perforated plate with 130 orifice, see Su and Heindel;[25] for the star spargers with 4, 6, and 8 stars, see Barghi et al.,[26] Al-Masry and Ali,[27] and Tang and Heindel,[28] respectively.

$$b(t_j) = \begin{cases} 1 \text{ if } s(t_j) > th_\alpha = 0.1(s_a - s_w) + s_w \\ 0 \text{ else} \end{cases} \quad (1)$$

The local gas fraction is obtained as follows:

$$\alpha = \frac{\sum_{j=1}^{N} b(t_j) \cdot \Delta t_s}{N \Delta t_s} \quad (2)$$

in which N is the total number of samples and Δt_s is the sample time. Figure 3 schematically shows the signal of a single bubble passing the four-point probe.

The bubble velocity is calculated by following a specific procedure.[23] First of all, the signal of the central tip is used to find the starting point of a bubble. This time is used as a reference to find the times the bubble is hitting the other three probes. For an axially symmetric bubble such as ellipsoidal bubbles, the trajectory of the central probe through the bubble upon hitting the bubble at its top is the bubble minor axis, so the three other probes respond almost simultaneously. The three time differences, τ_{ic}, are calculated:

$$\begin{gathered} \text{If } s_c(t_s) > th_v, \text{ bubble hits the central tip at time } t_s \\ \text{If } s_i(t_k) > th_v, \text{ bubble hits tip } i \text{ at time } t_k \\ \tau_{ic} = t_k - t_s \end{gathered} \quad (3)$$

The average of times of flight of a bubble from the central tip to the other tips, τ, is calculated as follows:

$$\tau = \frac{1}{3} \sum_{i=1}^{3} \tau_{ic} \quad (4)$$

A tolerance value is used to evaluate if these three time differences are coinciding:

$$\text{If} \left| \frac{\tau_{ic} - \tau}{\tau} \right| < \beta \forall i, \text{ the detected bubble is accepted} \quad (5)$$

The bubble velocity is determined as

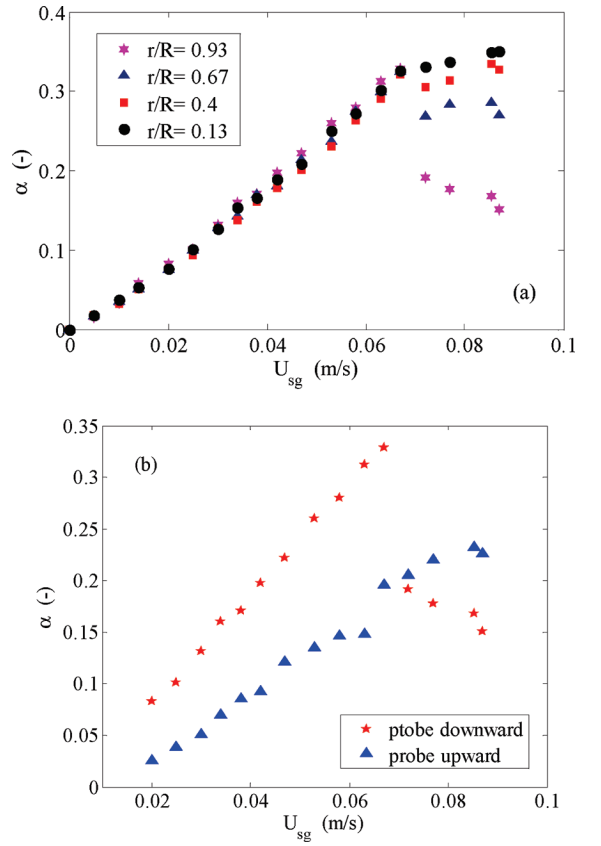

Figure 6. (a) Local radial gas fraction for an air−water system in the 3D column with the needle sparger.[4] (b) Effect of probe orientation on the gas holdup in the wall region (z = 47 cm).

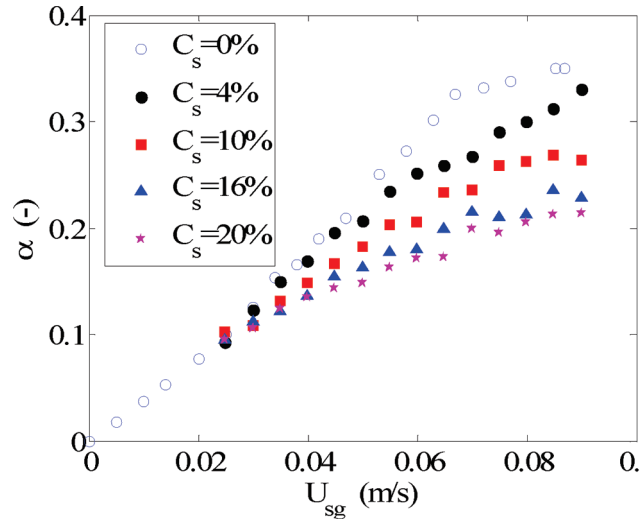

Figure 7. Effect of solids volume fraction (volume %) on the gas fraction in the center of the 3D column with needle sparger (z = 47 cm).

$$U_b = \frac{\Delta S}{\tau} \quad (4)$$

and the bubble chord length is calculated from

$$L_b = U_b T_0 \quad (5)$$

T_0 is the time the central probe is in the bubble.[15] Next, the search for the next bubble that hits the probe starts. The value we consider for the tolerance β is 0.25, which introduces a biasing in the bubble velocity data. This value limits the accepted

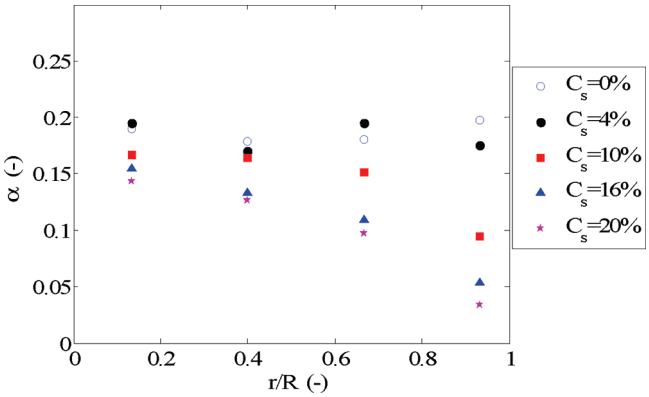

Figure 8. Effect of solids volume fraction (volume %) on local gas holdup profile in the 3D column with needle sparger (U_{sg} = 0.045 m/s, z = 47 cm).

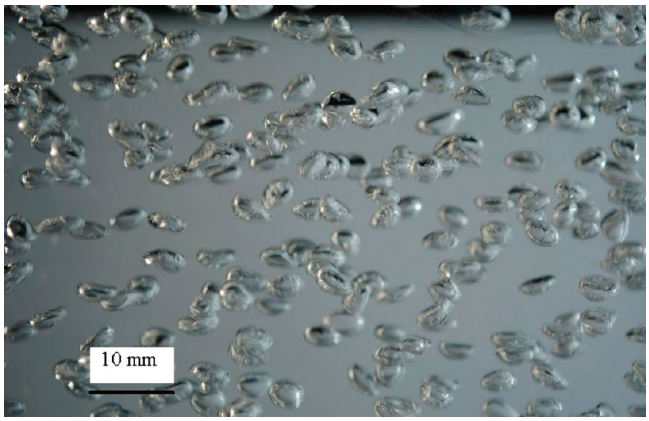

Figure 9. Image captured 40 cm above the sparger for an air−water system in the 2D bubble column, U_{sg} = 0.008 m/s.

bubbles to those bubbles that are rising vertically; it has been determined empirically.

3.2. Accuracy. We checked the accuracy of our measurements by repeating the measurements for different sampling times and chose Δt_s = 104 s as a proper and accurate sampling time for our experiments with the optical probes. The voltage signals are collected at a sampling frequency of 20 kHz.

To achieve accurate and reliable experimental results, both the reproducibility and sensitivity of the measurements with the optical probe are investigated. Figure 4 illustrates the repeatability of the bubble velocity and the bubble chord length measurements through three runs of experiments. The results of 3 different runs show that the average bubble velocity changes 6% and the average bubble chord length only changes 1.2%.

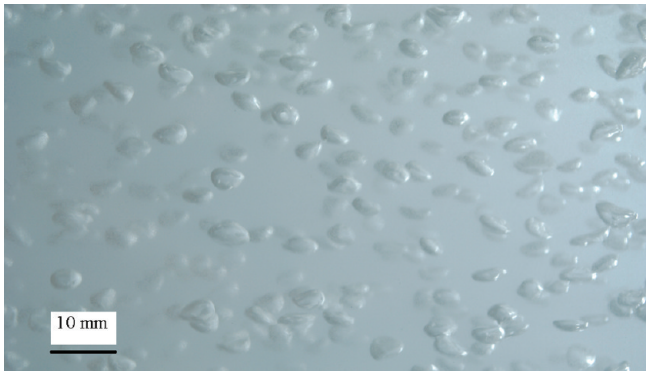

Figure 10. Image captured 40 cm above the sparger for a 1 vol % of a slurry system in the 2D column, U_{sg} = 0.008 m/s.

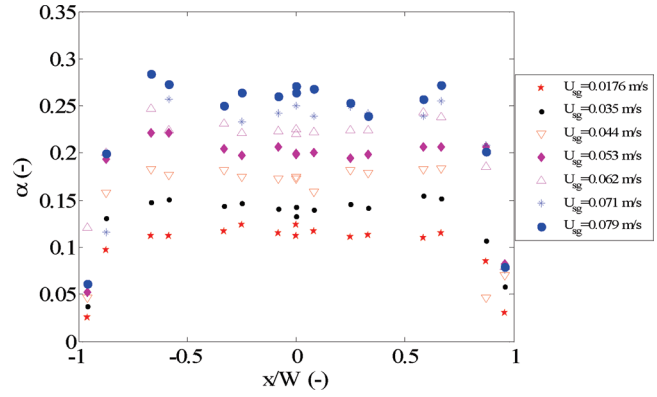

Figure 11. Effect of superficial gas velocity on the gas fraction profile in the 2D column with needle sparger (C_s = 10%, z = 27 cm).

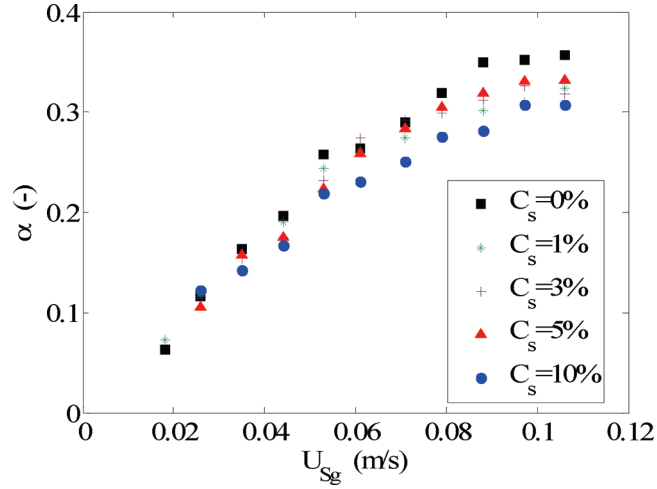

Figure 12. Effect of solids volume fraction (volume %) on gas volume fraction in the center of the 2D column with the needle sparger (z = 27 cm).

The threshold values we choose in our data analysis introduce a biasing both in the gas fraction and the bubble dynamics values. The criteria to choose a proper threshold value to calculate the gas fraction is to remove the unwanted noises to avoid an overestimate of the gas fraction. The threshold value of 10% is a proper value to estimate the gas fraction. Variation of the threshold lower than 10% shows that variation of the gas fraction with the threshold value is steep. Above the 10%, the sensitivity to the choice of the threshold value is $d\alpha/dth_\alpha = -0.16$. The threshold value of 60% is used for bubble velocity and chord length determination.

The average bubble velocity and the average bubble chord length are insensitive to the tolerance value of β. The tolerance value of 0.25 is sufficient to filter the accepted bubbles to those which are rising vertically. Changes in the value of β change the number of accepted bubbles but only slightly change the average values of the bubble velocity and bubble chord length and also the standard deviations. Changing the β from 0.15 to 0.35 results in $d\langle U_b\rangle/d\beta = 0.18$, $d\sigma(U_b)/d\beta = 0.13$, $d\langle L_b\rangle/d\beta = 0.4$, and $d\sigma(L_b)/d\beta = 0.74$.

4. Results and Discussion

4.1. 3D Column. A comparison between the results of the gas fraction measurements in our 3D column equipped with the needle sparger and other gas-injection systems shows that, with the needle sparger, higher gas loading can be achieved at higher superficial gas velocities (see Figure 5).

At low superficial gas velocities, the flow regime is homogeneous and the gas fraction increases almost linearly with increasing superficial gas velocity. The transition from the homogeneous flow regime to the heterogeneous flow regime occurs at $U_{sg,trans}$.

Measuring the radial gas fraction profile (at $r/R = 0.93$, 0.67, 0.4, and 0.13) in a 3D bubble column (with the needle sparger) with single-point glass fibers shows that, at a gas velocity < 0.06 m/s, the gas fraction in the cross section of the column is rather flat. This illustrates that vortical structures and backmixing are virtually absent and a uniform flow exists in the column. At higher gas velocity, the wall region has the lowest gas fraction (see Figure 6a). It supports the visual observation of a downward motion of the liquid, driving bubbles away from the wall. Note that bubbles that are dragged downward have a smaller probability of being pierced by the probe. Figure 6a shows that, near the center of the column, the gas fraction still increases with U_{sg}.

To investigate the effect of probe orientation on the gas fraction measurement in the wall region, we measure the gas fraction using a single probe pointing downward at $r/R = 0.93$. Figure 6b shows that, at low superficial gas velocities as we expected, the majority of the bubbles are rising upward and, therefore, the probability of being pierced by the probe facing downward is higher. Moreover, downward orientation of the probe gives a better idea of entering the heterogeneous flow regime than the case in which it faces upward. This figure illustrates that, at churn-turbulent flow regime, it is very difficult to measure the local gas fraction accurately in the wall region due to the fact that making an average value of measured gas fraction with two probes with two different orientations is not easy.

We find that an increase in solids volume fraction from 0 to 20% in the system results in a decrease in gas fraction and a shift of $U_{sg,trans}$ from 0.065 to 0.04 m/s (see Figure 7). Furthermore, Figure 8 shows that adding solids to the system at low superficial gas velocity ($U_{sg} = 0.044$ m/s) changes the gas fraction distribution from a flat profile to a decreasing profile toward the wall region. This graph suggests that we have changed the flow regime from a uniform bubbly flow regime to a turbulent flow in which the gas fraction distribution due to the presence of vortical structures in the column is not flat. This phenomenon also supports the conclusion from Figure 7 that adding solids changes the transition point from a higher superficial gas velocity to a lower one.

4.2. 2D Column. For a better understanding of the behavior of the system, we measured the bubble dynamics in our 2D setup, which makes it possible to visually observe the trajectories of the bubbles. Figure 9 shows an image of bubbles in an air−water system in $U_{sg} = 0.0088$ m/s. Image processing yielded an average vertical chord length of 2.0 mm. This is in reasonable agreement with the average chord length of 1.8 mm we obtained from the optical probe at the same gas velocity (see Figure 16). When solids are added to the system, the contrast decreases and visual observation becomes more cumbersome. Figure 10 shows that, already for a solids volume fraction of 1%, the contrast is considerable lower; for the higher solids loadings (we typically used 5 and 10%), individual bubbles are almost impossible to see.

Figure 11 shows that the gas fraction in the center of the 2D column strongly increases with superficial gas velocity, while the gas fraction near the walls hardly changes. This suggests that higher velocities change the slurry flow to upward in the center and downward close to the walls. The lower probability of piercing the bubbles that are moving downward should be considered.

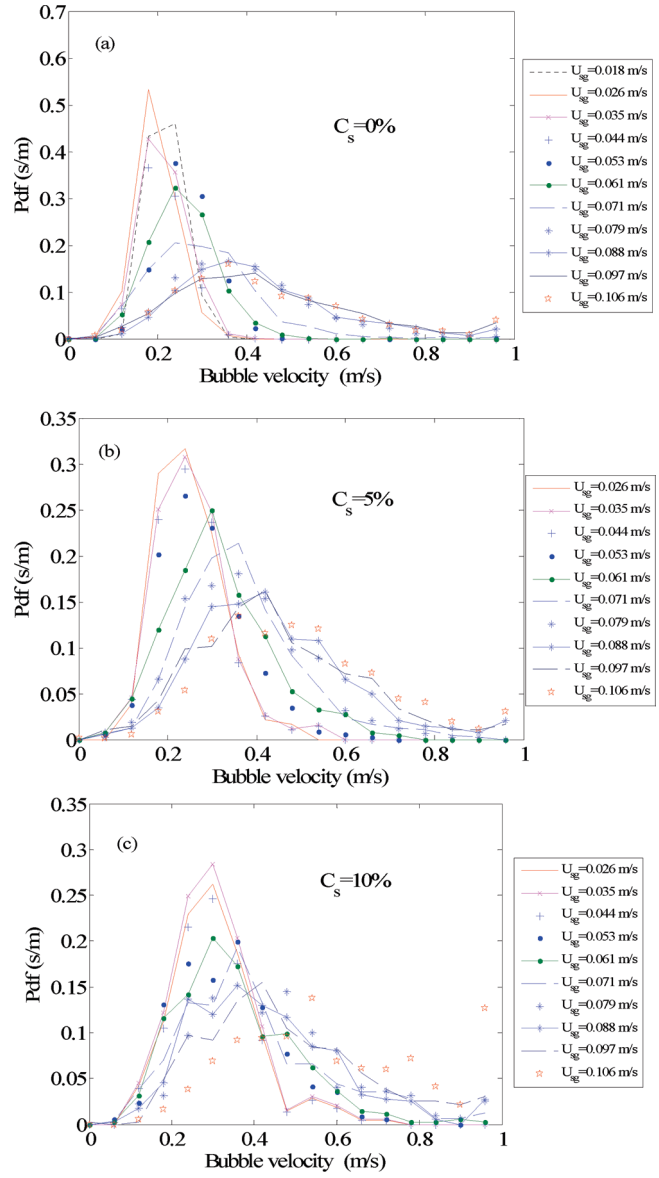

Figure 13. Effect of superficial gas velocity on bubble velocity profile in the 2D column with different solids volume fraction (volume %): (a) $C_s = 0\%$, (b) $C_s = 5\%$, and (c) $C_s = 10\%$ ($z = 27$ cm).

The effect of solids volume fraction on the gas fraction in the 2D column is shown in Figure 12. Similar to what we have seen in the cylindrical column, adding solids to the system decreases the gas fraction in the 2D column. Visual observations support the results from the optical probe: the presence of solids enhances liquid circulation and formation of some larger bubbles in the system.

With the four-point probe, we also measured the bubble velocity and bubble chord length distribution. In Figures 13 (bubble velocity) and 14 (bubble chord length), the results are presented in the form of probability density functions (pdfs) for three different solids volume fractions ($C_s = 0\%$, 5%, and 10%) as a function of the superficial gas velocity. For the bubble velocity, we find that the pdfs shift to higher velocities and widen when increasing the superficial gas flow rate for all three solids volume fractions. In Figure 15, we have summarized this by presenting the mean bubble velocity (Figure 15a) and its

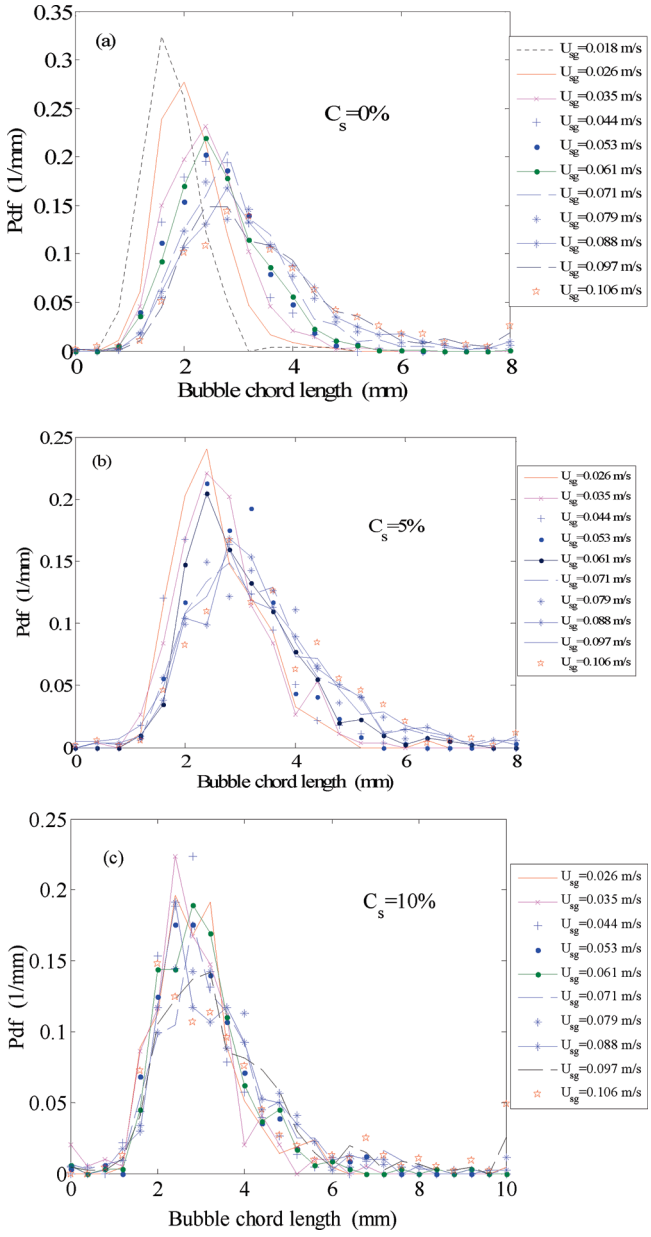

Figure 14. Effect of superficial gas velocity on bubble chord length profile in the 2D column with different solids volume fraction (volume %): (a) C_s = 0%, (b) C_s = 5%, and (c) C_s = 10% (z = 27 cm).

normalized standard deviation (Figure 15b) for all cases. The mean bubble velocity follows the same trend for all three solids volume fractions: the mean velocity increases by roughly 60−100% from the low superficial gas velocities to the highest one we used. The increase in the standard deviation is even higher. Furthermore, at the higher superficial gas velocities, the standard deviation becomes more or less independent from the solids volume fraction. On the other hand, the bubble chord length pdfs are much lower depending on the solids volume fraction. This is most likely caused by the special needle sparger that we use: the needles individually control the bubble size virtually independent of the flow conditions close to the bottom of the column. Using the needle sparger makes our bubble chord length distribution results different than what Wu et al.[22] have reported. The situation for C_s = 0% at the lower superficial gas velocities (U_{sg} < 0.035 m/s) is the exception: the chord length distribution is more narrow and centered around L_b = 2 mm. Only in these cases, the flow pattern is not disturbed at all, neither by liquid eddies nor by particles. For all other cases,

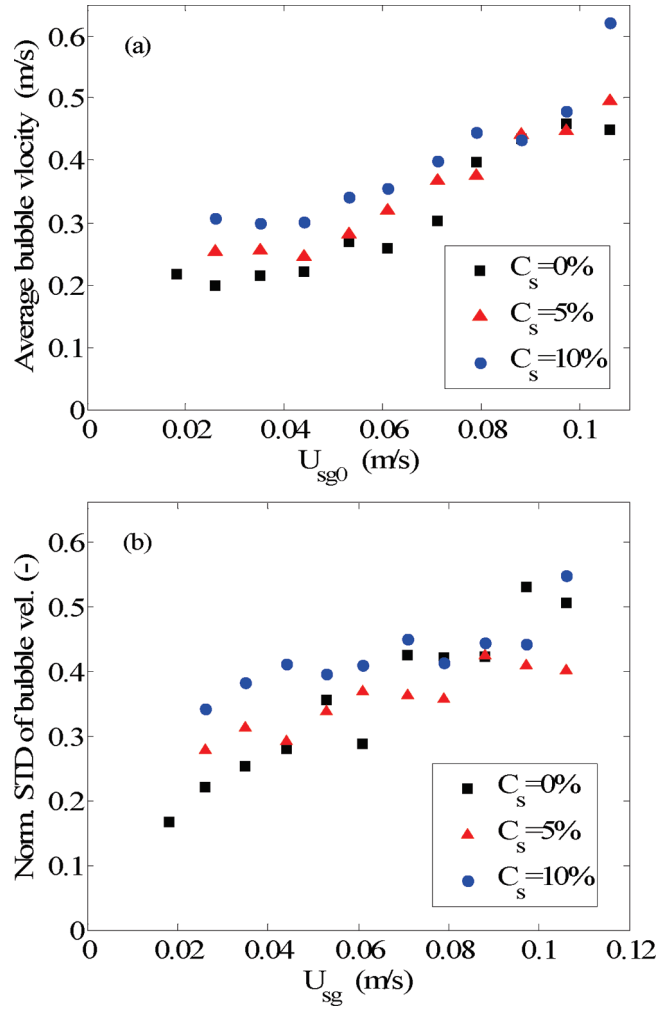

Figure 15. (a) Effect of solids volume fraction (volume %) on average bubble velocity in the 2D column (z = 27 cm). (b) Effect of solids volume fraction on standard deviation of bubble velocity in the 2D column with needle sparger (z = 27 cm). Note: The standard deviation of the bubble velocities has been normalized by dividing them by the average bubble velocity.

the chord length distribution is concentrated in the range 2−4 mm with an increasing tail up to 6−8 mm with increasing gas flow rate. This is summarized in Figure 16 by the mean chord length and the normalized standard deviation. Especially for U_{sg} > 0.04 m/s, the distributions for the different particle concentrations look alike. The mean chord length is an increasing function of the solids volume fraction, but the difference between the C_s = 0% and C_s = 10% case is only some 10%. From these observations, we conclude that the bubble velocity is changing not because coalescence is widening the bubble size but instead because the flow changes from homogeneous with almost zero liquid velocity to heterogeneous flow with vortical structures and overall liquid circulation.

If we treat the slurry as a pseudo-two-phase flow, with the continuous phase consisting of liquid with particles, a simple force balance on a bubble shows that the density of the pseudoliquid phase does not directly influence the terminal velocity: $V_b(\rho_{liq} - \rho_g)g = C_D A_\perp (1/2)\rho_{liq} v_s^2$. Taking the bubbles to be ellipsoidal, the ratio of $(V_b)/(A_\perp) = (2/3)L_b$ from which it follows that the slip velocity of the bubbles changes as $v_s \propto \sqrt{L_b}$. Our data indicate that the effect of solids is more complicated: the drag coefficient is not a constant for the various cases. However, the force balance does support our conclusion that the increase in bubble velocity with increasing superficial

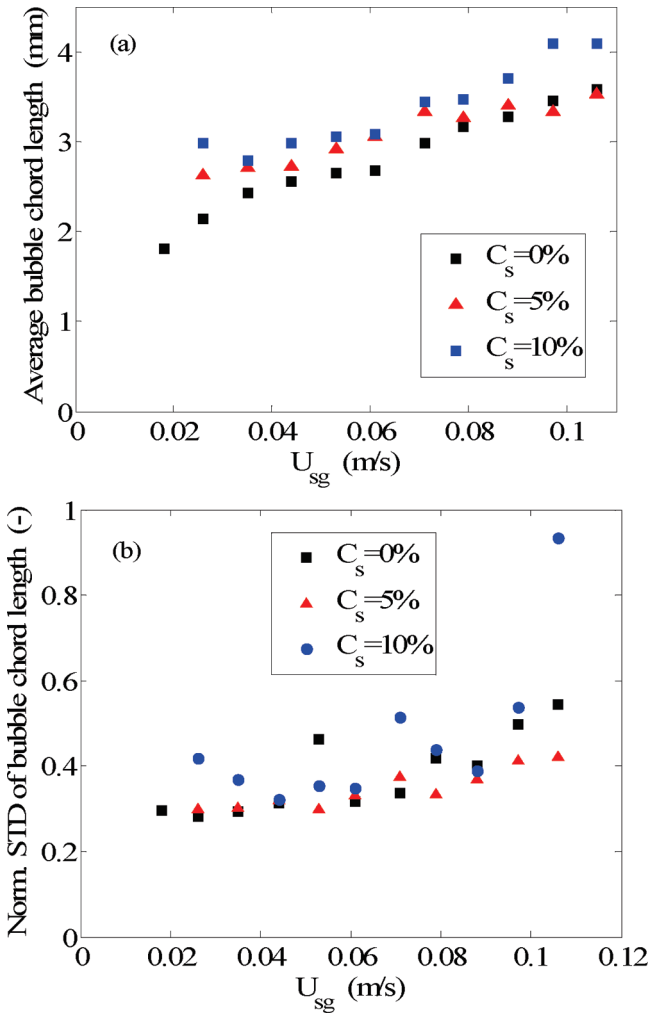

Figure 16. (a) Effect of solids volume fraction (volume %) on average bubble chord length in the 2D column (z = 27 cm).[4] (b) Effect of solids volume fraction on standard deviation of bubble chord length in the 2D column with needle sparger (z = 27 cm). Note: The standard deviation of the bubble chord length has been normalized by dividing them by the average bubble chord length.

velocity cannot be explained by the increasing bubble size. Moreover, at higher superficial gas velocities, the gas fraction increases and mutual hindrance should slow down the rising bubbles even more (see, e.g., ref 15).

From visual observations, we find that adding solids to the system increases the liquid circulation, and although some large bubbles form, there are still many small bubbles present in the column. We can conclude that the increase in bubble velocity is due not only to the appearance of larger bubbles but also to liquid circulation induced by a changing radial gas fraction profile. In future work, we will study the effect of liquid circulation patterns in more detail.

We compared our experimental achievements with the Richardson and Zaki[29] (R&Z) model and with the Garnier et al.[30] model to investigate if our three-phase system behaves as a quasi-two-phase system or not. These models are based on the slip velocity and are only valid in the homogeneous regime. By considering the fact that liquid velocity in the homogeneous flow regime is zero, the direct relations between the gas fraction and the superficial gas velocity are as follows:

$$U_{sg} = \alpha v_s(\alpha) = v_\infty \alpha (1 - \alpha)^{n-1} \text{ (R\&Z)} \qquad (5)$$

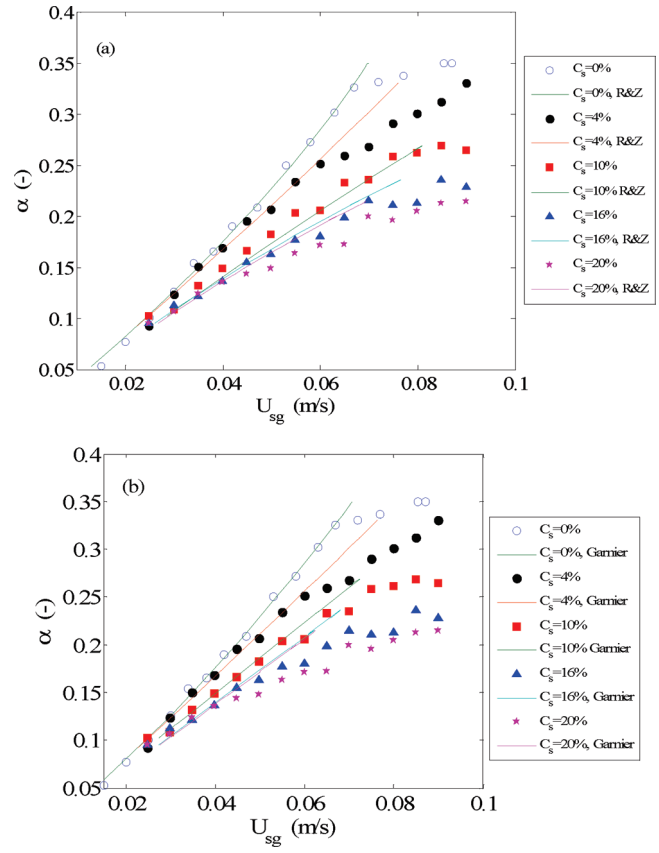

Figure 17. Gas fraction versus superficial gas velocity in different solids volume fraction (volume %) in the 3D column: (a) fitted with R&Z model and (b) fitted with Garnier et al. model.

$$U_{sg} = \alpha v_s(\alpha) = v_\infty \alpha (1 - C_\mu \alpha^{1/3}) \text{ (Garnier et al.)} \qquad (6)$$

v_∞ is the terminal velocity of a single bubble, n is the Richardson and Zaki power (= 2.39 for bubbles with the same size for which we measured $Re > 500$), and C_μ is the parameter in the Garnier et al. model (= 1 in their model). Both models are fitted to the gas fraction data from 2D and 3D columns up to the transition point (see Figures 17 and 18). The results are given in Tables 2 and 3.

The values of n we found are much lower than what Richardson and Zaki presented in their original model. The value of n = 1.57 for an air−water system in cylindrical column is quite close to the one mentioned by Mudde et al.[15] The value of v_∞ for an air−water system presented in Table 2 (0.255 m/s) is in a good agreement with what we expected for the velocity of a 4 mm single bubble (≈0.27 m/s). Our results are in line with the fact that the bubble velocity in a swarm is lower than the velocity of an individual bubble due to the mutual hindrance (e.g., see manuscript by Barnea and Mizrahi[31]).

The coefficient of the Garnier et al. model, C_μ, is found to be 0.54, which differs from the value of 1 that Garnier et al. reported. Data presented in Table 2 show that the value of n decreases with an increase in solids volume fraction from 1.57 to 0, which shows that our results deviate from R&Z's relation. Also, the values of C_μ decrease from 0.541 to 0. We should not forget that, at low superficial gas velocities, less liquid circulation results in solids settling, which decreases the effect of solids on the hydrodynamics. Both results from 2D and 3D clearly show that what we found for n and C_μ is not in good agreement with what R&Z and Garnier et al. reported, but the values of v_∞ close to 0.25 m/s are realistic. This can be explained by the fact that we fitted the homogeneous part of our results

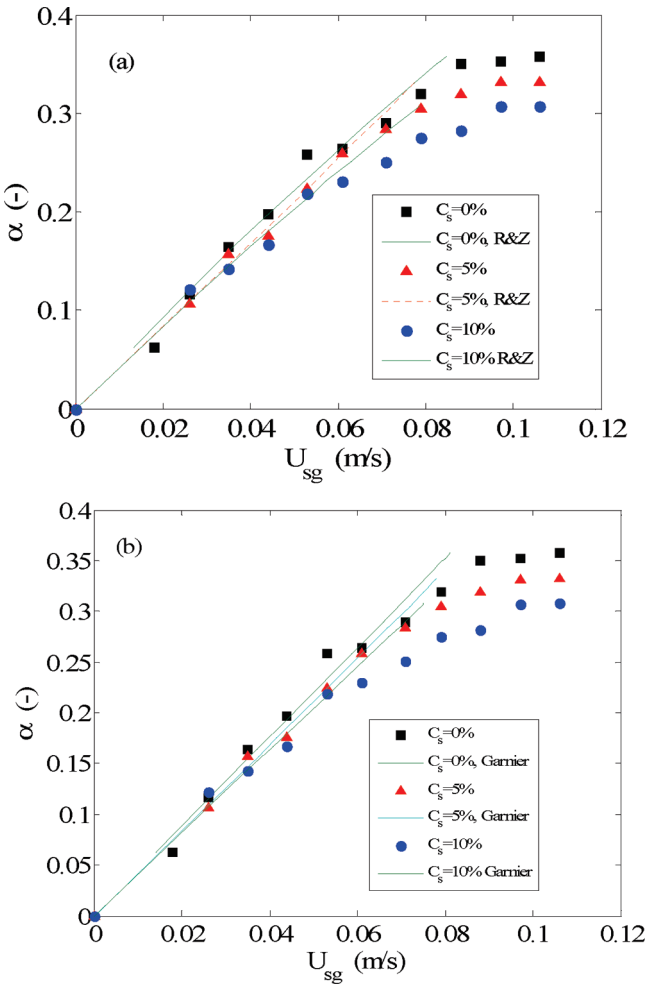

Figure 18. Gas fraction versus superficial gas velocity in different solids volume fraction (volume %) in the 2D column: (a) fitted with R&Z model and (b) fitted with Garnier et al. model (z = 27 cm).

Table 2. Fit Parameters for Different Solids Volume Fraction in 3D Column

	R&Z			Garnier et al.		
	v_∞ (m/s)	n	Pearson correlation coeff.	v_∞ (m/s)	C_μ	Pearson correlation coeff.
C_s = 0%	0.255	1.57	0.9991	0.326	0.541	0.9994
C_s = 4%	0.247	1.183	0.9978	0.274	0.233	0.9977
C_s = 10%	0.252	0.655	0.9978	0.268	0	0.9974
C_s = 16%	0.24	0	0.9983	0.286	0	0.9958
C_s = 20%	0.254	0	0.9959	0.29	0	0.9896

Table 3. Fit Parameters for Different Solids Volume Fraction in 2D Column

	R&Z			Garnier		
	v_∞ (m/s)	n	Pearson correlation coeff.	v_∞ (m/s)	C_μ	Pearson correlation coeff.
C_s = 0%	0.21	0.73	0.9845	0.22	0	0.9819
C_s = 5%	0.242	1.08	0.9974	0.25	0.096	0.9974
C_s = 10%	0.231	0.731	0.9929	0.244	0	0.9927

to the models in which the relation between the gas fraction, slip velocity, and superficial gas velocity is linear.

5. Concluding Remarks

In this paper, we have reported experimental results of a 2D and a 3D slurry bubble column equipped with needle spargers. Using optical probes, we have shown that we can achieve direct information about the bubble dynamics in the system. Measuring the gas fraction profile has shown a higher gas fraction in the center of the column and a lower one in the wall region for the highest superficial gas velocities used. This result supports the visual observation that a downward motion of liquid is present, driving bubbles away from the wall. We found that an increase in solids volume fraction decreases the gas fraction and shifts the transition point from homogeneous to heterogeneous to lower superficial gas velocities.

With the four-point optical probe, we measured the bubble dynamics and showed that, for different solids volume fractions, increasing the superficial gas velocity widens the probability density function. Moreover, adding solids increases the mean bubble velocity by 60−100% from the low superficial gas velocity to the highest one, but it has much less effect on the mean chord length.

We have applied different existing relations to find out if our three-phase system behaves as a pseudo-two-phase system. Fitting our experimental results to Richardson and Zaki's and also to Garnier's model illustrates that the presence of solids in the system makes the hydrodynamics more complicated than for a two-phase system. Contrary to previous reports on the hydrodynamics of the slurry bubble columns, we think that the decreasing gas fraction at high solids volume fraction is not only due to the presence of larger bubble but also due to the liquid flow pattern. We will study the liquid circulation in more detail in the near future.

Using the needle sparger, we have shown that a very even feeding of the gas results in increasing the transition point from the homogeneous to the heterogeneous regime. We will use the obtained insight to make further steps in structuring slurry bubble columns.

Nomenclature

b = binary value
C_D = drag coefficient
C_s = solids volume fraction in gas-free slurry
C_μ = Garnier model parameter
D_T = column diameter (m)
d_p = radial distance between central tip and other tips (m)
d_s = solid average diameter (m)
L_B = bubble chord length (m)
n = Richardson and Zaki parameter
N = number of samples
r = radial position (m)
R = column radius (m)
ΔS = axial distance between central tip and other tips (m)
s_a = output value of the tip in air (V)
s_w = output value of the tip in water (V)
t = time (s)
th_α = threshold value for gas fraction
th_v = threshold value for bubble velocity estimation
T_i = 0, 1, 2, 3 = time interval that tip i spend in the bubble (s)
Δt_s = sample time (s)
U_b = bubble velocity (m/s)
U_{sg} = superficial gas velocity (m/s)
$U_{sg,trans}$ = transition superficial gas velocity (m/s)
V_b = bubble volume (m^3)
v_s = bubble slip velocity (m/s)
v_∞ = single bubble terminal velocity (m/s)
x = width distance (m)
z = height above the gas distributor (m)

Greek Letters

α = gas fraction
β = tolerance value
ρ_{liq} = liquid density (kg/m^3)
σ = standard deviation (various)
τ = average of times of flight (s)

Literature Cited

(1) Kreutzer, M. T.; Kapteijn, F.; Moulijn, J. A. Shouldn't catalysts shape up? Structured reactors in general and gas−liquid monolith reactors in particular. *Catal. Today* **2006**, *111* (1−2), 111–118.

(2) Pangarkar, K.; Schildhauer, T. J.; van Ommen, J. R.; Nijenhuis, J.; Kapteijn, F.; Moulijn, J. A. Structured packings for multiphase catalytic reactors. *Ind. Eng. Chem. Res.* **2008**, *47* (10), 3720–3751.

(3) Vervloet, D.; Kamali, M. R.; Gillissen, J. J. J.; Nijenhuis, J.; van den Akker, H. E. A.; Kapteijn, F.; van Ommen, J. R. Intensification of co-current gas−liquid reactors using structured catalytic packings: A multiscale approach. *Catal. Today* **2009**, *147* (Suppl.), S138–S143.

(4) Hooshyar, N.; Hamersma, P. J.; Mudde, R. F.; van Ommen, J. R., Intensified Operation of Slurry Bubble Columns Using Structured Gas Injection. *Can. J. Chem. Eng.* **2010**, *88* (4), 533−542.

(5) Van den Bleek, C. M.; Coppens, M. O.; Schouten, J. C. Application of chaos analysis to multiphase reactors. *Chem. Eng. Sci.* **2002**, *57* (22−23), 4763–4778.

(6) Ellenberger, J.; Krishna, R. Improving mass transfer in gas−liquid dispersions by vibratiion excitement. *Chem. Eng. Sci.* **2002**, *57* (22−23), 4809–4815.

(7) Ellenberger, J.; Krishna, R. Intensification of slurry bubble columns by vibration excitement. *Can. J. Chem. Eng.* **2003**, *81* (3−4), 655–659.

(8) Knopf, F. C.; Ma, J.; Rice, R. G.; Nikitopoulos, D. Pulsing to improve bubble column performance: I. Low gas rates. *AIChE J.* **2006**, *52* (3), 1103–1115.

(9) Knopf, F. C.; Waghmare, Y.; Ma, J.; Rice, R. G. Pulsing to improve bubble column performance: II. Jetting gas rates. *AIChE J.* **2006**, *52* (3), 1116–1126.

(10) Waghmare, Y. G.; Dorao, C. A.; Jakobsen, H. A.; Knopf, F. C.; Rice, R. G. Bubble size distribution for a bubble column reactor undergoing forced oscillations. *Ind. Eng. Chem. Res.* **2009**, *48* (4), 1786–1796.

(11) Kulkarni, A. V.; Badgandi, S. V.; Joshi, J. B. Design of ring and spider type spargers for bubble column reactor: Experimental measurements and CFD simulation of flow and weeping. *Chem. Eng. Res. Des.* **2009**, *87* (12), 1612–1630.

(12) Hebrard, G.; Bastoul, D.; Roustan, M. Influence of the gas sparger on the hydrodynamic behaviour of bubble columns. *Chem. Eng. Res. Des.* **1996**, *74* (3), 406–414.

(13) Thorat, B. N. Effect of sparger design and height to diameter ratio on fractional gas hold-up in bubble columns. *Chem. Eng. Res. Des.* **1998**, *76* (A7), 823–834.

(14) Harteveld, W. K. Bubble columns: structures or stability? Ph.D. dissertation, Delft University of Technology, Delft, The Netherlands, 2005.

(15) Mudde, R. F.; Harteveld, W. K.; van den Akker, H. E. A. Uniform Flow in Bubble Columns. *Ind. Eng. Chem. Res.* **2009**, *48* (1), 148–158.

(16) Xue, J.; Al-Dahhan, M.; Dudukovic, M. P.; Mudde, R. F. Bubble Dynamics Measurements Using Four-Point Optical Probe. *Can. J. Chem. Eng.* **2003**, *81* (3−4), 375–381.

(17) Chen, W.; Tsutsumi, A.; Otawara, K.; Shigaki, Y. Local bubble dynamics and macroscopic flow structure in bubble columns with different scales. *Can. J. Chem. Eng.* **2003**, *81* (6), 1139–1148.

(18) Magaud, F.; Souhar, M.; Wild, G.; Boisson, N. Experimental study of bubble column hydrodynamics. *Chem. Eng. Sci.* **2001**, *56* (15), 4597–4607.

(19) Chaumat, H.; Billet-Duquenne, A. M.; Augier, F.; Mathieu, C.; Delmas, H. On the reliability of an optical fibre probe in bubble column under industrial relevant operating conditions. *Exp. Therm. Fluid Sci.* **2007**, *31* (6), 495–504.

(20) Zhang, L. J.; Li, T.; Ying, W. Y.; Fang, D. Y. Experimental study on bubble rising and descending velocity distribution in a slurry bubble column reactor. *Chem. Eng. Technol.* **2008**, *31* (9), 1362–1368.

(21) Xue, J.; Al-Dahhan, M.; Dudukovic, M. P.; Mudde, R. F. Bubble velocity, size, and interfacial area measurements in a bubble column by four-point optical probe. *AIChE J.* **2008**, *54* (2), 350–363.

(22) Wu, C.; Suddard, K.; Al-Dahhan, M. Bubble dynamics investigation in a slurry bubble column. *AIChE J.* **2008**, *54* (5), 1203–1212.

(23) Mudde, R. F.; Saito, T. Hydrodynamical similarities between bubble column and bubbly pipe flow. *J. Fluid Mech.* **2001**, *437* (1), 203–228.

(24) Jamialahmadi, M.; Muller-Steinhagen, H. Effect of solid particles on gas hold-up in bubble columns. *Can. J. Chem. Eng.* **1991**, *69* (1), 390–393.

(25) Su, X.; Heindel, T. J. Gas holdup in a fiber suspension. *Can. J. Chem. Eng.* **2003**, *81* (3−4), 412–418.

(26) Barghi, S.; Prakash, A.; Margaritis, A.; Bergougnou, M. A. Flow regime identification in a slurry bubble column from gas holdup and pressure fluctuations analysis. *Can. J. Chem. Eng.* **2004**, *82* (5), 865–870.

(27) Al-Masry, W. A.; Ali, E. M. Identification of hydrodynamics characteristics in bubble columns through analysis of acoustic sound measurements−Influence of the liquid phase properties. *Chem. Eng. Process.* **2007**, *46* (2), 127–138.

(28) Tang, C.; Heindel, T. J. In *Gas holdup in a cocurrent air−water−fiber bubble column*; Proceedings of the ASME Heat Transfer/Fluids Engineering Summer Conference 2004; HT/FED: Charlotte, NC, 2004; pp 497−505.

(29) Richardson, J. F.; Zaki, W. N. Sedimentation and fluidisation: Part I. *Trans. Inst. Chem. Eng.* **1954**, *32*, 35–53.

(30) Garnier, C.; Lance, M.; Marié, J. L. Measurement of local flow characteristics in buoyancy-driven bubbly flow at high void fraction. *Exp. Therm. Fluid Sci.* **2002**, *26* (6−7), 811–815.

(31) Barnea, E.; Mizrahi, J. A generalized approach to the fluid dynamics of particulate systems. Part 1. General correlation for fluidization and sedimentation in solid multiparticle systems. *Chem. Eng. J.* **1973**, *5* (2), 171–189.

Received for review March 8, 2010
Revised manuscript received August 31, 2010
Accepted September 1, 2010

IE100528C

Paper IV

Dynamics of single rising bubbles in neutrally buoyant liquid-solid suspensions

Has been submitted for publication in Physical Review Letters.

Dynamics of single rising bubbles in neutrally buoyant liquid-solid suspensions

Nasim Hooshyar,[1] J. Ruud van Ommen,[1] Peter J. Hamersma,[1] Sankaran Sundaresan,[2] and Robert F. Mudde[1,*]

[1] *Department of Chemical Engineering, Delft University of Technology, Julianalaan 136, 2628 BL Delft, The Netherlands*
[2] *Chemical Engineering Department, Princeton University, Princeton, New Jersey 08543*

(Dated: October 24, 2012)

We experimentally investigate the effect of particles on the dynamics of a gas bubble rising in a liquid-solid suspension while the particles are equally sized and neutrally buoyant. Using the Stokes number as an universal scale we show that when a bubble rises through a suspension characterized by a low Stokes number (in our case small particles), it will hardly collide with the particles and will experience the suspension as a pseudo-clear liquid. On the other hand, when the Stokes number is high (large particles), the high particle inertia leads to direct collisions with the bubble. In that case, Newton's collision rule applies, and direct exchange of momentum and energy between the bubble and the particles occurs. We present a simple theory that describes the underlying mechanism determining the terminal bubble velocity.

PACS numbers: 47.55.D-

Bubbles rising in clear liquids or liquid-solid mixtures are important in numerous fields such as oil and gas production [1, 2], food processing [3], biotechnology [4] and algae production [5]. The shape, oscillation, path and velocity of a gas bubble rising in clear liquids has been studied extensively [6–9]. As compared to the clear liquid case, there have been very few studies that focus on the dynamics of a gas bubble in liquid-solid suspensions. Fan and Tsuchiya [6] investigated the bubble wake in liquid-solid suspensions and measured the wake size. They showed that the wake size is sensitive to the extent of the disturbance in the liquid flow caused by the presence of the particles. Vera et. al [10] studied the instabilities of gas bubbles in a liquid-fluidized bed and described the series of instabilities induced by a downward liquid flow through a bed of gas bubbles. Although a few researchers proposed correlations for the bubble velocity in liquid-solid suspensions [11], no one looked into the underlying mechanism of particle-bubble interaction.

The objective of the present research is to study the influence of particles on the velocity of a single gas bubble rising in a liquid-particle suspension. We use spherical particles and make them neutrally buoyant [12] to prevent direct momentum exchange of particles colliding with a bubble due to their gravitational settling. We categorize the system in terms of the ratio between the Stokes relaxation time of the particles ($\tau_p = \rho_p d_s^2/18\mu$, with the particle density ρ_p, the solid diameter d_s, and the liquid viscosity μ) and the characteristic time of the rising bubble ($\tau_b = d_b/v_b$, with the bubble diameter d_b and the bubble velocity v_b), St=τ_p/τ_b [13]. We experimentally show that the Stokes number (St) is the most important parameter for understanding the bubble dynamics with a regime transition from the direct to indirect particle interaction around St=1.

In this Letter we report detailed experiments on the terminal velocity of a single bubble rising through a neutrally buoyant liquid-particle suspension. Experiments were performed in a rectangular column (Fig. 1(a)). The column (cross section 50 mm $\times$ 50 mm, height 200 mm) was filled with a water-glycerol mixture having the same density as the suspended,

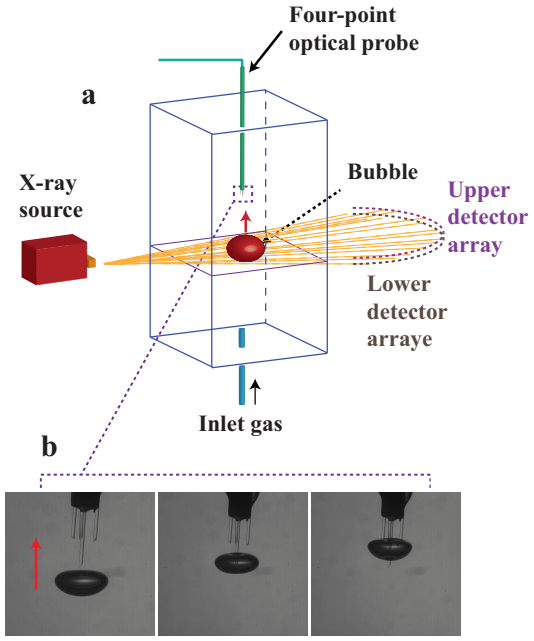

FIG. 1: (color online) Gas bubble formation, motion and detection in water- glycerol-polystyrene mixture. (a) Schematic of the set-up, (b) sequences of a single rising bubble being pierced with the four-point optical probe.

spherical polystyrene particles (d_s= 78 μm, 587 μm, 2.0 mm and 4.0 mm). The liquid mixture density was 1054 kg/m^3, slightly varying with the different particles used. An air bubble with an equivalent diameter of about 3.0 mm was injected via a needle with an ID of 0.8 mm located at the bottom center of the column. The flow behaviour of the rising bubble and the surrounding particles in suspensions containing particles at very low volume fractions was recorded using a high-speed camera (1000 fps). At higher particle volume fractions where the system is opaque, we obtained information on the bubble motion and shape by using a four-point optical probe (Fig. 1(b)) [14]. For large particle sizes (2.0 and 4.0 mm),

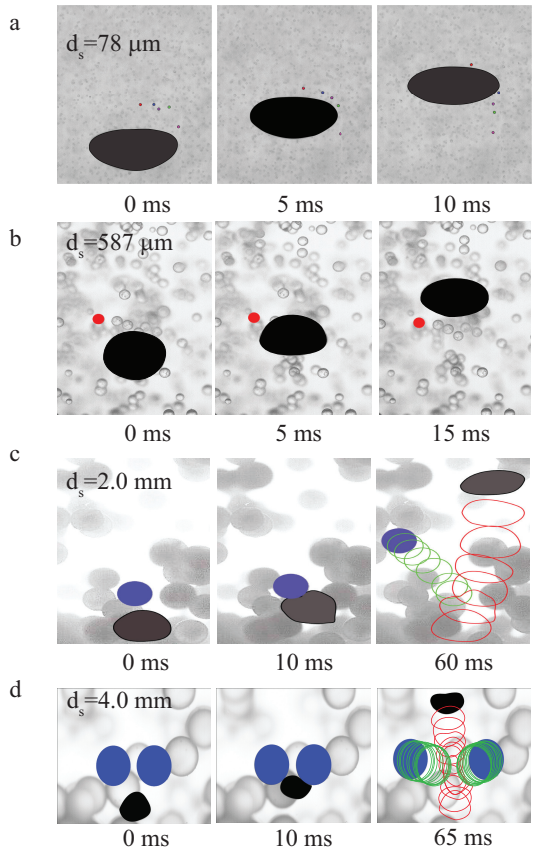

FIG. 2: (color online) Gas bubble motion in water- glycerol-polystyrene mixture: (a) and (b) 78 and 587 μm particles with St $\ll 1$ remain in the streamline of the liquid and do not collide on the bubble surface, (c) 2.0 mm particle with St $\gg 1$ and $d_s < d_b$ collide with the bubble and changes the bubble's direction of the motion and (d) 4.0 mm particles with St $\gg 1$ and $d_s > d_b$ encounter the rising bubble. For more details, see Supplementary Movies 1-3.

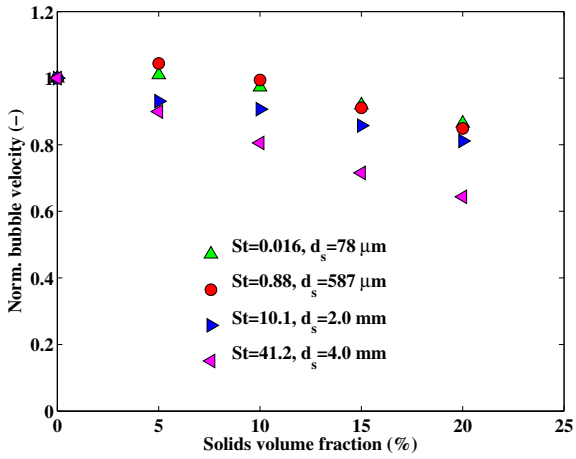

FIG. 3: (color online) Effect of Stokes number (St) on the bubble velocity: the superficial gas velocity. The results of systems with 78 and 587 μm particles are from measurements with the four-point optical probe and are the average of the bubble velocity values in different vertical elevations. The bubble rise velocities in suspensions with 2.0 and 4.0 mm particles are the results of measurements with the X-ray densitometry. The velocity values are normalized to the velocity obtained in clear liquid.

where the optical probe could not be used reliably, the bubble characteristics were measured using fast X-ray densitometry [15]. The consistency of the measurements with different techniques has been ascertained (see Supplementary Information).

The motion of a single rising bubble in a water-glycerol mixture at 25 $\pm$ 0.5°C was captured in the series of images shown in Fig. 2(a)-(d). We categorize the systems in terms of the Stokes number. Fig. 2(a) shows that for the system with 78 μm particles (St = 0.016 $\ll$1), the particles remained virtually on the streamlines of the liquid flowing around the bubble (see Supplementary Movie 1) and the mixture of liquid and particles behaved as a pseudo-clear liquid. The motion of the bubble could be described by replacing the suspension with a clear liquid having the same viscosity and surface tension as the liquid-solid suspension. The influence of the suspended particles was merely to increase the viscosity. The same is true for suspended particles of 587 μm diameter (St = 0.88). Fig. 2(c) shows that with 2.0 mm particles (St = 10.1 $\gg$1, but the particle size still smaller than the bubble size), the particles collided with the bubble (see Supplementary Movie 2). With 4.0 mm particles (St = 41.2, and the particles are larger than the bubble) collisions between the particles and the rising bubble were very prominent (see Fig. 2(d) and Supplementary Movie 3). Clearly, above a critical value of the St number the particles no longer migrate with the liquid around the bubble but collide with the bubble and change its direction of motion.

Fig. 3 illustrates that the bubble rise velocity decreases with an increase in the particle volume fraction for all St and that the extent of reduction depends on St. The observed reduction in the bubble velocity for St $\ll$ 1 is to be expected. As the small particles do not directly collide with the bubble, their effect is felt as an (apparent) increase in the viscosity of the mixture. A commonly used model for the effective viscosity, μ_{eff}, of a suspension of small particles (St $\ll$ 1) capturing the increase in μ_{eff} with increasing solids volume fraction, C_s, is [16]:

$$\frac{\mu_{eff}}{\mu_0} = (1 - C_s/C_m)^{-n} \qquad (1)$$

where μ_0 is the viscosity of solids-free liquid and C_m is the random close packing concentration for a given system. We set $n = 2.5C_m$ so that at small C_s values one recovers the Einstein equation for the viscosity of a dilute suspension of solids in a liquid [17]: $\mu_{eff}/\mu_0 = (1 + 2.5C_s)$.

The viscosity and the surface tension of suspensions of 78 μm particles were measured. The surface tension was found to be independent of the solids concentration. For the high-

est solids fraction examined in this study the apparent viscosity was almost double that of the suspending liquid. Eq. (1) with C_m = 0.65 [18] captures the data satisfactory. Using a force balance between the drag and buoyancy for the single rising bubble, along with the drag relation proposed by Tomiyama [19] for contaminated systems, we estimated the expected bubble velocities for different particle volume fractions. The calculated results are displayed in Fig. 4 along with experimental data. At low particle volume fractions where the drag force is dominated by surface tension effects, there is little change in the rise velocity with C_s. At somewhat higher particle loading levels and hence higher viscosities, the viscous effect becomes more important than surface tension and the bubble velocity begins to decrease with increasing particle volume fraction. In order to ascertain that the increased viscosity is the reason for the reduced bubble rise velocity at St $\ll$ 1, we performed bubble rise experiments using a clear liquid having the same viscosity as the suspension by adjusting the glycerol fraction. Fig. 4 confirms that for St $\ll$ 1, the rise velocity of the bubble in the presence of particles can be found by replacing the mixture with a clear liquid having the same viscosity and surface tension as the suspension. As can be seen in Fig. 4, the bubble rise velocity seems to go up from μ_{eff}= 2.3 to 2.7 mPa.s and in Fig 3 at St$\ll$ 1 from C_s=0 to 5%. The velocity again drops with a further increase in the μ_{eff} and C_s. It is due to the fact that at low μ_{eff} the bubble follows a zig-zag path (see Fig. 3 in Supplementary Information). With an increase in the μ_{eff} the bubble path becomes slightly tighter and therefore, the bubble travels vertically a longer height in a given time than for the 0% solid loading. With further increase in particle volume fraction the bubble velocity decreases as a result of the increase in the apparent viscosity.

Particles with a higher inertia, i.e. St $\gg$ 1, do literally collide with a bubble. Fig. 2(c) (Supplementary Movie 2) and (d) (Supplementary Movie 3) are examples of such collisions. In the first phase of the collision, the bubble slows down and gets deformed, while the particle gains momentum. In the second phase, the particle and bubble separate again; the bubble will regain its shape, but will have lost energy. We use a simple energy conservation argument to estimate the energy transferred from the bubble to the particle. The deformation of the bubble increases the bubble surface area. The associated increase in surface energy, $\Delta E_\sigma = \sigma \Delta A$ (where σ is the surface tension and ΔA is the change of surface energy) goes about at the expense of the kinetic energy of the bubble. For the latter we take $m_v v_b^2/2$ (where m_v is the virtual mass of the bubble). During the collision, a portion of the deformation energy is transferred to the particle, while the remainder is dissipated as heat. The bubble will continue to migrate with a reduced kinetic energy: $m_v v_{ac}^2/2 = m_v v_{bc}^2/2 - \sigma \Delta A$ (with v_{bc} the bubble velocity just before collision and v_{ac} just after collision).

Subsequently, the bubble will accelerate in clear liquid due to the buoyancy force until it collides with the next particle and the cycle repeats. The accelerating part is governed by Newton's equation of motion: $m_v dv_b/dt = F_B - C_D A_\perp (\rho_{liq} v_b^2/2)$ with $m_v = \rho_{liq} V_B/2, F_B = \rho_{liq} V_B g$. V_B is the bubble volume and ρ_{liq} the liquid density. C_D and $A_\perp$ are the drag coefficient and the frontal bubble area, respectively. For constant C_D the equation of motion is readily solved, giving the bubble's position and velocity as a function of time.

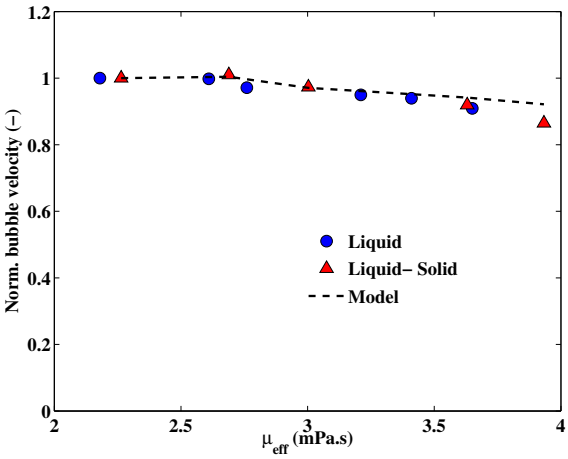

FIG. 4: (color online) Influence of the effective viscosity on the bubble velocity.A single rising bubble in a neutrally buoyant suspension of 78 μm polystyrene particles is found to be the same as that in clear liquid with the same effective viscosity. The velocity values are normalized to their velocities at μ = 0.0022 Pa.s. The dashed line corresponds to a simple model balancing the buoyancy and drag forces (see text).

The bubble will travel on average a mean free path, λ_{mf}, between two successive collisions which are modeled as instantaneous events. We get the bubble travel time between two successive collisions from the sequence: (i) collision : $v_{bc}(i) \rightarrow v_{ac}(i)$, (ii) acceleration over one mean free path: $v_{ac}(i) \rightarrow v_{bc}(i+1)$ in a duration $\Delta\tau_{mf}$. In a steady state the bubble will acquire such a velocity that $v_{bc}(i) = v_{bc}(i+1)$ with a time $\Delta\tau_{mf}$ between collision. By solving the trajectory for this condition, we find the rise velocity of the bubble:

$$\overline{v} = \frac{\lambda_{mf}}{\Delta\tau_{mf}} \tag{2}$$

The mean free path is a function of the solids number density, n_p, and the particle and bubble diameter d_p and d_b, resp.:

$$\lambda_{mf} = \left[\sqrt{2}\pi n_p \left(\frac{d_p}{2} + \frac{d_b}{2} \right)^2 \right]^{-1} \tag{3}$$

This description should hold when the mean free path is large compared to the particle and bubble size. As the 2.0 mm and 4.0 mm particles are of the same size as the bubbles, we use the bubble size as the characteristic length to define a Knudsen number: Kn $\equiv \lambda_{mf}/d_b$.

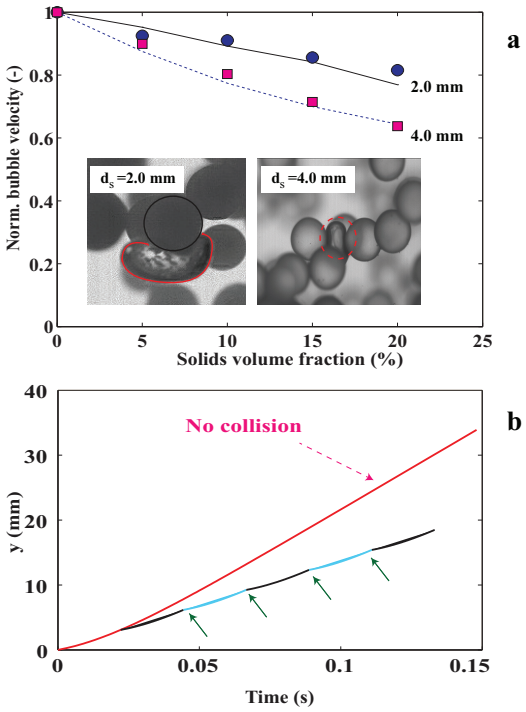

FIG. 5: (color online) Influence of 2.0 and 4.0 mm particles on the bubble velocity. (a) The solid and dashed lines correspond to the estimated values for the average bubble velocity and the symbols to the experimental results measured by X-ray densitometry; Inset, 2.0 mm case: the red line around the bubble shows its deformation and in 4.0 mm case: the red dashed line on the image denotes the squeezed bubble; (b) the modelled vertical position of the bubble, y, as a function of time for a 3 mm bubble. The red curve gives the position without taking the collision into account. The multiple colored curve indicates the results when the collisions are taking into account. The green arrows point to the collision event when the 4.0 mm and λ is 3.08 mm.

We argue that for Kn larger than one, the above reasoning should give a reasonable estimate of the bubble rise velocity. The mean free path for the 4.0 mm particles varies from 12.3 to 3.08, giving Kn ≥ 1. From the movies of the collisions we estimated that the bubble deforms to an ellipsoidal with a short axis of 2.0 mm. The energy spend in creating this increase in bubble surface area translates into a velocity reduction of 40% upon collision: $v_{ac}(i) = 0.6v_{bc}(i)$. This number was used to analyze the collision-acceleration trajectory of a bubble. The dashed line in Fig. 5(a) shows the outcome of such an analysis. The line describes the experimental points very well.

We performed a similar analysis for the 2.0 mm particles as well, where Kn was found to be order one or smaller and multi-particle collisions may become important rendering estimation of the energy loss very difficult. From the movies, it was estimated that the increase in bubble surface area associated with its deformation during collision with a single particle was not more than 1 mm^2. An increase in surface area of 1 mm^2 is equivalent to $v_{ac}(i) = 0.84v_{bc}(i)$; when this was combined with the above mean free path analysis, the average rise velocity was underpredicted. The solid line drawn in Fig. 5(a) matches the 2.0 mm data is we set $v_{ac}(i) = 0.95v_{bc}(i)$, which is equivalent to an increase in surface area by 0.34 mm^2. In spite of the difficulty in estimating the energy loss in a collision, it is encouraging that a model based on energy loss captures the experimental data.

Our study highlights that the microscopic behaviour of a gas, liquid and solid system changes with increasing St. When St $\ll 1$, the particles do not collide with the bubble and the bubble rises as in a clear liquid having the same viscosity and surface tension as the suspension. Collisions between particles and bubble, which occur at St $\gg 1$, lead to bubble deformation and a decrease in bubble velocity. When Kn ≥ 1, a mean free path analysis based on repeated collision between a single particle and the bubble adequately captures the effect of particles on the average bubble rise velocity. Although the average rise velocity of the bubble decreases with increasing solids volume fraction at both small and large St, the underlying microscopic events leading to the observed macroscopic behaviour differ significantly. It is crucial to understand this difference to properly interpret and model the dynamics of bubble rise in technological as well as natural contexts where the particle-bubble interaction is further complicated by gravitational settling of non-neutrally buoyant particles.

* Electronic address: r.f.mudde@tudelft.nl

[1] M. Al-Asimi et al., Oilfield Rev. **14,** 14-35+1+65 (2003).
[2] S. Guet and G. Ooms, Annu. Rev. Fluid Mech. **38,** 225 (2006).
[3] B. R. Pinzer et al., Soft Matter. **8,** 4584 (2012).
[4] F. Garcia-Ochoa and E. Gomez, Biotechnol. Adv. **27,** 153 (2009).
[5] L. Rodolfi et al., Biotechnol. Bioeng. **102,** 100 (2009).
[6] L-S. Fan, and K. Tsuchiya, Butterworth- Heinemann. (1990).
[7] N. Z. Handzy and A. Belmonte, Phys. Rev. Lett. **92,** 124501-1 (2004).
[8] G. Mougin and J. Magnaudet, Phys. Rev. Lett. **88,** 014502 (2001).
[9] W. L. Shew and J.-F. Pinton, Phys. Rev. Lett. **97,** 144508 (2006).
[10] M. U. Vera et al., Phys. Rev. Lett. **84,** 3001 (2000)
[11] X. Luo et al., Chem. Eng. Sci. **52,** 3693 (1997)
[12] N. T. Ouellette et al., Phys. Rev. Lett. **101,** 174504 (2008)
[13] Y. Tagawa et al., J. Fluid Mech. **693,** 201 (2012).
[14] R. F. Mudde and T. Saito, J. Fluid Mech. **437,** 203 (2001).
[15] R. F. Mudde, Powder Technol. **199,** 55 (2010).
[16] I. M. Krieger, Adv. Colloid Interface Sci. **3,** 111 (1972).
[17] A. Einstein, Ann. Physik. **324,** 289 (1906).
[18] J.-P. Matas et al., Phys. Rev. Lett. **90,** 014501/1 (2003).
[19] A. Tomiyama et al., JSME Int J. Ser. B. **41,** 472 (1998).

Supplementary Information: Methods

The opaque character of a gas-liquid-solids system makes the measurements and especially the visualization troublesome. Moreover, the presence of solids particles can damage intrusive fragile devices such as optical probes. This document gives information about the three measurement techniques that were used in this study to track the bubbles.

1 High speed camera

An Olympus high speed camera (CMOS 800 $\times$ 600 sensor) was used for visualization and measurement of the size and rise velocity of single bubbles. The high-speed camera measurements (made at 1000 fps) were used to validate the four-point optical probe and X-ray densitometry. The displacement of the centre of gravity in two consecutive frames was first calculated in pixels and (using a ruler) subsequently converted to mm, from which the bubble velocity was computed. Given the opaque nature of our suspensions at appreciable solids loading levels, the high speed camera could be used to make measurements at no or ultra-low ($\sim 0.03\%$) particle loading levels only.

2 Four-point optical probe

A four-point optical probe [1] was used to measure the dynamics of a single rising bubble in opaque systems where the visualization was not possible. The probes in our study worked on the principle of difference in light refraction between the probe material (plastic), liquid and air. The bubble velocity was obtained by analyzing the response from the probes. See Supplementary Movie 4 which shows the four-point optical probe piercing the rising bubble.

Fig. 1 shows the four-point probe configuration, with ΔS=2.0 $\pm$ 0.02 mm and d_p=0.6 mm. Tips T_1, T_2 and T_3 form an equilateral triangle in horizontal plane, while the central tip C is located a central distance of ΔS from this plane [2]. The fibers (250 μm diameter) were glued together and placed vertically, facing downward to detect the rising bubbles. The optical probe can be placed at different

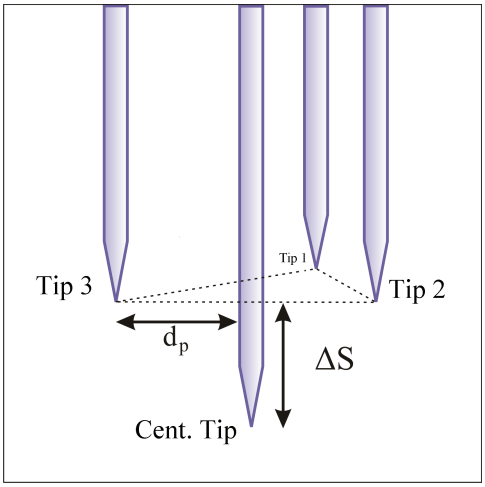

Figure 1: **Four-point probe configuration:** T_1 **,**T_2 **and** T_3 **refer to the three tips in the same plane.** T_c **refers to the central tip [2].**

elevations above the point where the bubble is injected. The procedure of signal analysis has been reported by Hooshyar et al. [2].

Fig. 2 shows the bubble rise velocity at several different elevations above the bubble injection port, measured by the optical probe as well as by the high-speed camera. The rise velocity increases initially and reaches a plateau after about 10 mm. The optical probe and high-speed camera measurements agreed with each other to within $\pm 1.9\%$. It should be noted that in this plateau the vertical component of the bubble velocity varied slightly with the phase of the oscillations (see Fig. 2). This variation is likely due to the zig-zag path followed by the rising bubbles (see Fig. 3). We measured the bubble rise velocity at 10 different elevations (separated by 1 mm) and averaged them to get the values reported in the paper.

3 X-ray densitometry

When dealing with suspensions having high particle loading, observation with a camera was not possible because of the opacity. Furthermore, the trajectory of the bubble departed significantly from a vertical path, especially for the large particles (2.0 and 4.0 mm) which made optical probe placement for accurate measurements difficult. Since the particles are to some extent transparent to X-rays, non-intrusive techniques based on X-ray densitometry or X-ray scan can be used for the measurements in the gas-liquid-solid experiments [3] . We employed X-rays to measure the velocity of a single bubble in a solid-liquid mixture. The time of the flight of the bubbles from one detector plane to a second plane (located a known distance above the first one) was measured. Using this procedure, we examined the effect of par-

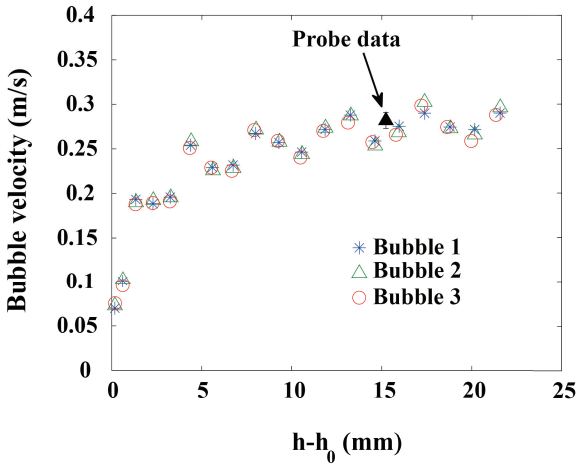

Figure 2: **Bubble rise velocity at different elevations, h, of the center of gravity of the bubble from the tip of the capillary through which the bubble is injected. h_0 = the elevation when detachment occurs =1.89 $\pm$ 0.03 mm. The figure shows data for three different bubbles rising in clear liquid, illustrating reproducibility.**

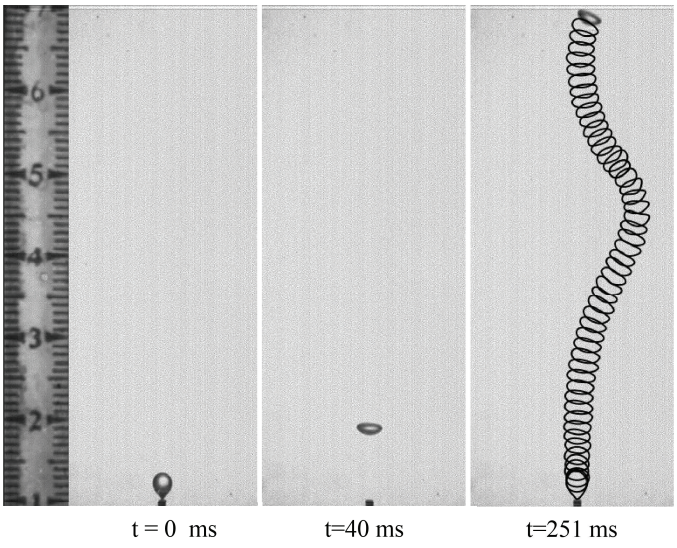

Figure 3: **An air bubble rising in a mixture of water and glycerol.**

ticle size and volume fraction on the bubble rise velocity.

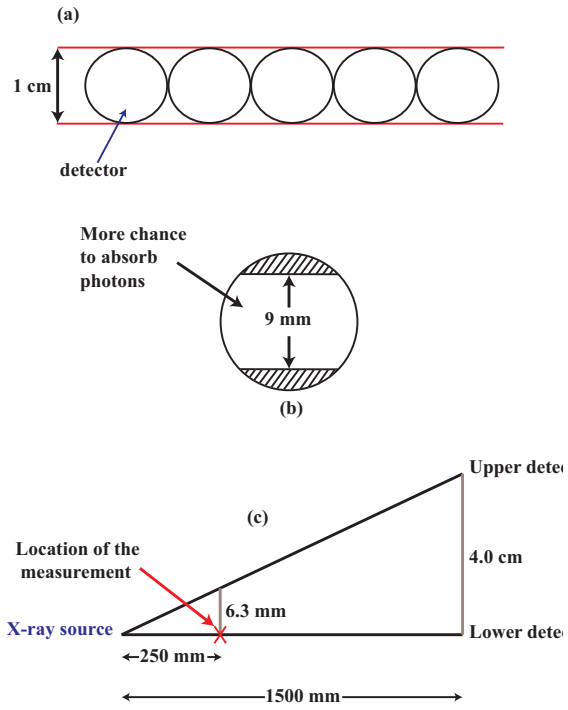

Figure 4: Schematic arrangement of the detectors in one plane: (a) series of detectors in one array, the distance between two sheets is 1 cm, (b) highlights the sensitive area of one sensor and (c) the distance between the source, measurement location and detectors. Note: the cross shows the location of the measurements in our study.

3.1 Facility

The X-ray source used in this study is manufactured by Yxlon Intentional GmbH. The maximum X-ray energy and tube current are 150 kV and 22.5 mA, respectively. The X-ray source generates a fan beam that is detected by two sets of 32 sensors placed opposite to the source. These two sets of detectors form two measuring planes 4 cm apart at the detector's position. The detectors are manufactured by Hamamatsu (type: S 1337- 1010BR) [4]. Fig. 4 schematically shows the arrangement of the detectors. The estimation of each measuring plane thickness at the measurement location is 1.5 mm.

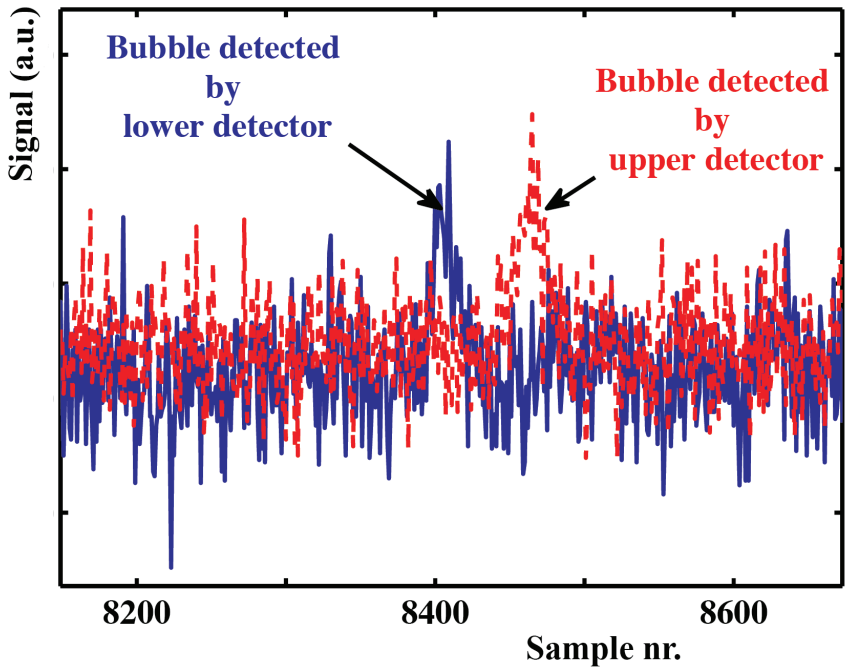

Figure 5: **Raw signals recorded by two different X-ray detectors located at two different planes. The effect of bubble passage is highlighted.**

3.2 Measurement

The rise velocities of single bubbles rising in suspensions containing 78 μm, 2.0 mm and 4.0 mm polystyrene particles were measured using X-ray densitometry. The bubble was injected at the bottom of a rectangular column. As it rose past the two detector planes, it altered the attenuation of the X-ray recorded by the 32 detectors. In each experiment, the typical duration of recording was 30 sec and each experiment was repeated four times.

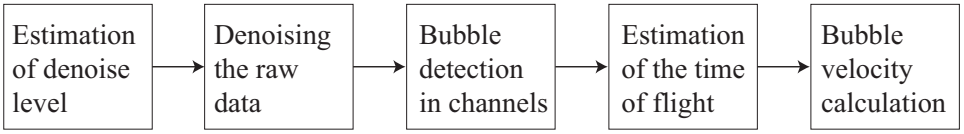

Figure 6: **Procedure of signal analysis for bubble velocity estimation.**

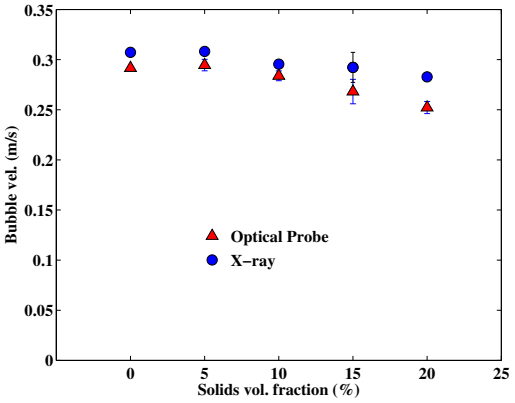

Figure 7: **Effect of particle volume fraction on the bubble rise velocity as measured by X-ray densitometry and four-point optical probe.**

3.3 Signal analysis

Fig. 5 illustrates the effect of bubble passage on the signals recorded by two detectors at two different elevations. The noisy signals were filtered using the Wavelet method (wdencmp function in Matlab). The rise velocity of the bubbles, v_b, can be estimated from $v_b = \Delta z/\Delta t_f$, where Δz is the distance between the two detector planes and Δt_f is the time of flight of the bubble. Fig. 6 summarizes the procedure of the bubble velocity estimation.

Bubble rise velocities measured by X-ray densitometry and the four-point optical probe are comparable at low particle volume fractions (see Fig. 7). The intrusive optical probe slows down the bubble, an effect that appears to be more pronounced at higher particle loading levels. Furthermore, at high solids loading, the signal becomes progressively noisier as the particle loading level increases; this, in turn, leads to larger uncertainties in measurements and analysis.

References

[1] Mudde, R. F. & Saito, T. Hydrodynamical similarities between bubble column and bubbly pipe flow. *J. Fluid Mech.* **437,** 203-228 (2001).

[2] Hooshyar, N., Hamersma, P. J., Mudde, R. F. & van Ommen, J. R. Intensified operation of slurry bubble columns using structured gas injection. *Can. J. Chem. Eng.* **88,** 533-542 (2010).

[3] Mudde, R. F. Time-resolved X-ray tomography of a fluidized bed. *Powder Technol.* **199,** 55-59 (2010).

[4] Mudde, R. F. Bubbles in a fluidized bed: A fast X-ray scanner. *AIChE J.* **57,** 2684-2690 (2011).